UNIVERSITY OF NAPLES FEDERICO II

DEPARTMENT OF PHARMACY

PHD IN

NUTRACEUTICALS, FUNCTIONAL FOODS AND HUMAN HEALTH - XXXV cycle.

IN VITRO MODEL SYSTEMS TO STUDY NUTRACEUTICAL PROPRIETIES

PhD Thesis

Dr. Cristina Santarcangelo

TUTOR:
PROF. MARIA DAGLIA

PHD COORDINATOR:
PROF. ALBERTO RITIENI

Academic Year 2022-2023

The most difficult person to deal with during a PhD is oneself.

CHAPTER 1: General introduction

1.1 3Rs principles

The use of animals for scientific experimentation represents one of the most controversial problems in human-animal relationships. Starting from the 1900 century the expansion of science has led to the exponential growth of the use of animals in scientific experimentation [1]. The ethical aspects of the use of animals in experiments were defined by the principles of the 3Rs: Replacement, Reduction, and Refinement, proposed by William M.S. Russel and Rex L. Burch in 1959 of the Universities Federation for Animal Welfare (UFAW), with the publication of their book "The Principle of Humane Experimental Technique" [2]. Since then, these concepts have evolved and updated according to modern research practices and have been integrated into national and international legislation and regulations on the use of animals in scientific procedures such us Directive 2010/63/EU on the protection of animals used for scientific purposes of 3 June 2010.

The definitions of the 3Rs principles are explained below:

- Replacement refers to methods that minimize the number of animals used or avoid their use in experiments or scientific studies. The replacement could be absolute when the animals are substituted by computer models or relative when vertebrates are replaced with animals with a lower pain perception potential, such as invertebrates. At the present, replacement principal definition had updated according to modern research practices. The modern concept of replacement indicates the development and use of robust and predictive models or tools to address important scientific questions without the use of animals.
- Reduction involves minimizing the number of the animal used in the experiment. This can be achieved by intelligently designing experimental studies.
- Refinement refers to the modification of experimental procedures to minimize pain and distress and to enhance the welfare of an animal used in science from the time it is born until its death. The latest *in vivo* technologies and the new knowledge in research animal welfare helps to improve understanding of the impact of welfare on scientific outcomes.

For many years animal experimentation has been used to answer important scientific questions including those related to human health. Currently, the golden standard in different research fields like toxicological and safety studies is still animal models. Animal models are often costly and time-consuming and depending on the research question present scientific limitations, such as poor relevance to human biology [3]. Looking to the future, alternative models can address some of these concerns: *in vitro* models must be easy to implement, relevant, predictive to the human situation [2]. In the last decade, advances in science and technologies have meant that there are now realistic opportunities to replace the use of animals. The development and validation of new *in vitro* cell

systems could significantly contribute to the good experimental practice proposed by the "3Rs" model.

1.2 The small intestine: Anatomy and Functions.

Foods and among them the class of dietary supplements are orally delivered and pass through the digestive system starting from the mouth, passing through the oesophagus and the stomach, and terminating the travel in the large intestine. Along the alimentary canal, foods are processed thanks to the action of enzymes at the acid pH of the stomach and then passes to the level of the small intestine where the nutrients are absorbed [4,5]. The intestine is a component of the digestive system allowing essential functions: digestion and absorption of foods and nutrients, protective function against pathogens through the synthesis of immune cells, molecules secretion [5]. The length of the small intestine varies with an average length of approximately 6.5 meters in adult [6]. Intestine is divided into three sections (Fig.1). The first section is the duodenum, which is the shortest section, on average measuring from 20 cm to 25 cm in length. It is the most proximal section of small intestine, which is connected to the antrum of the stomach, separated by the pylorus. Bile and pancreatic enzymes are secreted in the duodenum via the duodenal papilla. The second section is the jejunum, which is almost 2.5 meters in length. In the jejunum the typical small intestinal macroscopic structure appears consisting of a highly folded mucous membrane containing villi at the top protruding into the lumen, which is much longer than those in the duodenum or ileum. This results in an enlarged surface that facilitates the absorption of the products of digestion. Ileum, which is approximately 3.5 meters in length and absorbs nutrients that got past the jejunum. The ileum terminates at the ileocecal junction and continues as the large intestine [7,8].

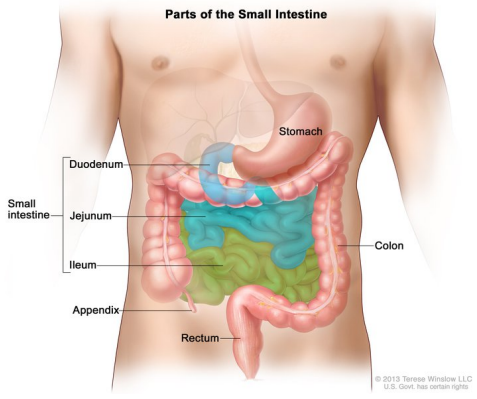

Figure 1: Part of the small intestine© 2013 Terese Winslow LLC, U.S. Govt. has certain rights. Exported from National Cancer Institute website with permission.

The intestinal tissue consists in four layers: mucosa, submucosa, muscularis externa, and the serosa (Fig 2).

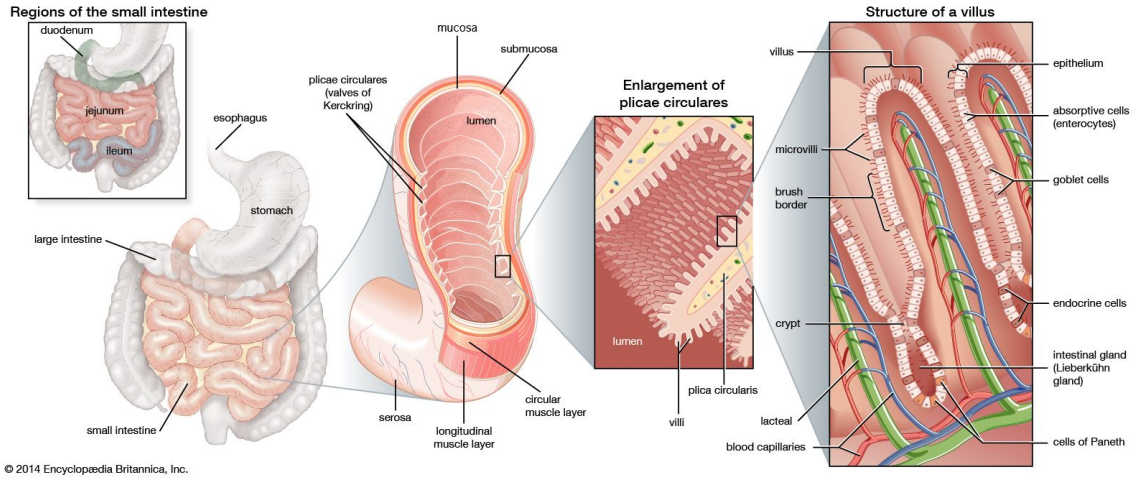

Figure 2: Anatomy of the small intestine. The duodenum, jejunum, and ileum are shown in relation to other GI tract organs; the enlarged views show the structure of villi and microvilli in the duodenum (exported https://www.britannica.com/science/small-intestine#/media/1/549336/107046)

The intestinal mucosa is the innermost layer of the small intestine. As such, it directly faces the lumen of the intestine, in close contact with foods. Below the mucosa, proceeding outwards, there are the remaining tunics: submucosa, the muscularis mucosae and the serosa. The intestinal mucosa is in turn made up of three distinct portions: a single layer of epithelial cells, a connective tissue that keeps the epithelium in place with a dense vascular and lymphatic network (the lamina propria), and a small layer of smooth muscle, called muscularis mucosae, which separates it from the tunic underneath and it is playing an important role in intestinal peristalsis and contraction [9,10]. Different cell types are present in intestinal epithelium, each performing different functions. The most common cell in intestinal epithelium are enterocytes, which are polarized columnar cells involved in absorption function thanks to the presence of characteristic brush border formed by exposed microvilli in the luminal part of the intestine [11]. Other cell types are present in the intestinal epithelium are secretory cells, including goblet, enteroendocrine, Paneth cells, tuft cells and stem cells [12-15]. Goblet cells are located between enterocytes and are involved in the mucus production, which covers the intestinal layer and protects it by microbial infection and in the maintenance of intestinal homeostasis [16]. Enteroendocrine cells produce hormones such as serotonin, glicentin and somatostatin, which are correlated with tissue repair, angiogenesis, enterocytes differentiation and polarization. Enteroendocrine cells represent up to 1% of all cells in the epithelium [17]. In the intestinal epithelium, cell proliferation take place in the basal part of crypts where are located epithelial stem called columnar intestinal stem cells (ISCs) [18,19]. The side-to-side connections between the

intestinal cells are due to tight junctions, adherent junctions and desmosomes, which are different in protein composition and functions. Differently, the connection between the basal part of the cells and the extracellular matrix (basal lamina) occurs through integrins proteins that form hemidesmosomes. These types of junctional proteins provide cells and tissues mechanical support and contribute to intracellular signalling to transmit information to the nucleus [20].

Cell	**Function**	**Structure**	**Localization**
Enterocytes	Most abundant absorptive cells of the small intestine	Columnar ceels with microvilli on the apical side; bound to each other by different junctions	Crypt- villus axis
Paneth cells	Secretory cells that secrete lysozyme, antibiotic proteins and may regulate intestinal flora	Pyramid-shaped cells with eosinophilic cells granules that contain glycoprotein such us lysozyme	Base of crypts
Enteroendocrine cells	Hormone producing cells (i.e. somatostatin, serotonin, glicentin).	Basal-granulated cells that represent up to 1% of all cells in the epithelium.	Embedded between enterocytes
Goblet cells	Mucin-secreting cells		Located between the enterocytes.
M cells	Epithelial cells without microvilli	Specialized intestinal epithelial cells that sample antigens and pathogens through endocytosis.	Peyer's patches.
Cup cells	Cup cells	Still unknown function	
Stem cells	Progenitor cells of epithelial cell lineages	Columnar cells	Crypt base

Table 1: Intestinal epithelial cell types, function, structure and localization.

Mucus represents the first protective layer of the gastrointestinal tract that still allows nutritional uptake; it is composed of 98% water, which makes it transparent and microscopically invisible. In addition to water, another important component of mucus are mucins [21]. The MUC2 mucin is the most representative mucin in the small intestine and protects the intestinal tract from self-digestion and microorganism infections. Goblet cells are involved in the MUC2 mucin production, which covers the villi forming an inner mucus layer, dense and with a thickness of about 200 μm (human)

[22]. In the outermost layer thanks to proteolytic activities the mucus turns into a less viscous and expanded layer that allows bacteria to enter and uses the mucins as a nutritional source and bacterial habitat [23].

1.3 Absorption and Transport.

The intestinal barrier offers the possibility of limited passage of substances into two different directions. The absorption of substance and nutrient in the intestinal epithelium can be occur through several routes and it depends by the chemical-physical characteristics of the molecule such us molecular weight and hydrophobicity. Basically, the transport can be a passive transport, which is a free energy transport following the concentration gradient [24], and active transport, which is a transport requiring an energy source to drive molecules or ions through the cell membrane. Passive transport may occur via the transcellular pathway, in which molecules cross through the cell membrane and the paracellular pathway, in which hydrophilic chemicals pass through the intercellular spaces (cell junctions). Transcellular transport can be simple diffusion, in which chemicals directly pass through the hydrophobic membrane, or facilitated diffusion, in which diffusion is facilitated by transport channels or carriers. Active transport is a form of transcellular transport that requires energy to drive molecules or ions through the cell membrane. Specific transporter can mediate the selective transport of specific molecules or vesicles can internalize compounds inside the cells. Some examples of vesicular transport are endocytosis, pinocytosis, phagocytosis, and receptor-mediated endocytosis [25].

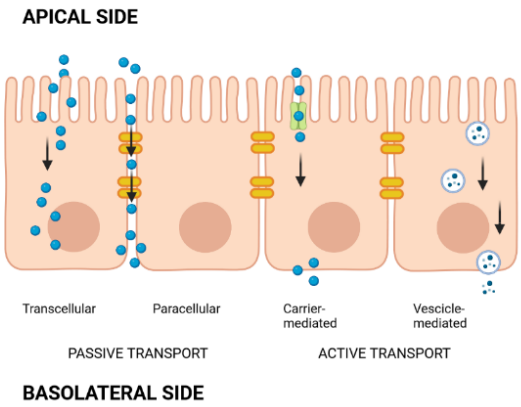

Figure 3: Transport pathways of substances across the intestinal epithelium; absorption can occur in parallel involving passive (transcellular and paracellular) and active (transcellular carrier-mediated and vesicle mediated) mechanisms (Biorender).

1.4 Linking with immune system.

The intestinal barrier acts as a protection against the attack by pathogens and toxins. The intestinal epithelium is a complex physical barrier that selectively absorbs the molecules. Furthermore, an immunological barrier is present bring able to secrete IgA by M cell, which block the access to epithelial receptor, a phenomenon known as immune exclusion [26]. The enterocytes can detect pathogens through Toll-like receptors, which activate transduction signals such us: nuclear factor (NF)-κB, the mitogen-activated protein kinases (MAPKs) and the interferon regulatory factor (IRF) mediated pathways [27, 28]. Consequently, the activation of these patterns determines the release of different cytokines and interleukins, which play a key role in the barrier permeability. [29]. The intestinal epithelium, covered by a mixture of water, mucus, and glycocalyx, is permeable to nutrients, water, and small molecules but constitutes a protective wall against bacteria and pathogens [30]. Despite mucus layer is responsible by a rapid particle clearance due to the quick turnover [31]. Paneth cells produce proteins with antibiotic action and defensins playing a primary role in innate immunity and gut protection [32].

1.5 In vitro models for intestinal permeability studies.

Different animal alternative models were developed to better mimic the physiological human conditions and to respect the 3Rs principles. Although animal models are still widely used, it is known that they have limitations especially for oral absorption. For instance, mice and rats are the most common animal model because they are small and are less expensive that rabbits, dogs and pigs. However, the physiology of the rodent gastrointestinal tract is different from that found in humans (lower intestinal pH and shorter intestinal transit time in rodents compared to humans). This might affect the behaviour and absorption of the compounds of interest differently leading to inadequate predictions for humans [33-35]. On the hand, animal models can resemble the physiology of an entire human organism but present different disadvantages such us ethical considerations, high costs and the difficulties in extrapolating results to humans due to differences between species. *In vitro* models also have limitations but there are different types of models with different levels of complexity that simulate the real situation [36]. To evaluate intestinal absorption, there are two groups of *in vitro* models currently used to determine the bioavailability of orally delivered drug: synthetic models and cell-based model.

1.5.1 Synthetic models

Synthetic models consist of lipid membrane. They are used to study passive diffusion processes and offer highly reproducible and robust results [37]. Cell based systems are more reliable in terms of intestinal absorption and represent a model with intermediate level of complexity in terms of

physiological conditions [38]. Among the synthetic *in vitro* models, Parallel Artificial Membrane Permeability Assay (PAMPA) are the best known for predicting the passive transport and permeability of one or more compounds of interest across the cell membrane [39-42]. This system is composed of two compartments (apical and basal) separated by a synthetic membrane, on which a phospholipid solution (dissolved in organic solvent) is placed to reproduces in artificial way enterocytes human biological barrier as reported in figure x [43]. PAMPA is a robust, fast, and low-cost model system to measure the permeability of lipophilic molecules through different biological barriers such us the intestine, the blood brain barrier, skin. It resulted to be very useful in limiting the use of animals. [44]. The versability of PAMPA is linked to the possibility of differentiating the phospholipidic composition, using different organic solvents and pH conditions [45]. Moreover, PAMPA represents a useful tool for the compound screening in early-stage ADME test as it allows to obtain information about the drug absorption potential [46]. In fact, several studies show a relationship between the permeation rate in PAMPA and Caco-2 cell-based model for hydrophobic compounds that cross the membrane thanks to transcellular transport [47]. On the contrary, PAMPA is not a good model for the evaluation of hydrophilic molecules that very often need membrane transporters. due to the absence of cells and the presence of organic solvents [48].

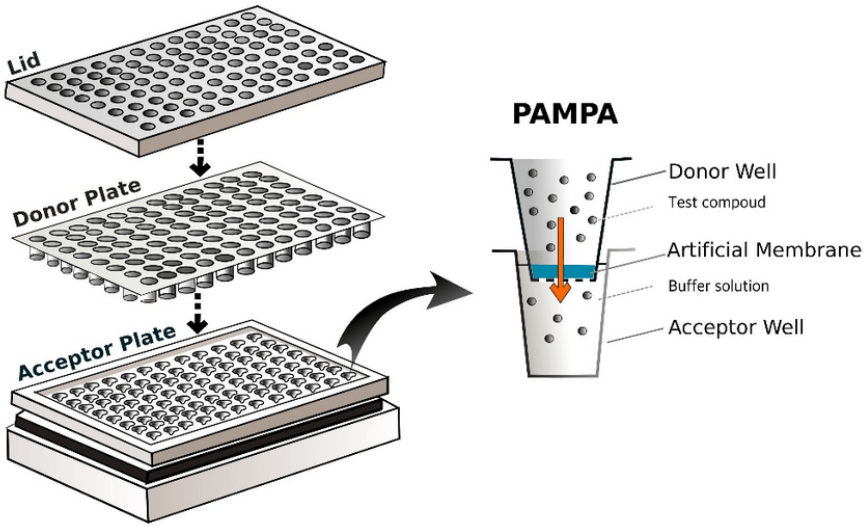

Figure 4: Parallel Artificial Membrane Permeability Assay (PAMPA) 96-well setup (left); a single well of PAMPA (right).

1.5.3 Cell-based model

In traditional *in vitro* cell culture models, suitable for high-throughput screening, cells are grown as two-dimensional (2D) monolayers on a flat surface, or on permeable membranes (Transwell® inserts). Transwell® model is the accepted *in vitro* model to perform the permeability, metabolic and toxicological studies in both pharmaceutical and nutraceutical research fields [49]. This system is

composed by a multi-well plate where the insert to obtain a basolateral compartment and apical compartment corresponding to the intestinal lumen and the epithelial are placed, respectively [50]. To separate apical and basal compartment there is a porous membrane, which consist of polyester or polycarbonate where there are cells either in mono- or co-culture to mimic the complex functions and morphology of the intestinal epithelium (Fig. 5) [51]. Cell lines or primary cells can be used for this purpose. In additions, models based on the use of stem cells have recently been developed. Primary human intestinal epithelial cells are obtained from the small intestine or the colon and express all intestinal epithelial cell types. Primary cells are collected from the small intestine or colon, when they are seeded in Transwell® insert form a cell monolayer and express all gut specific markers [52 – 54]. However, primary cell cultures of small intestinal tissue have several disadvantages as low reproducibility and the short life span. For this reason, primary cell cultures of small intestinal tissue have been replaced by cell lines derived from gastrointestinal cancer. The easy maintenance, accessibility and reproducibility of the cell lines make them suitable for high throughput screening studies. There are several models of intestinal immortalized cells including Caco-2 cell line, which are the most studied [55,56].

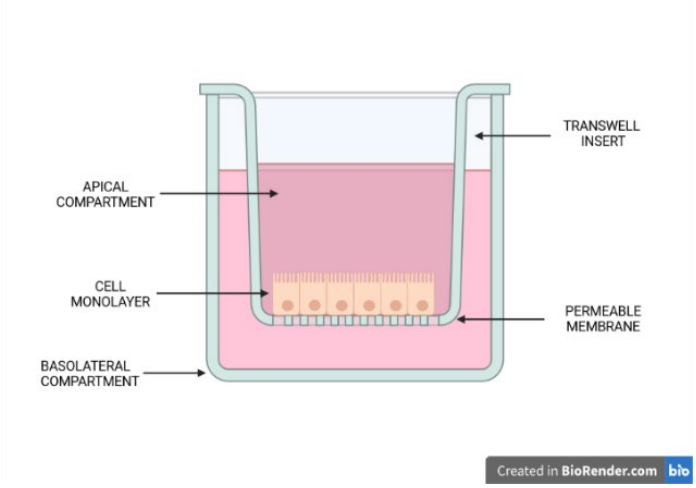

Figure 5: Scheme of cell-based monolayers setup in Transwell® system.

Caco-2 cell line derived from human epithelial colorectal adenocarcinoma cells and were first isolated in 1979 by Fogh and co-workers [57]. This cell line represents a reference model for permeability assay of different compounds, which can cross the enterocyte layer by passive paracellular or transcellular route, or carrier-mediated route and transcytosis [58]. Caco-2 cells are cultured in the Transwell® system for 21 days, in the initial stages of growth these cells do not show the morphological and functional characteristics of the intestinal epithelium but when they reach confluence and form a monolayer, they acquire the phenotypical characteristic showing polarized cells, tight junctions and apical microvilli [59]. The proteomic characterization of Caco-2 cells has

allowed us to understand which type of enzymes and transporters are expressed by Caco-2 cells in cultures on Transwell® [51, 61]. These studies revealed that Caco-2 cells express markers characteristic of enterocytes but there is difference in the expression of transporters between Caco-2 and human gut cells [62]. Some examples concern the expression of the P-gp transporter, which is highly variable and the metabolic enzyme CYP3A4 is low or absent in Caco-2 cell line [63, 64]. Caco-2 cells show tighter junctions (3.7 ± 0.1 Å) in comparation with human small intestine. This condition represents a limitation for hydrophilic compounds, which are transported across the membrane by paracellular pathway [65]. In physiological conditions the molecules that are slowly absorbed remain for a long time in the intestinal lumen and precipitate in the areas of the crypt where the junctions are more permeable and this phenomenon does not occur in the Transwell® model, since it is a flat cell monolayer and does not have the 3D structure villus crypt [66]. Moreover, the Caco-2 cell does not produce mucus, which is the first layer with the molecules come into contact [67]. In comparing studies performed in different laboratories, Caco-2 model presents a great variability among the obtained data. The experimental conditions (i.e. protocols, passage number of cells, type of cell clone) affect the inter-laboratory variability [63, 69, 70]. Despite these limitations, the Caco-2 model is still nowadays the best model for *in vitro* prediction of intestinal drug permeability and absorption of nutraceutical and pharmaceutical compounds. In fact, this model has obtained excellent results in terms of correlation to the paracellular transport pathway, which represents the most common molecules absorption route [39; 69]. There are more than 30 years of studies conducted on the Transwell® model using Caco-2 and several laboratories have gained experience in reproducing this model. For this reason, Caco-2 cells are the gold standard method for the investigation of intestinal compound permeation processes accepted by regulatory authorities [72 - 74]. Caco-2 is a characterized cell line, but 21 days are required when they are cultured in Transwell® inserts to obtain a mature monolayer ready for permeability studies. In this regard, several researchers have tried to simplify the protocols and reduce the maturation times of these cells adding growth factor and hormones in the culture media [75, 76]. An interesting study conducted by Chong et al. (1997) used a BioCoat® intestinal epithelial cell environment to achieve a mature Caco-2 monolayer suitable to perform absorption assay in only 3 days [77]. However, these protocols obtain a monolayers ready for transport studies, but often, under these culture conditions, Caco-2 cells may not express transport carriers or tight junctions, which are essentials for a functional intestinal model [78]. Good results were obtained by Peng and collaborators who obtained a good correlation between the 7-days model and the traditional 21-days model in terms of efflux ratio and permeability value. In this experiment Caco-2 cell line was cultivated in collagen-coated Transwell® [79]. However, the validation of new

protocols for Caco-2 cell models is difficult due to variability in transporter expression and cell morphology [80].

1.5.3 Alternative to the Caco-2 model.

To mimic the human gut permeability, several cell lines have been studied to find a better and more reliable model of Caco-2 cell line. There is interest from scientists in developing an alternative *in vitro* model that can be used in different stage of molecule discovery and development. The most used cell-based model, after Caco-2, for permeability studies is represented by TC-7 cells, which are a clone of the Caco-2 cell line. Consequently, both cell lines have the same morphological characteristics such as the presence of polarized cells with brush border microvilli and the expression of tight junctions [81]. Unlike the latter, TC-7 cells have a more homogeneous and reproducible cell population with higher enzyme levels. Studies conducted in several laboratories show robust results [82]. However, more recent studies have shown that the use of this cellular model is not useful for studying the permeability of lipophilic compounds or molecules that need transporters to cross the intestinal membrane [83]. Different co-culture models have been developed to obtain *in vitro* models more faithful to the physiological conditions. One such co-culture model is based on the union of Caco-2 cells and HT-29 cells. HT-29 cells originate from human colon adenocarcinoma cell and express also intestinal secretory cells to mimic Goblet cells and mucus production [84]. This model is widely used in bioavailability studies because it reproduces an environment like that of the human gut where substances meet mucus as the first layer. [85]. Furthermore, the contemporary presence of Caco-2 and HT29 can modulate the junction distribution to obtain a monolayer more like those of small intestine [86]. Caco-2/HT-29 model thanks to properties of the secreted mucus is employed to investigate the intestinal immune response to bacterial infections [87]. The culture conditions affect the phenotypic of this model, especially the level of glucose in the culture medium is essential to obtain the differentiated and polarized cells [88].

Another model that has been studied involves the use of Caco-2 cell line in combination with Raji-B cell line, which derived from Burkitt's lymphoma. The Raji-B cell line exhibits a B-lymphocyte-like phenotype and can induce the differentiation of Caco-2 in Microfold cells (M cells) -like cells [89]. The main function of these cells in this type of *in vitro* model is the transport of antigens and pathogens due to their transcytosis activity. Thereby, the Caco-2/ Raij-B co-culture model is used to study to investigate the role of M cells in the uptake of molecules with antibiotic action or vaccine [90-92]. A new co-culture protocol has recently been developed where human Raji B lymphocytes are not in direct contact with the Caco-2 cells, but they were added to the basolateral chamber of the Transwell® at 14th day of culture [90]. Although lymphocytes were not in direct contact with Caco-

2 cells, it was possible to observe that some cells developed M cell-like morphology, allowing the establishment of a system that better resembles the physiological conditions [93]. To further expand the complexity of the *in vitro* cell-based model system, a new triple co-culture was development using Caco-2, HT29-MTZ and Raji-B cells [94]. These three cell lines keep their functions when cultured together mimicking an environment closer to the human intestinal epithelium [95].

Stem cell and induced pluripotent stem cell (iPSCs) are now under study as intestinal model for intestinal transport and toxicity studies. iPSCs are induced to differentiate into enterocytes and express drug-metabolizing enzymes (CYP 3A4, CYP2C9, carboxylesterase) and sodium-dependent transporter (SLC28A3) [96 – 99]. However, only a limited number of studies have been performed due to the high cost that stem cells require for growth and differentiation. An example of their application is the study conducted by Komada and co-worker, they used iPSCs to obtain enterocyte-like cells and predict the oral absorption of paracellularly absorbed compounds [100].

1.5.4 3D model system.

In biology, the relationship between structure and function is well known. The function of a cell is usually directly related to its structure. Furthermore, the cells receive signals and stimuli from the surrounding environment, which modulates the cellular processes. To create an intestinal model that mimics the *in vivo* scenario, it is necessary to consider the fundamental role of the cellular matrix and stromal cells. For this reason, numerous advances have been made in the development of 3D models [101, 102]. An innovative 3D model was developed using a quadruple culture of Caco-2, HT29-MTX, fibroblasts in type I collagen, and macrophages [103]. Comparing the data collected with these 3D models and the monoculture of Caco-2, fibroblasts improve the growth of the epithelium and HT29-MTX cells allow obtaining an intestinal epithelium with a lower expression of tight junctions and mucus production [104]. The expression of efflux transporters (P-gp) is altered in 3D models in comparison with *in vivo* data and the presence of macrophages can alter the absorption of different molecules [105, 106]. Moreover, the intestinal villi architecture in this model does not reflect the *in vivo* scenario and this represents a problem especially for bioavailability prediction of slowly absorbed molecules. Taking this in consideration, several laboratories have started to use collagen scaffolds [107, 108]. *In vitro* models with cellular complexity are represented by intestinal organoids, which are self-organized 3D tissue [109, 110]. Intestinal organoids are also called mini-gut and enteroids can mimic the *in vivo* tissue in terms of physiologic functions and morphology [111, 112]. Intestinal organoids derived from stem cells (pluripotent, fetal or adult) as they can be induced to differentiate, forming all the cells of the adult intestine [113, 114]. Organoids represent an improvement for research, especially in the field of personalized medicine, the investigation of

molecules permeability, which represent a challenge. Moreover, the production and maintenance of these systems is expensive and it is difficult to obtain reproducible results [115].

1.5.5 Dynamic model system.

All the models described above are static while it is known that the intestinal *in vivo* microenvironment is stimulated by mechanical stimuli and fluid flow [116]. A recent development in the field of *in vitro* models is the introduction of microfluidic technology that is used to develop novel cell culture dynamic model systems. The growing interest in the development of fluid platform is linked to the evidence that fluid flow and mechanical stimuli can alter gene expression compared to static systems (23.000 genes targeted) [117]. Fluid platforms (bioreactor and microfluidic chips) of human intestine usually are formed of an apical compartment and a basolateral compartment separated by a porous membrane over, which intestinal epithelial cells are seeded. Dynamic conditions are established thanks to a pump that allows the circulation of the culture medium in the system [118].

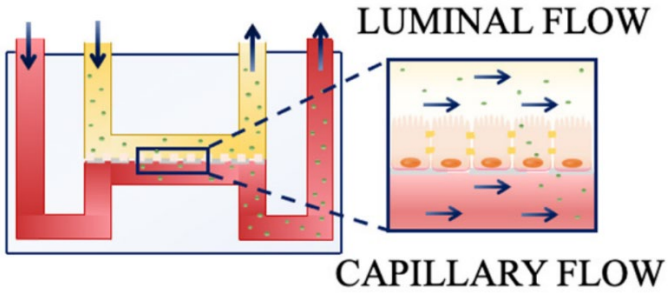

Figure 6: Typical design of an intestine dynamic model system composed of two channels mimicking the lumen and the blood circulation, separated by a membrane over, which cells are cultured [119].

The most used material for the manufacture of these platforms is polydimethylsiloxane (PDMS) for its low costs and gas-permeable proprieties. In additions. It is biocompatible, shows microscope compatibility and has fast fabrication properties [120]. However, gas-permeable proprieties can be a limitation since the evaporation of media can occur during an experiment and take effect on cellular microenvironments [121]. Nowadays, several dynamic models have been developed with geometric shapes and various flow rates or patterns. The perspectives that these dynamic models are interesting especially for the effects that the fluid flow can determine in immortalized cells lines such as Caco-2. Numerous studies conducted on Caco-2 cells have shown that under dynamic conditions these cells can complete their differentiation in 5-7 days [122-126]. Moreover, Caco-2 monolayer can build a phenotypic with 3D villi-like structure and basal crypts as a consequent of a fluidic stimulus [127]. Literature revealed the potential of dynamic models to be used to evaluate compound permeability,

improve the culture conditions compared with static models, and approach to *in vivo* scenario. Studies also report an increase of cytochrome P450 expression, mucus production and increase of aminopeptidase activity compared with cells cultured under static conditions [123, 126, 128, 129]. Dynamic systems were used to studies the permeability of different compound across intestinal epithelium and the results were compared with traditional Transwell®. For instance, Kulthong and co-workers performed permeability studies of different compound with high and low permeability in static and dynamic culture conditions. The obtained results showed permeability value similar to that obtained to BSC classification and a reduced uptake of the compounds compared with static conditions [123]. In another study, the permeability values for compounds such as curcumin, caffeine mannitol and dextran in Caco-2 cells cultured in a fluidic system resulted to be very similar to human data [123, 127, 130]. Dynamic Cell-Based Models are models that are still under development and are therefore not yet accepted by regulatory authorities. This is due to the fact that most of the studies conducted have limitations due to the intra-laboratory variability and these models have been developed without following Good Manufacturing Practices (GMP) or Good Laboratory Practices (GLP). To validate intestinal cell-based dynamic *in vitro* model system is essential to verify the suitable as barrier model in terms of monolayer integrity, differentiation cell markers and functionality. For Caco-2 cell *in vitro* model, as proposed in this thesis, the barrier integrity was monitored thought the measurement of transepithelial electrical resistance (TEER), the paracellular transport is modulate by tight junctions and small molecules such us lucifer yellow, mannitol and FITC-dextran can cross the membrane by paracellular transport. The morphology assessment was evaluated through immunohistochemistry or the expression of specific transporter [131].

1.6 Compounds relevant to this thesis

1.6.1 Vitamin C

Vitamin C, also known as ascorbic acid (Fig. 7), is a water-soluble molecule that can be found in foods. This molecule is an essential micronutrient for humans, which thanks to its ability to donate electrons exhibits an antioxidant activity, protecting cells from damage caused by free radicals and external factors such as: pollution, cigarette smoke and ultraviolet radiation [132]. Vitamin C is involved in collagen production and improves the absorption of iron from plant foods [133]. Furthermore, it is a cofactor for the regulation of gene expression and the biosynthesis of numerous enzymes. The vitamin C contribution in supporting the immune system takes place through different cellular functions of the innate and adaptive immune system. Vitamin C can trigger events such as chemotaxis and phagocytosis in neutrophils thus favouring the elimination of bacteria thanks to the

formation of reactive oxygen species (ROS) [134]. It also plays a key role in apoptosis and in the elimination of neutrophils at the site of infection by macrophages, thus reducing potential tissue damage. The role of vitamin C in lymphocytes is not yet understood but it appears to promote differentiation and proliferation of T and B cells [135].

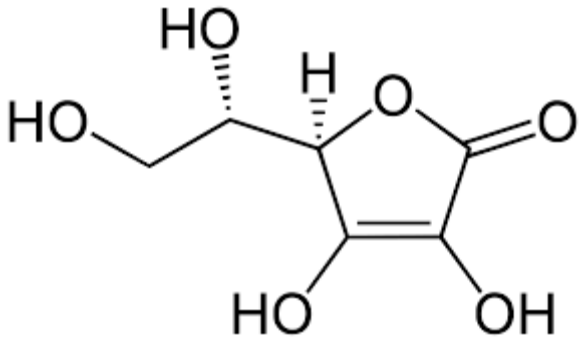

Figure 7: Molecular structure of vitamin C. Downloaded from https://www.acs.org/molecule-of-the-week/archive/a/ascorbic-acid.html.

Vitamin C protects biomolecules such as proteins, lipids, carbohydrates and nucleic acids from oxidative damage generated during cellular metabolism or due to exposure to toxins and pollutants [136]. Vitamin C deficiency results in scurvy, a disease that leads to weakening of collagen structures and reduced immunity. Individuals with scurvy are highly susceptible to life-threatening infections such as pneumonia [137 – 139]. The chemical-physical characteristics among, which the high solubility of vitamin C, prevent the accumulation in the body tissue and on the other hand, can induce hypovitaminosis C. The reference values define hypovitaminosis C when plasma levels of vitamin C are below 23 μmol/L, and deficiency when plasma levels are below 11 μmol/L [140, 141]. The reasons that can determine a state of hypovitaminosis or vitamin C deficiency are intake of fresh foods to reach the minimum recommended dietary levels of vitamin C, smoking, alcohol abuse or use of drugs that can lead to a reduction in the levels of vitamin C absorbed. Furthermore, environmental phenomena such as pollution or reduced exposure to sunlight can negatively affect the vitamin C status in an entire population [142, 143].

1.6.1.2 Vitamin C: Absorption, Distribution, Metabolism, Excretion

The main source of vitamin C is determined by diet and dietary supplements. Vitamin C is ubiquitous in nature, being particularly present in fruit and vegetables, which contain high concentrations. Healthy subjects can reach sufficient concentrations of vitamin C through the diet, but some diseases could negatively affect its absorption. The absorption and distribution of vitamin C is mainly regulated by a family of saturable sodium dependent vitamin C transporters (SVTC) and its absorption/elimination is strongly related to the administered dose [144]. Tissue-specific expression

of the transporters results in a compartmentalized distribution of vitamin C uptake that operates between 0.2 mM in muscle and heart, up to 10 mM in the brain and adrenal gland. The homeostasis of vitamin C is influenced by multiple factors including genetics, environment, lifestyle, diet, and any previous pathologies [145]. The hydrophilic nature of ascorbic acid results in the inability to cross the cell membrane through passive route. In 2002, Sotiriou and co-worker discovered that SVTC receptor was essential for the survival of the organism. Its inactivation led to respiratory failure and cerebral haemorrhage [146]. In the following years, multiple polymorphisms of this protein were discovered [147]. Generally, low molecular weight molecules are metabolized by a series of enzymes with oxidation and conjugation reactions that transform the molecule, increasing the solubility of the compound and promoting clearance. Vitamin C, on the other hand, takes part in numerous reactions in, which it acts as an electron donor, carrying out an antioxidant action on free radicals and undergoing a dismutation reaction, which forms dehydroascorbic acid [148]. This molecule, under optimal conditions, has a half-life of a few minutes and is again reduced to ascorbic acid at the intracellular level.

Absorption. Vitamin C exists mainly in two forms, reduced and oxidized, which is predominant in the tissues [149]. Its absorption occurs by passive diffusion, facilitated diffusion and active transport. Vitamin C is mainly present in the anionic form and at neutral pH, it is highly soluble. For this reason, Vitamin C can cross slowly the plasma membrane when the concentration gradient is favourable. Facilitated diffusion across the membrane, on the other hand, is promoted by carrier proteins, but like passive diffusion it depends on the electrochemical gradient. Among these transporters we also mention the glucose transporters, in fact vitamin C competes with glucose in the intestine to be absorbed intracellularly (Fig. 8) [150]. The most significant absorption of vitamin C occurs via active transporters, first discovered in the 1970s [151]. It is known that increasing the intake of vitamin C results in less absorption. Many authors hypothesize that this is due to saturation of intestinal transporters [152]. Numerous experiments have shown that intestinal absorption of vitamin C is mainly passive due to the low presence of active sodium-dependent transporters, which however have a high absorption capacity. However, literature data record the cellular release of vitamin C into the circulatory system with a C_{max} value of only 3h [153]. This evidence suggests the presence of other carriers unknown to date. Briefly, Ingested vitamin C crosses the intestinal epithelium through membrane transporters in the apical brush border membrane, either as ascorbate by sodium-coupled active transport via the SVCT1 transporter or as dehydroascorbic acid (DHA) through facilitated diffusion via GLUT1 or GLUT3 transporters. Once inside the cell, DHA is efficiently converted to ASC or transported to the blood stream by GLUT1 and GLUT2 in the basolateral membrane, hereby maintaining a low intracellular concentration and facilitating further DHA uptake. ASC is conveyed

to plasma by diffusion, possibly also by facilitated diffusion through volume-sensitive anion channels or by yet unidentified active transporters; the precise efflux mechanisms remain unknown [150].

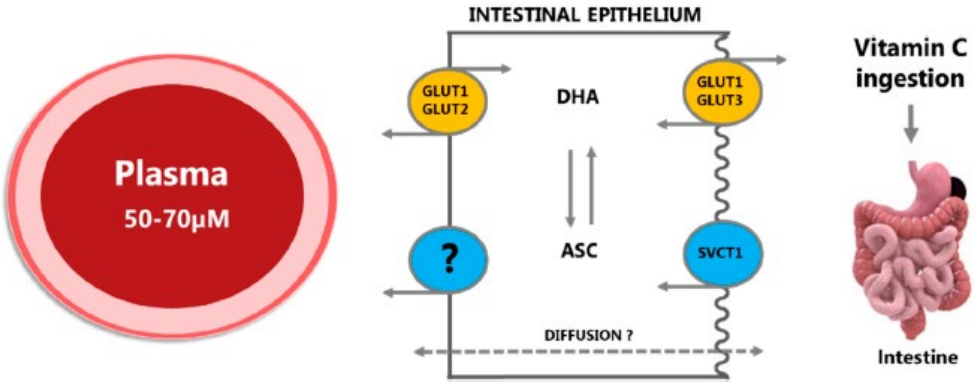

Figure 8: Transport mechanisms between intestines and blood. [150].

Distribution. The distribution of vitamin C is compartmentalized, the intracellular concentrations are between 0.5 and 10 mM while the plasma concentrations have values between 50 and 70 µM in healthy individuals (Fig. 9). Glucose transporters operate by facilitated diffusion and are expressed ubiquitously in the tissues and determine the absorption of vitamin C [154]. The oxidated form of vitamin C is predominantly in the circulatory system, indicating a predominance of transporters for glucose versus active transporters. An exception is represented by erythrocyte, which do not have any active transporters and are the only ones to absorb vitamin C by facilitated diffusion [155]. Erythrocytes can recycle the oxidized form of vitamin C into ascorbic acid for maintain intracellular levels like plasma concentrations. It has been estimated that erythrocytes alone can reduce all the amount of vitamin C in the blood every 3 minutes [156].

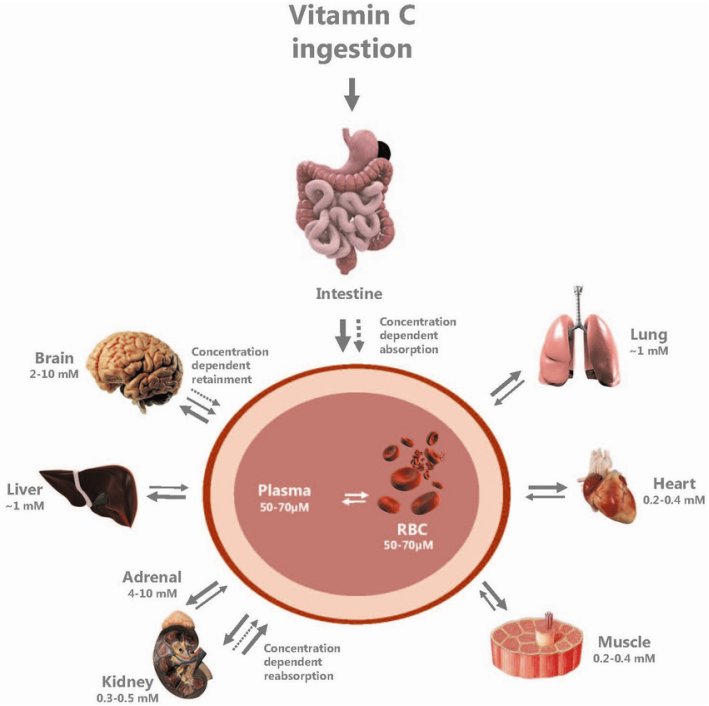

Figure 9: Illustration of the different distribution of vitamin C in the body. Several organs have concentration-dependent mechanisms for the retention of vitamin C, maintaining high levels during times of inadequate supply at the expense of other organs [150].

Metabolism and excretion. The metabolism of vitamin C is related to its antioxidant activity. The oxidized form of vitamin C is reduced intracellularly while preserving the pool of ascorbic acid. Therefore, the turnover of vitamin C is related to the catabolism of its oxidized form through the hydrolysis of 2,3-diketogluconic acid and the decarboxylation of L-xylonate and L-lixonate, which can enter the pentose pathway through degradation [156]. Ascorbic acid is filtered at the glomerular level by hydrostatic pressure and concentrated in pre-urines. Here, at the pH of 5 the non-ionized form of ascorbic acid increased. Ascorbic acid increases from 0.01% in plasma up to 15% in pre-urines with a concentration gradient of 1500:1 promoting the passive reabsorption of vitamin C following the concentration gradient. Vitamin C recovery in the proximal renal tubules is mediated by active SVTC1 transporters (Fig.10) [157].

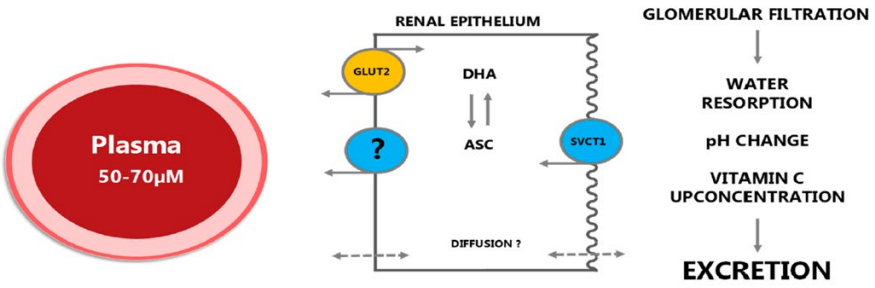

Figure 10: Vitamin C is filtered by glomerulus to the renal tubule lumen and the reabsorption (under vitamin C deficient conditions) is primarily achieved by SVCT1 transporters in the apical side of renal epithelium. GLUT2 transporters are in the basolateral membrane enabling transport of DHA to plasma [150].

1.6.1.3 Natural source of vitamin C.

The main sources of vitamin C are citrus melon, cherries, kiwi, mango, papaya, strawberries, watermelon and tomatoes. Among vegetables, the most important sources of vitamin C are represented by cabbage, broccoli, Brussels sprouts, bean sprouts, cauliflower, kale, red and green peppers, peas, tomatoes, and potatoes [158]. Although vitamin C is present in many types of fruit and vegetables, the deficiency is common in the population. In fact, the food processing can reduce the vitamin C content in the foods. This phenomenon occurs due to sensitivity of vitamin C at light and heat. Food supplements may contain synthetic source vitamin C or vitamin C extracted from natural sources. Chemically, there are no differences between synthetic and natural vitamin C, however, natural sources also contain other molecules (phytocomplex), which play an important role in the overall biological action of the supplement. The best-known natural source for its high vitamin C content is acerola (Malpighia punicifolia L.), which contains 1500-4500 mg of vitamin C per 100 g of product. The fruit also contains phytonutrients including carotenoids, flavonoids, anthocyanins, which provide added value to its biological properties [159]. Acerola contains numerous macro and micronutrients, such as glucose, fructose and sucrose, which are the main sugars present in the ripe acerola fruit. [153]. Among organic acids, malic acid represents 32% of the total acids present in ripe fruit while citric acid and tartaric acid are present to a lesser extent [159]. The main phytocompounds present in acerola include carotenoids, phenols, alkaloids, compounds containing nitrogen and sulphur groups. The fruit also contains pro-vitamin A, vitamins B1 and B2, niacin, albumin, iron, phosphorus and calcium [155]. Among the polyphenols there are procyanidins, anthocyanins, flavan-3-ols, flavonols. Mezadri and colleagues evaluated total polyphenols in commercial acerola products, yielding values ranging from 452 – 1060 mg gallic acid equivalents per 100 g (GAE/100 g) [160]. Lima and colleagues evaluated the carotenoid content of 12 different acerola genotypes. The collected

data show a content of 9.4-40.6 μg/g of carotene equivalents. [161]. Another source of vitamin C is Myrciaria dubia (Kunth) McVaugh, commonly called camu-camu, which is a plant from the Amazon rainforest known for its high vitamin C content and high nutritional value [163]. Camu-camu contains numerous bioactive compounds including anthocyanins (cyanidin 3-glucoside, delphinidin 3-glucoside), flavonols (myricetin, quercetin), ellagic acid, ellagitannins, proanthocyanidins and carotenoids (lutein, β-carotene, violaxanthin and luteoxanthin) [164]. Literature data indicate that the vitamin C content present in camu-camu is between 1.9 and 2.3 g/100 g, based on the degree of ripeness a value comparable to that of acerola [165]. In recent years, numerous studies have been conducted on the antioxidant activity of the polyphenols present in camu-camu [166], which appear to be involved in numerous beneficial effects on human health [167]. Commercial interest in camu-camu has grown considerably especially as an ingredient (dried powders) for the formulation of food supplements. The drying process of the fruit allows for the elimination of water, which is responsible for the loss of vitamin C during the storage phases, thus preserving the nutritional value of the camu-camu [168]. Rosa canina L. is a precious source of vitamin C and polyphenols. Rose hips provide about 426 mg of vitamin C per 100 g of fruit. The chemical composition of rose hips has been studied over the years by numerous researchers [169]. These studies revealed that the chemical composition of rose hips exhibits significant variability based on growing region, climate, degree of ripeness, cultivation practices, and storage conditions [170]. The total polyphenol content in rose hips is approximately 96 mg gallic acid equivalents per g of extract (dry weight). From rosehip fruits a compound was extracted and identified, identified as (2S) -1,2-di-O-[(9Z, 12Z, 15Z)-octadeca-9,12,15-trienoyl] -3-O -β-D-galactopyranosyl glycerol (GOPO), which appears to have a significant anti-inflammatory action [171]. Synthetic vitamin C is chemically identical to the vitamin C normally found in food sources. However, fruits and vegetables are rich in other micronutrients and phyto-complexe and some of these may affect the bioavailability of vitamin C. Furthermore, for several decades it has been demonstrated that the typical flavonoids of plants can perform an antioxidant action, also showing a protective action towards vitamin C [172-174]. In this regard, Uchida and co-worker. evaluated the bioavailability of vitamin C following administration of commercial ascorbic acid in single doses of 50, 100, 200 and 500 mg in young Japanese males. Blood and urine were collected from all subjects up to 6h after administration, assessing ascorbic acid levels. Subsequently each subject received diluted acerola juice containing 50 mg of ascorbic acid by repeating the blood and urine analyses. In plasma, the bioavailability values of synthetic ascorbic acid compared to acerola, as a source of vitamin C, tend to be higher when compared with ascorbic acid alone. Acerola could therefore enhance the absorption and excretion of this vitamin [175] Yuka et al. were evaluated the effect of vitamin C absorption in the Transwell model after 2, 3, 4, 8 and 24 hours by treating

intestinal Caco-2 cells with acerola juice. This study highlighted a promotion of ascorbic acid absorption with an increase in gene expression of the protein involved in its transport and absorption thanks to acerola treatment [176]. The limited results present in the literature eventually lead to the conclusion that further studies on vitamin C should be conducted. One of the few relevant studies (double blind with placebo) confirmed the antioxidant and anti-inflammatory action of M. dubia [176]. As regards the bioavailability of M. dubia, further studies should be conducted to determine the bioactive metabolites, trying to demonstrate the effective biological relevance of these compounds in the context of nutrition and health. For acerola, camu camu and rosa canina, given the scarce scientific literature available, further in vitro and in vivo studies should be conducted to evaluate the beneficial actions and their safety profile. The bioaccessibility and bioavailability of vitamin C in natural sources of acerola, camu camu and rosehip will in fact be evaluated in the studies described in the following paragraph. However, the intake of natural vitamin C is recommended to take advantage of the health benefits of the phytocomplex [176].

1.6.2 Vitamin D.

Vitamin D, also known as calciferol, comprises a group of fat-soluble seco-sterols. The two major forms are vitamin D2 and vitamin D3. Vitamin D2 (ergocalciferol) is largely human-made and added to foods, whereas vitamin D3 (cholecalciferol) is synthesized in the skin of humans from 7-dehydrocholesterol and is also consumed in the diet via the intake of animal-based foods. Both vitamin D3 and vitamin D2 are synthesized commercially and found in dietary supplements or fortified foods. The D2 and D3 forms differ only in their side chain structure. The differences do not affect metabolism (i.e., activation), and both forms function as prohormones. When activated, the D2 and D3 forms have been reported to exhibit identical responses in the body, and the potency related to the ability to cure vitamin D–deficiency rickets is the same [177]. Askew and colleagues first identified the structure of vitamin D2 in 1931. Subsequently, the structure of vitamin ***D3 was identified synthetically. From a chemical point of view, the two compounds can be considered steroids with the B ring open between carbons 9 and 10 (secosteroids); Ergocalciferol differs from cholecalciferol in that it has a methyl group at carbon 24 and a double bond between carbons 22 and 23 in the side chain [178]. In 1971 the bioactive form of vitamin D, 1,25-dihydroxyvitamin D*** (calcitriol), was isolated from intestinal extracts by mass spectroscopy. The fact that this compound could not be isolated from the intestine of nephrectomized animals led to the conclusion that the kidney was the site of synthesis of the active form of vitamin D. Calcitriol was subsequently synthesized through a double hydroxylation in positions 25 and 1 of cholecalciferol. The observation that in nephrectomized animals a correct intestinal absorption of calcium was restored with the

administration of 1,25-dihydroxyvitamin D and not of 25-hydroxyvitamin D led to the conclusion that the biologically active vitamin D was the dihydroxylated form (Fig. 11).

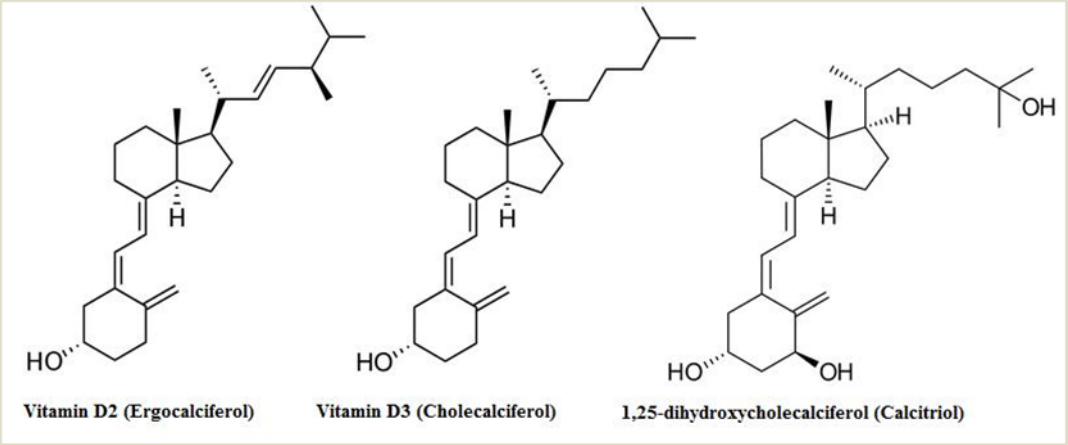

Figure 11: Vitamin D2, vitamin D3 and active metabolite calcitriol.

Vitamin D is localized in target tissues thank to specific transport protein at an extra- and intra-cellular level. Calcitriol is an that active form of vitamin D, which could function as a hormone, as a substance produced by an endocrine cell, i.e. an internal secretion, which is released into the bloodstream causing functional responses in cells located at various distances from its production site [177]. The European Food Safety Authority (EFSA), in 2016, defined the values of daily adequate intake (AI) for vitamin D, in different segments of the population (Table 2). This parameter represents a dietary recommendation used when there is insufficient data to calculate an average requirement [176].

Age	*Daily intake* (AI)
7-11 anni	10[(a)]
1-3 anni	15[(a)]
4-6 anni	15[(a)]
7-10 anni	15[(a)]
11-14 anni	15[(a)]
15-17 anni	15[(a)]
≥ 18 anni[(b)]	15[(a)]

Table 2: Daily dietary recommendation intake related to age. (a) Assuming minimal dermal synthesis of vitamin D. (b) Including pregnancy and lactation.

For pregnant and breastfeeding women, EFSA's Panel considers the AI to be the same as for non-pregnant and non-breastfeeding women, i.e. 15 µg/day. Data from surveys on vitamin D dietary intake in European countries suggest that in Italy, Spain and Portugal, the population consumes less than 1 µg/day to about 3 µg/day of this vitamin [179]. Vitamin D3 is present in foods of animal origin and the main sources are fish, offal (especially liver), meat and meat products and eggs (yolk). Fish, especially fatty fish and fish liver, has the highest natural content of vitamin D3, presumably derived from dietary microalgae, which contain both vitamin D3 and 7-dehydrocholesterol. Egg yolk also has a high vitamin D3 content, which is strongly related to the content of the vitamin in the feed. The vitamin D content of meat products depends, among other factors, on the vitamin D and fat content of the forage and on the latitude where the animals grazed. Vitamin D2, on the other hand, is contained in several species belonging to the plant kingdom, including fungi, algae and plants contaminated by fungi. Vitamin D2 in fungi and yeasts is synthesized by exposure to ergosterol UVB rays, and the amount depends on the intensity and time of exposure to light [180 – 185]. In Italy, supplement foods may contain vitamin D2 and/or D3, for a maximum daily intake of 50 µg, as established by the guidelines of the Ministry of Health "Daily intakes of vitamins and minerals allowed in food supplements - April 2019 revision". Vitamin D2 used for this purpose is produced by UV irradiation of ergosterol, contained in yeasts, while vitamin D3 derives from irradiation of 7-dehydrocholesterol derived from lanolin, an animal product secreted by the sebaceous glands of sheep, which is obtained for extraction and purification from wool. Both forms of vitamin D, when taken, induce an increase in blood levels of 25-hydroxyvitamin D. However, although both forms are equally absorbed in the intestine. Different studies indicates that vitamin D3 causes an increase of 25 - increased hydroxyvitamin D, which in turn, increases the duration of the increase, compared to vitamin D2. This aspect is detailed in the section on bioavailability [186 – 188]. Vitamin D, in the D3 form, is also produced endogenously from the precursor 7-dehydrocholesterol, by the action of solar radiation. This contribution is estimated to be equal to 80% of the circulating vitamin D and depends on various factors, linked for example 1) to environmental conditions (season, hours of light, smog, cloud cover), 2) to genetic factors (percentage of melanin present in the epidermis, a high percentage inhibits its synthesis) and between individuals (for example, age, as the elderly have a reduced capacity for skin synthesis, 3) to lifestyle, since UVB radiations are not able to penetrate through the windows of the houses and therefore during the hours spent in the buildings skin synthesis does not occur and the use of sun-screen cream [189]. Several studies have shown correlation between vitamin D deficiency and chronic or acute diseases. Furthermore, deficiency conditions are often accompanied by alteration of energy homeostasis, immune and endocrine systems [190]. Vitamin D deficiency in children

determine rickets, which is a pathology discovered in the seventeenth century by Francis Glisson, characterized by a lack of mineralization of bone tissue, with consequent skeletal deformities. In addition to bone deformities and pain, severe rickets can cause failure to thrive, developmental delay, hypocalcemic seizures, tetanus spasms, cardiomyopathy, and dental abnormalities. In adults and adolescents, vitamin D deficiency can lead to osteomalacia a condition, which bone is incompletely or defectively mineralized during the remodeling process, resulting in bone fragility. Signs and symptoms of osteomalacia are like those of rickets and include bone deformities and pain, hypocalcemic seizures, tetanus spasms, and dental abnormalities [191].

1.6.2.1 Endogenous synthesis

Vitamin D3 is synthesized in the skin starting from 7-dehydrocholesterol in the plasma membranes of epidermal keratinocytes and dermal fibroblasts is converted to previtamin D3, which immediately after its formation, isomerizes to vitamin D3 (cholecalciferol) [192]. Cutaneously synthesized vitamin D3 is released from the plasma membrane and enters the systemic circulation bound to vitamin D-binding protein (DBP) (Fig. 12) [193]. As a lipid-soluble molecule, vitamin D3 can be taken up by adipocytes and stored in subcutaneous or omental fat for later use [194]. Once in the circulation, vitamin D is converted by a hepatic hydroxylase into 25-hydroxyvitamin D (25(OH)D; calcidiol). The circulating 25(OH)D level is an indicator of the vitamin D status. As needed, 25(OH)D is converted in the kidney to its active hormonal form 1,25-dihydroxyvitamin D (1,25(OH)2D; calcitriol) in a process, which is usually tightly controlled by the parathyroid hormone, which levels start rising at 25(OH)D cut-off levels of 75 nmol/L or lower [194].

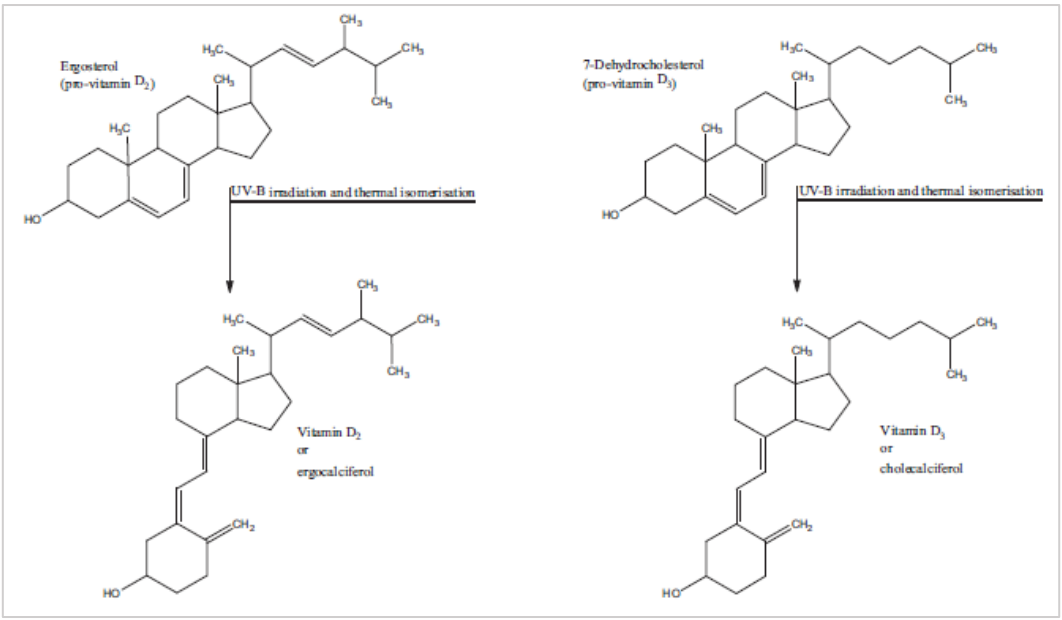

Figure 12: Biosynthesis of vitamins B2 and B3 [193].

1.6.2.2. Vitamin D: Absorption, distribution, metabolism, excretion.

Intestinal absorption (CALCIFEROL). Vitamin D from food is absorbed in the small intestine, mainly in the distal tract. Studies using radiolabelled compounds indicate that vitamin D absorption efficiency ranges from 55% to 99% in humans, with a Average value of 78%, with no significant differences between vitamin D2 and D3 absorption [195-200]. The absorption process of vitamin D takes place in the presence of bile salts and is more efficient when there are fatty substances inside the food bolus. Within the intestinal lumen, vitamin D is included in micelles, formed of bile acids, which enter the enterocytes by passive diffusion, through a non-saturable mechanism when there are high concentrations of vitamin D inside the bolus, while, at low concentrations, intestinal absorption requires the action of three transmembrane proteins, positioned on the enterocyte, which have a primary function of cholesterol transporters [201, 202]. A systematic review suggests that an oil carrier improves vitamin D absorption, as demonstrated by a greater response in serum 25-hydroxyvitamin D peak elevation, compared to a powder (cellulose and lactose) or an ethanol-based vehicle [203]. Vitamin D absorbed in the intestine is incorporated for 80% in chylomicrons, lipoproteins which collect, in addition to vitamin D, also triglycerides and cholesterol introduced with the diet. Within these structures, vitamin D, which due to its lipophilic nature, would have found various difficulties in entering and being transported in the blood stream, is easily conveyed in the lymphatic system and from here reaches the circulatory system [204]. The chylomicrons present in the blood reach various organs and tissues, until they reach the liver at the end of their cycle.

Hepatic metabolism (CALCIFEROL 25-HYDROXYVITAMIN D). Vitamin D activation involves two steps. The first occurs after calciferol is released in the liver, where it undergoes the first hydroxylation at the C25 position and is transformed into 25-hydroxyvitamin D. This hydroxylation is carried out by a mitochondrial enzyme (CYP27A1) or microsomal enzymes (including CYP2R1, CYP3A4 and CYP2J3) [205]. The rate of hydroxylation of calciferol in the liver has been observed to be higher in the presence of low serum levels of 25-hydroxyvitamin D [206].

Renal metabolism (25-HYDROXYVITAMINA DCALCITRIOL) and distribution. Once 25-hydroxyvitamin D has reached the kidneys, it undergoes a second hydroxylation at the 1α position in the proximal tubules, which transforms it into the active form of vitamin D, calcitriol. The enzyme involved is 1α-hydroxylase CYP27B1, which is also found in other parts of the body, such as bone tissue, parathyroids and the placenta. It follows that the synthesis of the active form also takes place at the level of these tissues. The enzymatic activity of 1α-hydroxylase is regulated by the concentration of calcium, phosphorus and parathyroid hormones. Other types of hydroxylation can also occur in the kidney, for example in the C24 position, which lead to the formation of inactive

metabolites, which are eliminated in the urine as water-soluble conjugates (Fig. 13) [206]. Calcitriol is a steroid with a carbon bond in position C9 and C10 in the B ring of the cyclopentanoperhydrophenanthreic structure, which represents the carbon skeleton of steroids. The flexible nature of calcitriol is essential for interaction with DBP proteins and vitamin receptors [206].

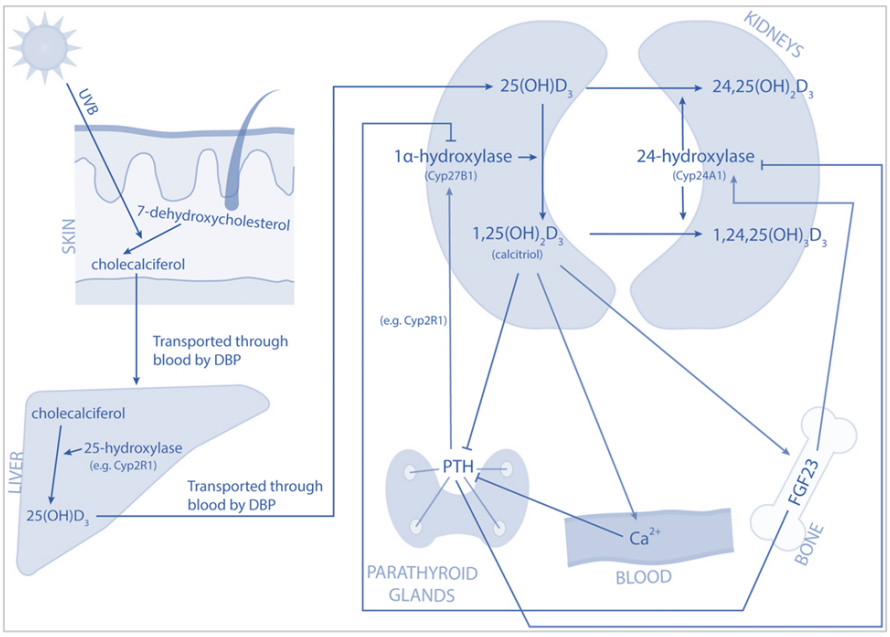

Figure 13: Vitamin D biosynthesis and metabolism [207].

Elimination. The catabolism of 25-hydroxyvitamin D and calcitriol involves inactivation by hydroxylation at the C24 position, by the enzyme CYP24A1, which gives rise to 24,25-dihydroxyvitamin D, preventing the conversion of 25-hydroxyvitamin D to calcitriol, and the 1,24,25-Trihydroxyvitamin D (calcitrioic acid). These elimination products may also regulate bone mineralization and suppression of PTH production. While urinary excretion of vitamin D metabolites is low due to active renal reuptake. CYP24A1 catalyses a lactone excretion pathway where 23-hydroxylation leads to the formation of 25-hydroxyvitamin D-26,23 lactone and 1,25-dihydroxyvitamin D-23,26-lactone [208]. As previously reported, the presence of lipids making vitamin D more accessible to enterocytes, facilitating the penetration of the lipid bilayer through a multi-step process: (1) lipids mediate the diffusion of vitamin D from the food matrix to the enterocyte, as they behave as a hydrophobic “bridge” phase, (2) lipids stimulate the secretion of bile salts, resulting in the formation of micelles, (3) digestive enzymes catalyse the release of fatty acids from lipids, which are involved in the formation of micelles [209]. Vitamin D3 appears to be more bioavailable than D2, producing a higher and more persistent increase in the serum concentration of 25-hydroxyvitamin D, the circulating form of the vitamin. Studies carried out in this regard have shown that the administration of vitamin D2 supplements reduces the percentage contribution of

vitamin D3 to the pool total vitamin D in the 25-hydroxylation phase, and that this decrease is accompanied by an absolute decrease in serum 25-hydroxyvitamin D concentrations [210]. The data suggest that vitamin D3 may be the preferred substrate for hepatic hydroxylation at the 25-position and other data suggest a greater metabolism and clearance for vitamin D2, respectively in the hepatic and renal districts, accelerating its degradation [211].

1.6.2.3 Biological activity

In recent years there has been a growing literature consisting of clinical studies, on experimental animals or *in vitro* models, which investigate the classical and non-classical biological activities of vitamin D. However, the fact that still a significant part of clinical studies interventional trials with negative outcomes have limitations in the study design, such as indistinct recruitment of individuals with and without vitamin D deficiency, lack of randomization, not taking into account body mass index variability, small sample size , or, again, the use of non-standardized methods for measuring the serum concentration of vitamin D, has led some exponents of the scientific community to think that the effect of this compound on human health is underestimated, concluding that, although vitamin D cannot be regarded as a panacea and is very likely to have more significant effects are obtained in people who have a previous deficiency, vitamin D, thanks to the high margin of safety, registered at the dosages allowed in food supplements, and to the numerous evidences of efficacy, can be considered as a valid and economic aid in maintaining a good state of health [212]. The discovery of the link between calcitriol and its VNR receptors was a key element in the research relating to the biological actions exerted by vitamin D [213]. In 1975 it was demonstrated that a VDR protein was able to associate with chromatin following its link with the calcitriol. In the following years, the use of the radiolabelling technique made it possible to determine the presence of the VDR in numerous cell lines and multiple tissues, such as the pancreas, placenta, pituitary gland, ovary, testicles, mammary gland, nervous tissue and the cardiovascular system [212]. Today we know that VDR can be present both on the nuclear membrane of cells (nuclear receptor - nVDR) and on the outer cell membrane (membrane receptor - mVDR). The different positioning of the protein determines a different mechanism of action of calcitriol [214]. (Figure 15). Genomic action (nVDR). In the first case, in fact, the compound exerts a genomic action, transforming the calcitriol-nVDR complex into a real ligand-dependent transcriptor, which forms a heterodimer with the 9-cis-retinoic acid receptor (RXR), in turn called the D-VDR-RXR complex, which interacts directly with a region of DNA called the Vitamin D Response Element (VDRE). The D-VDR-RXR complex thus modulates gene expression, by inhibiting or inducing the synthesis of certain functional proteins. Non-genomic rapid action (mVDR). In the presence of mVDR receptors, calcitrol, by binding to the protein exposed on the outer plasma membrane, leads to the activation of transduction signals that regulate kinase activity

and the ion flux of calcium and chloride. The latter mechanism is called rapid non-genomic action because, compared to genomic action, it occurs much faster. Both forms of receptors, mVDR and nVDR are involved in the classic action of vitamin D to regulate calcium homeostasis and bone mineralization, detailed in the following section [215].

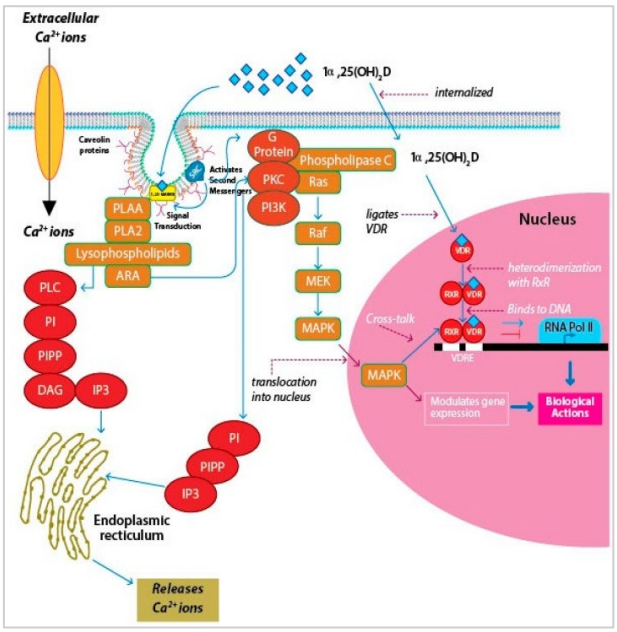

Figure 14: Different mechanism of action of calcitriol receptors [215].

The main function of calcitriol is the maintenance of serum levels of calcium and phosphate (2.5 mM), essential for various biological processes. Calcitriol aids in effective utilization of calcium by improving its intestinal absorption or mobilization from bone, in the absence of dietary calcium (Fig.14). When calcium concentrations drop below the physiological level, the parathyroid glands secrete parathyroid hormone (ParaThyroid Hormone – PHT), which stimulates the activity of the 1alpha-hydroxylase enzyme in the kidneys, leading to an increase in serum levels of calcitrol, which in turn, restores the blood calcium concentration to normal levels, through three main mechanisms:

1) The increase in the efficiency of calcium absorption in the intestine.

2) Decreased renal calcium elimination.

3) The mobilization of calcium from bone tissue, through the action of osteoclasts, whose synthesis is modulated by vitamin D. The parathyroid glands possess calcium-sensitive transmembrane proteins that are coupled to a G protein system, which are activated in the presence of low calcium levels, stimulating the production of PHT. The hormone reaches the bone tissue and cells of the proximal convoluted tubules in the kidney within seconds. When serum calcium levels exceed the calcium sensing system set point, the parathyroid gland-induced cascade of events is disrupted. C cells present

in the thyroid gland secrete calcitonin in response to high serum calcium levels. Calcitonin is a 32 amino acid peptide that blocks the mobilization of calcium from bone. When calcium levels return to normal, the enzyme 24-hydroxylase in the kidney is stimulated, leading to the formation of the inactive form of vitamin D [215].

Vitamin D acts as a potent modulator of the immune response with the most scientific evidence to support it. The hypothesis initially derived from two observations. First, many cells of both innate and adaptive immunity express the VDR receptor. Second, antigenic cells of the innate immune system, such as macrophages and dendritic cells, have the enzyme 1alpha-hydroxylase and, therefore, can convert 25-hydroxyvitamin D to calcitriol. The latter will bind to the VNR receptors that present the same, promoting transcriptional regulation. This mechanism appears to be central to two key features of immune function: innate antibacterial activity and antigen presentation to cells of adaptive immunity, such as T lymphocytes. In macrophages and monocytes, cellular sensing of pathogens, such as Mycobacterium tuberculosis, through recognition receptors, such as Toll-like receptors, enhances the expression of 1alpha-hydroxylase and VDR. The resulting effects, including increased expression of the antibacterial proteins cathelicidin and B-defensin 2 and increased autophagosome formation, improve the response to bacterial infection. Insufficiency or deficiency of vitamin D can therefore impair the innate immune response, predisposing the individual to infectious diseases. Some studies have revealed that calcitriol is able to preserve the integrity of the epithelial barrier, as well as that of the gastrointestinal barrier, primary defenses of our body [216]. The effect of vitamin D on the respiratory system is link to the immunomodulatory, anti-inflammatory and anti-infective action of calcitriol. The anti-inflammatory activity was found directly in the lung, with the inhibition of the NF-kB factor ("nuclear factor kappa-light-chain-enhancer of activated B cells") and of the MAPK protein, reducing the inflammatory secretion of cytokines and chemokines involved in lung inflammation and the number of inflammatory proteins infiltrating the lung interstitial tract. Calcitriol is also implicated in the reduction of oxidative stress, by regulating the nuclear transcription factor erythroid-2 (Nrf2), which in turn affects the transcription of genes involved in the oxidative process. Finally, calcitriol, in addition to stimulating the proliferation of monocytes and macrophages, inhibits the expression of various metalloproteinases in airway smooth muscle cells and alveolar macrophages, thus being involved in the tissue remodelling process through the regulation of the activation muscle activation of the bronchial tissue and in the deposition of the extracellular matrix by fibroblasts [217]. During the SARS-CoV-2 pandemic, several studies have been published suggesting a potential correlation between vitamin D deficiency and worsening of the course of infected hospitalized patients. However, more data are needed to confirm this link. Nevertheless, several relevant bodies, such as the Society Royal, have produced recommendations regarding the

assessment of the patient's vitamin D nutritional status during hospitalization and strategies for supplementation [218].

1.6.2.4 Natural source of vitamin D.

Lichens have been used for centuries in traditional medicine in many countries against a range of conditions like tuberculosis or throat irritation, as well as being used to promote general health [219]. The medicinal indications accepted by the European health authorities for human use are dry cough and irritation of the upper respiratory tract, laryngitis, and lack of appetite. Also, the lichen is employed to treat gastritis and other gastric complications. For example, products containing the aqueous extract of C. islandica are sold in Germany and Iceland as a treatment for coughs and sore throats. Polysaccharides are produced in considerable quantities by many species of lichens and there are studies conducted *in vitro*, which attest to their beneficial effects on the immune system. C. islandica has significant amounts of polysaccharides, among which lichenan and isolichenan have been isolated and appearing. The study of their immunomodulatory potential has shown that they can induce phagocytosis and complement activation. Furthermore, a recent study demonstrated that they affect cytokine production by human dendritic cells. C. islandica also contains several secondary metabolites, such as protolycesteric acid and fumarprotocetraric acid, which have been isolated and structurally traceable. The study of these single compounds showed that fumarprotocetraric acid has weak inhibitory effect on HIV-integrase *in vitro* and protolycesteric acid has antibacterial activity *in vitro* against H. pylori and inhibits 5-lipoxygenase [220].

1.7 The aim of this thesis

The present research aimed to develop new *in vitro* model system to evaluate the permeability proprieties of nutraceuticals. This resulted in the following research objectives:

- To evaluate the bioaccessibility and bioavailability of two different vitamin from natural source and synthetic source.

- To optimize and characterize a dynamic model system in terms of morphology and compound barrier functions.

- To compare the characteristics and functionality of MIVO® plaform with the classic and static Transwell® model system.

- To determine the potential permeability of vitamin C from synthetic source and from natural source using MIVO® platform and Transwell®.

CHAPTER 2: Comparative study of bioaccessibility and bioavailability of vitamins from natural sources and vitamins of synthetic origin.

2.1 Experimental.

2.1.1 Chemicals and reagents.

LC-MS-grade water, LC-MS grade acetonitrile, LC-MS grade methanol, ammonium acetate, and standard L-ascorbic acid (#A92902) were acquired from Sigma Aldrich Chemical Company (Milano, Italy). Vitamin C and D from natural sources and vitamin C and D from chemical synthesis. All compounds used for *in vitro* oral, gastric, and duodenal digestion processes were as follows: potassium chloride (KCl), dihydrogen potassium phosphate (KH_2PO_4), sodium carbonate ($NaHCO_3$), magnesium chloride ($MgCl_2$), ammonium carbonate ($NH_4)CO_3$, calcium chloride ($CaCl_2$), sodium chloride (NaCl), hydrochloric acid (HCl), and sodium hydroxide (NaOH). All materials were provided by Carlo Erba (Milan, Italy). Pancreatin from porcine pancreas (extract of pig bile), α-amylase from *Bacillus licheniformis*, pepsin from porcine gastric mucosa, porcine bile extract, and formic acid solution (1 M). MultiScreen-IP plate (0,45 μm), clear, non-sterile (MAIPNTR10), piastra MultiScreen Transport plate Clear, Non-Sterile; Transport Receiver Plate, non-sterile, styrene (MATRNPS50), Phosphate buffered saline (PBS), dodecane, dimethyl sulfoxide, *brilliant cresyl blue*, lucifer yellow CH, lithium salt, caffeine, furosemide, all reagents were acquired by Merk – Milano Italy. All the media and reagents were purchased from *Gibco* (Milan, Italy). Hanks' balanced salt buffer (HBSS) and 3-(4,5-dimethylthiazol-2-yl)-2,5-diphenyltetrazolium bromide (MTT) were obtained from Sigma-Aldrich (Milano, Italy).

2.1.2 Development of HILIC-UHPLC-MS method for determination of vitamin C.

HILIC-UHPLC-MS analysis was performed using Ultimate 3000 SD UHPLC system, equipped with quaternary pump, autosampler, and column heater compartment. The chromatographic system was connected using an ESI source at an LTQ XL™ Linear Ion Trap Mass Spectrometer (Thermo Fischer Scientific, Milan, Italy). A HILIC-Luna Polar column (100 × 2.1 mm, 1.6 μm), from Phenomenex (Torrance, CA, USA), was used. The mobile phase contained acetonitrile (eluent A) and water (eluent B), and 100 mM ammonium acetate pH 5.8 (eluent C) was eluted in isocratic mode as follows:93% A, 2% B, and 5% C. The total run time was 10 minutes. The flow rate was maintained at 0.4 mL/min, and the column temperature was maintained at 25 °C. A 5 μL injection volume was used. The MS spectra data were acquired under negative ionization mode and analysed in tandem mass, SRM (*Selected reaction monitoring*) 175 →115 (±2) using Xcalibur software. To obtain MS2 data, a collision energy of 35 % %was applied. A preliminary experiment was performed to optimize MS operating conditions: 10 μg/mL of ascorbic acid in H_3O^+ (0,1% formic acid)/acetonitrile 50:50 %v/v was directly infused through the ESI interface at a flow rate of 25 μL/min into the mass spectrometer.

The optimal conditions for the assay were as follows: capillary temperature, 160 ◦C; source temperature, 310 °C; capillary voltage, 35 V.

2.1.3 HILIC-UHPLC-MS quantitative analysis.

Quantification of vitamin C samples was performed using the previously reported HILIC-UHPLC-MS method using the external standard method. Before quantification, the analytical method was validated according to the ICH guidelines**.** Each vitamin C sample was carefully weighed (10 mg) and solubilized in 10 mL of water to obtain a concentration of 1 mg/mL. The samples were diluted according to the content of vitamin C reported in the datasheet to obtain aliquots at a concentration of 1 µg/mL vitamin C. A calibration curve was prepared using standard vitamin C to quantify the vitamin C content in the samples. The concentration range, calibration curve, and correlation coefficient were determined, as shown in Table x. The analytical method was linear within the concentration range of 0.156–5 µg/mL. The correlation coefficients were greater than 0.99. Repeatability was established by triplicate injections of sample and solutions at low, medium, and high concentration levels of the calibration curve, with the same chromatographic conditions and analyst both on the same day and within two consecutive days, showing good retention time and µg/mL extract repeatability with maximum CV% values of ≤ 0.07 and 8.02, respectively. The limits of detection (LODs) and quantification (LOQs) were calculated from the ratio between the standard deviation (SD) and the analytical curve slope multiplied by 3 and 10, respectively, to obtain a value of 0.150 µg/mL. All samples were analysed in triplicate.

Sample	Range of concentration	Calibration curve	Coefficient of correlation (R^2)
Vitamin C	0.156 - 5 µg/mL	y = 727890x – 203343	R^2 = 0.9956
	0.156 - 5 µg/mL	y = 854258x – 408841	R^2 = 0.9907
	0.156 - 5 µg/mL	y = 834571x – 356783	R^2 = 0.9934

Table 3: Calibration curve parameter: Sample, range of concentrations, linear equation, coefficient of correlations (R^2).

2.1.4 Development of RP-UHPLC-MS method for determination of vitamin D.

RP-UHPLC-MS analysis was performed using the same system reported above. A Kinetex®-XB-C18 100 A° (100 mm x 2,1 mm; 2,6 µm), (Torrance, CA, USA), was used. The mobile phase contained 0.1% acidified with formic acid water (eluent A) and methanol (eluent B) was eluted in gradient mode as follows: 85% B for 1.5 min, from 85% to 90% B in 6 min, and from 90% to 85% B in 5 min. The total run time was 16 minutes. The flow rate was maintained at 0.3 mL/min, and the column temperature was maintained at 40 °C. A 5 µL injection volume was used. The MS spectra data were acquired under negative ionization mode and analysed in tandem mass, SRM (Selected reaction

monitoring) 385 →367 (±2) using Xcalibur software. To obtain MS^2 data, a collision energy of 35 % was applied. A preliminary experiment was performed to optimize MS operating conditions: 10 µg/mL of vitamin D in H_3O^+ (0.1% formic acid)/acetonitrile 50:50 %v/v was directly infused through the ESI interface at a flow rate of 25 µL/min into the mass spectrometer. The optimal conditions for the assay were as follows: capillary temperature, 160 ◦C; source temperature, 310 °C; capillary voltage, 25 V.

2.1.5 Quantification of vitamin D samples.

Quantification of vitamin D samples was performed using the previously reported RP-UHPLC-MS method using the external standard method. Before quantification, the analytical method was validated according to the ICH guidelines. Each vitamin D sample was diluted to obtain a concentration of 2 µg vitamin D each sample. A calibration curve was prepared using standard vitamin D. Briefly, 10 mg of standard vitamin D were solubilized in 10 mL of DMSO to obtain 1 mg/mL stock solution of vitamin D. Serial dilutions were prepared in methanol in the range of concentration between 0.047 – 3 µg/mL. Table 4 reported concentration range, calibration curve, and correlation coefficient (R^2). All analysis were performed in triplicate. The correlation coefficients were greater than 0.99. Repeatability was established by triplicate injections of sample and solutions at low, medium, and high concentration levels of the calibration curve, with the same chromatographic conditions and analyst both on the same day and within two consecutive days, showing good retention time and µg/mL extract repeatability with maximum CV% values of ≤ 0.07 and 8.02, respectively. The limits of detection (LODs) and quantification (LOQs) were calculated from the ratio between the standard deviation (SD) and the analytical curve slope multiplied by 3 and 10, respectively, to obtain a value of 0.030 µg/mL.

Compound	Range of concentration	Calibration curve	correlation coefficients (R^2)
Vitamin D	3-0.047 µg/mL	y = 101759x + 9166,2	R^2 = 0.9940
	3-0.047 µg/mL	y = 155068x + 13158	R^2 = 0.9939
	3-0.047 µg/mL	y = 121589x + 27358	R^2 = 0.9947

Table 4: Calibration curve parameter: Sample, range of concentrations, linear equation, coefficient of correlations (R^2).

2.1.6 In vitro bioaccessibility of vitamin C and D samples using simulated orogastric and duodenal digestion processes.

To verify the effect of orogastric and duodenal digestion processes on the vitamin C and D samples we followed a protocol by Milekus et al. with some modifications [221] (Fig. 15).

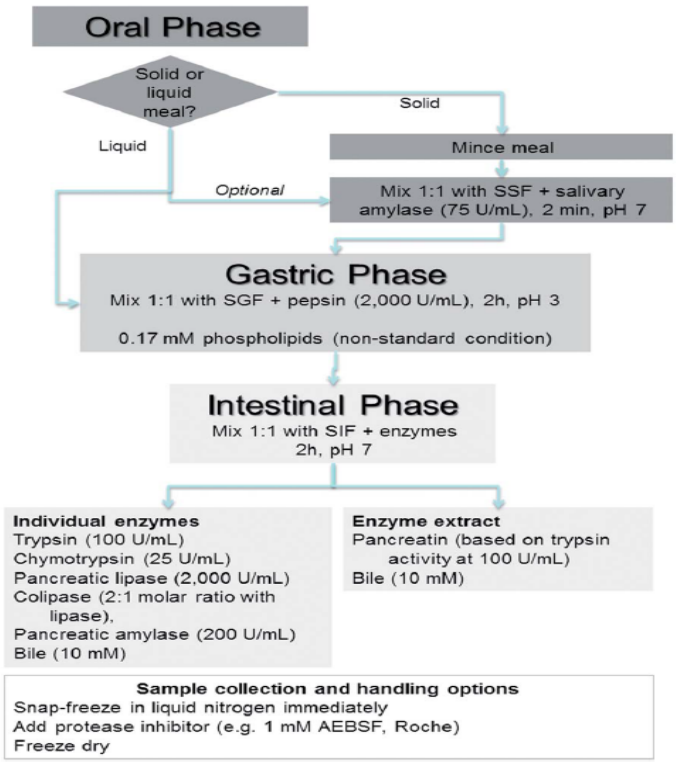

Figure 15: Flowchart of simulated *in vitro* digestion [221].

Briefly, 5 g of sample was dissolved in 3.5 mL of previously prepared simulated salivary fluid (SSF). The same procedure was followed for the blank sample, using 5 mL of water instead of the vitamin C sample. Then, 0.5 mL of fresh α-amylase solution (1500 U/mL) was added to both the samples. Finally, water was added to a final volume of 10 mL, and the samples were incubated for 2 min at 37 °C. The bolus obtained in the previous phase was mixed with 7.5 mL of simulated gastric fluid (SGF) and 1.6 mL (25,000 U/mL) of fresh pepsin, and the pH was adjusted to 2.00 ± 0.02 using 1 M HCl. The samples were brought up to 20 mL volumes and the mixture was incubated at 37 ◦C for 2 h in a shaking water bath. In two further samples, vitamin C and a blank were used to simulate only the duodenal digestion step. For this, 5 g of vitamin C sample or 5 mL of water was added to 20 mL of water to simulate the gastric chyme. Subsequently, 5 mL of fresh pancreatin (800 U/mL) was added to 2.5 mL of fresh pancreatin (160 mM) to reach a final volume of 32.5 mL. The samples were finally made up to a final volume of 40 mL, and the pH was adjusted to 7.00 ± 0.02 using 1 M NaOH, incubated at 37 ◦C for 2 h. At the end of the digestion process, the orogastric-duodenal digested

samples were freeze-dried and maintained at 4 ◦C prior to analysis under the experimental conditions described above. The dried samples were weighed (100 mg) and diluted in water to obtain a stock solution with a concentration of 1 mg/mL. Each sample was further diluted in water to obtain a final concentration of 1 µg/mL vitamin C. Calculations for the dilutions were carried out considering the vitamin C content reported in the technical specifications provided by the product datasheet. This preliminary analysis was conducted to verify the suitability of the analytical method for the analysis of digested samples. Subsequently, the tests were repeated on samples containing a vitamin C concentration equal to 5 µg / mL. All samples were analysed using the HILIC-UHPLC-MS method described above.

2.1.7 Parallel Artificial Membrane Permeation Assay (PAMPA).

2.1.7.1 Preparation of PAMPA plates.

Before preparing the plates, the samples were dissolved in 5% DMSO and PBS at pH 6.5 to preparation of solutions with a known content of vitamin C. Lecithin in dodecane solution (1% w/v) (~500 µL/plate) was prepared, and the mixture was sonicated to ensure complete dissolution. An aliquot of a 5 µL lecithin/dodecane mixture was carefully pipetted into each PVDF donor plate. Next, 300 µL of 5% DMSO and PBS at pH 7.4 was added to each acceptor plate and 150 µL of vitamin C samples-containing donor solutions. Donor and acceptor plates were assembled and incubated at room temperature for 16 h. At the end of the incubation period, 100 µL of solution was collected from the donor wells, 250 µL was collected from the acceptor wells, and stored at -20°C until analysis. Each test used a positive control with high permeability (caffeine) and a negative control with low permeability (furosemide) according to the Biopharmaceutical Classification System (BCS). Both compounds were solubilized in 5% DMSO, PBS (pH 6.5), and treated under the same conditions as the vitamin C samples used during the assay. Solutions of caffeine (200 µM) and furosemide (500 µM) were prepared. At the end of the assay, the permeability of lucifer yellow (LY) and brilliant cresyl blue (BCB) was measured to evaluate the integrity of the artificial membrane. A stock solution of 0.1 % (w/v) BCB was prepared, and 10 mL of this solution was placed in a beaker with 10 mg of LY to prepare the lucifer yellow (LY) stock solution. The final brilliant cresyl blue/lucifer yellow test solution was prepared by mixing the stock solutions in a 9:1 ratio and nine parts of BCB to one part of LY. Upon completion of the PAMPA assay, the acceptor plate was rinsed out, any remaining liquid in the donor wells was removed, 150 µL of BCB/LY test solution was added to the donor wells, and 300 µL of 5% DMSO and PBS at pH 7.4 were putted to the acceptor wells. The donor/acceptor plates were then assembled and incubated for 3 h. At the end of the incubation period, lucifer yellow and cresyl blue permeability was evaluated through a visual analysis of the passage of cresyl blue and the

absence of lucifer yellow in the acceptor compartment. For each sample, the effective permeability coefficient (Pe) was calculated using the following equation:

$$\log P_e = \log \{C \bullet -1n(1 - \frac{[drug]_{acceptor}}{[drug]_{equilibrium}})\} \text{ where } C = (\frac{V_D \bullet V_A}{(V_D + V_A)\ Area \bullet time})$$

Eq.1: $LogP_e$ calculation equation.

To evaluate membrane integrity, calibration curves for caffeine and furosemide were prepared as shown in Graphic 1 and 2 at concentrations of 0-200 µM and 0-600 µM for caffeine and furosemide, respectively. Spectrophotometric analysis was performed using a multiplate reader (Perkin Elmer, Waltham, Massachusetts, USA) at 273 nm for caffeine and 330 nm for furosemide in a 96-well quartz plate (Hellma Analytics). Table 5 and 6 shows the standard concentrations (µM), absorbance, and average measurements with blank correction.

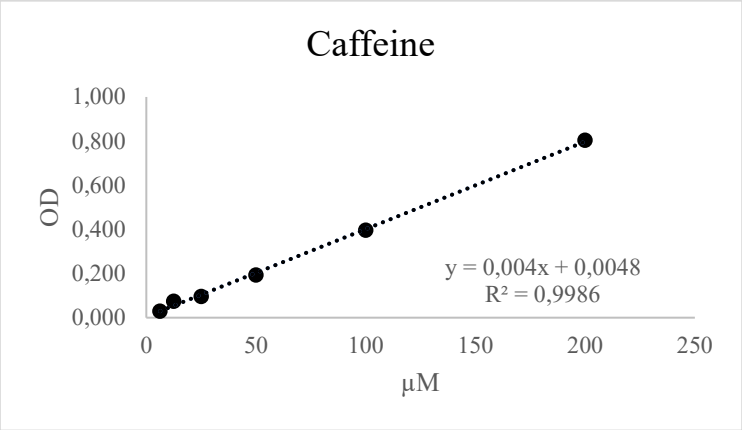

Graphic 1: Calibration curve Caffeine

Concentration [µM]	OD 1	OD 2	OD 3	Average	Average blank corrected
200	0,852	0,882	0,885	0,873	0,803
100	0,468	0,463	0,466	0,466	0,396
50	0,29	0,239	0,259	0,263	0,193
25	0,183	0,156	0,158	0,166	0,096
12,5	0,118	0,121	0,193	0,144	0,074
6,3	0,102	0,102	0,093	0,099	0,029
Blank	0,08	0,06	0,07	0,070	0,000

Table 5: Samples standard concentrations of caffeine (µM), absorbance, and average measurements with blank correction.

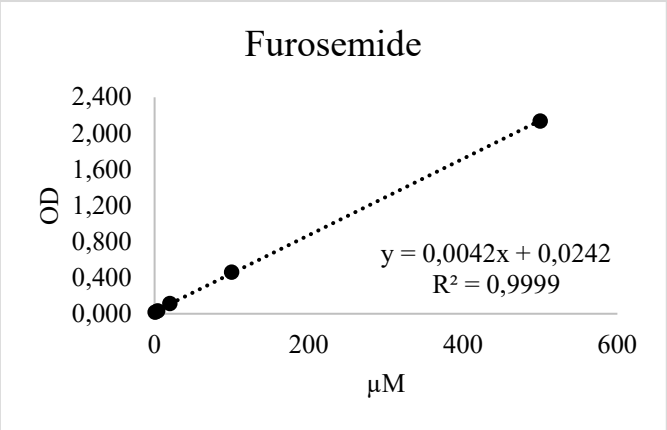

Graphic 2: Calibration curve Furosemide.

Concentration [µM]	OD 1	OD 2	OD 3	Average	Average blank corrected
500	1,93	1,85	1,93	1,903	1,837
100	0,61	0,589	0,572	0,590	0,524
20	0,213	0,19	0,213	0,205	0,139
4	0,121	0,123	0,124	0,123	0,056
0,8	0,101	0,1	0,093	0,098	0,031
Bianco	0,09	0,05	0,06	0,067	0,000

Table 6: Samples standard concentrations of furosemide (µM), absorbance, and average measurements with blank correction.

2.1.8 Transwell® assay.

2.1.8.1 Caco-2 cell line (ATCC® HTB-37™).

The Caco-2 cell line (ATCC® HTB-37™) from *the American Type Culture Collection* was cultivated in DMEM media with 10% FBS, 100 U/mL penicillin, and 100 µg/mL streptomycin ($DMEM^+$). The cells were incubated at 37°C with 5% CO_2, and the complete media was replaced every 48 h.

2.1.8.2 Cell viability test

The digested samples (100 mg) were solubilized in DMEM complete medium to obtain a stock solution of 1 mg/mL. Caco-2 cells (p12) were seeded in 96-well plates at a density of 5×10^4 cells/well. After 72 h, the cells were 70% confluent and treated with the samples in a concentration range of 500 - 7,81 µg/mL. For each sample, seven different concentrations of 1 mg/mL stock solutions were prepared. Untreated cells were used as a positive control, representing 100% cell viability. After 24 h, the treatments were removed, and the cells were rinsed with PBS before adding MTT solution (0.5 mg/mL). After 3 h of incubation, the medium was removed, and the cells were lysed with DMSO. Cell viability was determined by measuring the absorbance at 570 nm using an Envision microplate reader (Perkin Elmer, Waltham, Massachusetts, United States).

2.1.8.3 Seeding and culturing in Transwell® system.

The cells (p14) were seeded at a density of 3×10^5 cells on 12-well Transwell polyester inserts (0.4 µm pore size, Corning Amsterdam, The Netherlands) and cultured in complete DMEM for 21 days (Ref Nature). The medium was changed every two days. On day 21, transepithelial electrical resistance (TEER) was measured using an EVOM2 EndOhm (World Precision Instruments, Sarasota, FL, USA) apparatus to confirm the formation of the cell monolayer.

2.1.9 Permeability assay.

Before the experiment, each sample was solubilized in Hank's balanced salt solution (HBSS) at non-cytotoxic concentrations, as follows: sample 1, 31,25 µg/mL; sample 3, 15,62 µg/mL. The complete medium was removed from the donor and acceptor compartments and washed twice with pre-warmed PBS 1X. Sample solutions (0.5 mL) were added to the donor compartment while 1.2 mL of HBSS was added to the acceptor compartment. Transwell® plates were incubated at 37 °C and 5% CO2 with constant agitation (Corning® LSE™ Digital Microplate Shaker). At different time points (1h; 3h; 6h; 24h) aliquots (600 µL) were collected from the acceptor compartment and replaced with the same volume of HBSS. All liquids from the apical and basolateral chambers were collected at the last time point. All samples were stored at −20 °C before analysis. Before HILIC-HPLC-MS analysis, all samples were filtrated using a 0.22 µm membrane (MiniSart® Syringe Filter, Sartorius, Milano, Italy). In particular, the Cf samples were diluted to obtain a concentration of 5 µg/mL, which was within the linearity range of the calibration curve.

2.1.10 Cell uptake assay

Caco-2 cells were seeded in 12-well plates at a density of 3×10^4 cells/well and incubated at 37 °C and 5% CO_2. After 72h, the exhausted medium was removed and cells were treated with vitamin C samples for 24h. Subsequently, the cells were split using 0.25% trypsin-EDTA solution and transferred to a 2 mL microtube. The cells were centrifuged at 1200 rpm for 5 min to separate the cells from the culture medium. Cell pellets were resuspended in 200 µL of DPBS and centrifuged at maximum speed (14000 rpm for 10 min) to break the cells and allow the release of vitamin C. Supernatants were filtered and transferred to 2 mL microtubes and frozen at -80 °C until HILIC-UHPLC-MS analysis.

2.2 Results and discussion.

2.2.1 HILIC-HPLC-MS analysis and vitamin C samples quantification.

Figure 16 shows an example of the chromatogram and mass spectrum obtained from the analysis of the standard vitamin C using the analytical method developed, the operating conditions of which are reported in paragraph above.

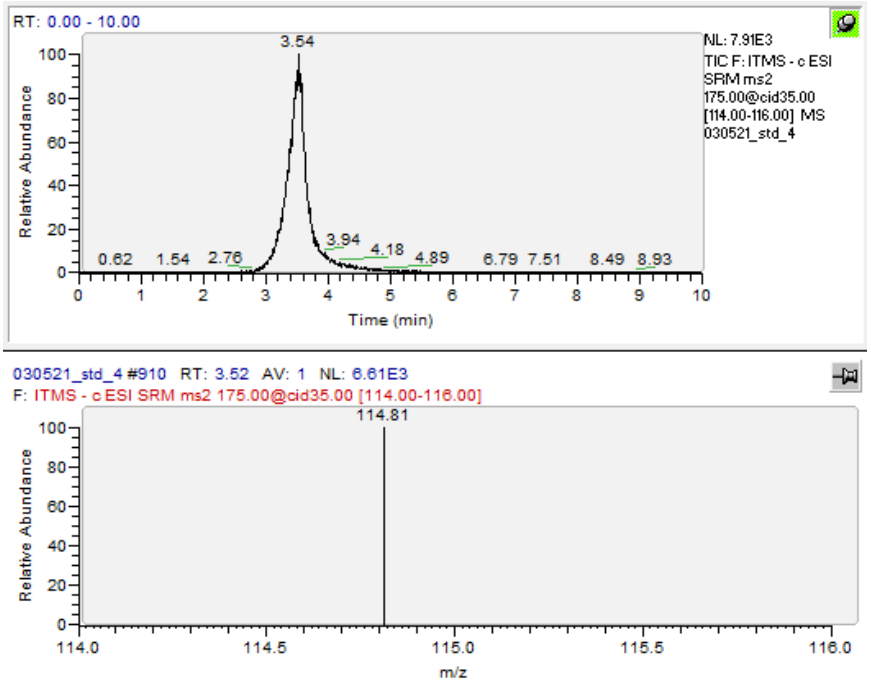

Figure 16: Chromatogram (TIC) and mass spectrum of standard vitamin C, mass spectrum of standard vitamin C, fragment ion with *m/z* 115.

Vitamin C samples were diluted to a theoretical concentration of 1 µg/mL. In fact, the results obtained by HILIC-UHPLC-MS analysis showed a vitamin C content between 0. 997 e 0.837 µg/mL, respectively, which were in line with the expected concentrations as reported in table 7.

ID samples	Peak area						Concentration µg/mL		
	Replicate			Replicate			Average	SD	RSD
	1	2	3	1	2	3			
VitC1	496234	503295	482364	0,955	0,965	0,936	0,953	0,015	0,015
VitC2	400623	438421	412579	0,824	0,876	0,840	0,847	0,027	0,031
VitC3	483086	535479	560092	0,937	1,009	1,043	0,997	0,054	0,054
VitC4	390778	403743	434633	0,810	0,828	0,871	0,837	0,031	0,037

Table 7: ID of samples, peak area fragment ion with m/z 115, concentration (µg/mL), average concentration, standard deviation (SD), relative standard deviation (RSD).

2.2.2 RP-HPLC-MS analysis and vitamin D samples quantification.

Figure 17 shows an example of chromatogram and mass spectrum obtained from the analysis of the standard vitamin D using the analytical method developed, the operating conditions of which are reported in paragraph x.Vitamin D samples at theoretical concentrations of 2 µg/mL were analysed through RP-UHPLC-MS, which revealed a vitamin D content in samples between 2,153 e 2,345 µg/mL (Table 7).

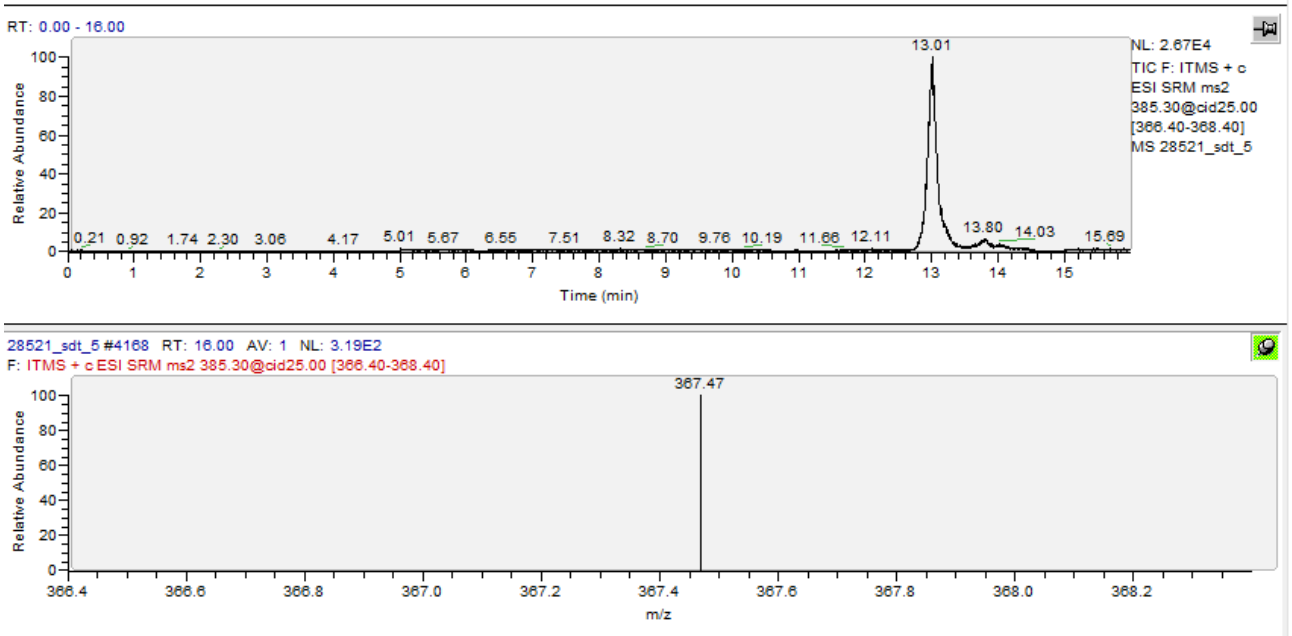

Figure 17: Chromatogram of standard vitamin D (cholecalciferol), mass spectrum fragment ion with *m/z* 367.4.

ID sample	Peak area Replicate			Concentration (µg/mL) Replicate			Average	SD	RSD
	1	2	3	1	2	3			
VitD1	383749	321358	373484	2,390	1,988	2,324	2,234	0,216	0,097
VitD2	367545	348338	335688	2,455	2,331	2,250	2,345	0,084	0,036
VitD3	321778	332327	331732	2,160	2,228	2,224	2,204	0,031	0,014
VitD4	341572	311950	387731	2,118	1,927	2,416	2,153	0,246	0,114

Table 8: ID of samples, peak area fragment ion with m/z 367, concentration (µg/mL), average concentration, standard deviation (SD), relative standard deviation (RSD).

2.2.3 Influence of simulated in vitro orogastric and duodenal digestion processes on vitamin C samples.

Table 9 shows the peak area and concentration of the samples after orogastric digestion. The theoretical concentration of the samples was 5 µg/mL of vitamin C. The experimental results showed

a concentration of vitamin C in the samples between 2,669 and 5,747 µg/mL, revealing a high sensitivity to orogastro and duodedal digestion of vitamin C samples of synthetic origin.

Theorical content of vitamin C (5 µg/mL)	Concentration µg/mL					
	1 replicate	2 replicate	3 replicate	Average	SD	RSD
VitC1	5,730	5,690	5,820	5,747	0,066	0,012
VitC2	5,487	5,184	5,515	5,395	0,184	0,034
VitC3	4,578	4,435	4,367	4,460	0,108	0,024
VitC4	1,627	1,640	1,735	1,6673	0,048	0,028

Table 9: reported the results obtained from digested vitamin D samples analysis. Experimental data show an average content of vitamin D between 1.996 and 2.324 µg/mL.

2.2.4 Influence of simulated in vitro orogastric and duodenal digestion processes on vitamin D samples.

Table 10 reported the results obtained from digested vitamin C samples analisis. Experimental data show an average of vitamin D between 1.996 and 2.324 µg/mL.

Theorical content of vitamin D 2 µg/mL	Concentration µg/mL					
	1 replicate	2 replicate	3 replicate	Average	SD	RSD
VitD1	1,955	1,974	2,060	1,996	0,056	0,028
VitD2	2,409	2,209	2,331	2,316	0,101	0,044
VitD3	2,318	2,231	2,423	2,324	0,096	0,041
VitD4	2,278	2,228	-	2,253	0,035	0,016

Table 10: ID samples, peak area related to ion with *m/z* →367, concentration in µg/mL, average, standard deviation (SD), relative standard deviation (RSD).

2.2.5 Pampa assay vitamin C samples.

Table 10 shows the results of the pampa experiment, such as the absorbance and concentration obtained from the acceptor compartment. Each measurement was performed in triplicates. PBS was used as a blank sample.

	Acceptor	
Tested compound	Concentrazion (µM)	OD
Caffeine	200	0,485
Caffeine	200	0,478
Caffeine	200	0,450
Furosemide	500	0,105
Furosemide	500	0,102
Furosemide	500	0,155
PBS (273 nm)	-	0,229
PBS (273 nm)	-	0,146
PBS (273 nm)	-	0,146

PBS (330 nm)	-	0,097
PBS (330 nm)	-	0,105
PBS (330 nm)	-	0,101

Table 10: Absorbance registered from acceptor compartment samples.

Table 11 presents the absorbance values obtained from spectrophotometry analysis and the concentration of the samples (μM) collected from the donor compartment. Each measurement was performed in triplicate and PBS was used as a blank.

Donor		
Sostanza testata	Concentrazione (μM)	OD
Caffeina	200	0,895
Caffeina	200	0,842
Caffeina	200	0,823
Furosemide	500	1,7
Furosemide	500	1,764
Furosemide	500	1773
Bianco PBS (273 nm)	0,179	0,179
Bianco PBS (273 nm)	0,17	0,17
Bianco PBS (273 nm)	0,208	0,208
Bianco PBS (330 nm)	0,179	0,155
Bianco PBS (330 nm)	0,17	0,158
Bianco PBS (330 nm)	0,208	0,141

Table 12: Absorbance registered from donor compartment samples.

The data show that only caffeine crossed the artificial membrane in detectable quantities. Furosemide, as expected, did not pass through the phospholipid membrane, demonstrating the integrity and functionality of the membrane. Since only caffeine passed the membrane for this compound, it was possible to determine the partition coefficient Log P_e, which agrees with what was expected based on literature data (Table 13).

Compound	% Retention	P_{app} cm/s	Log P_e
Caffeine	9,09	7,77 E-07	-6,11
Furosemide	-	-	-

Table 13: Apparent permeability coefficient (P_{app}) and Log Pe of standard samples.

Table 14 shows the data obtained from the analysis of various solutions at a concentration of 100 µg/mL vitamin C samples. However, because no quantifiable signal was obtained (LOD = 0.150 µg/ml) in the acceptor solutions, it was not possible to calculate the Pe of vitamin C.

ID SAMPLES	Theorical equilibrium (µg/mL)	DONOR concentration (µg/mL)	ACCEPTOR concentration (µg/mL)
VitC1	35,12 ± 0,22	43,85 ± 1,03	-
VitC2	28,27 ± 0,09	28,61 ± 0,75	-
VitC3	35 ± 0,23	49,08 ± 3,05	-
VitC4	28,46 ± 0,01	30,24 ± 3,01	-

Table 14: ID of samples, theorical equilibrium concentration, donor concentration and acceptor of vitamin C samples at 100 µg/mL concentration.

At the end of the experiment with vitamin C samples, membrane integrity tests were performed using cresyl blue solution and luciferin. All the wells tested presented intact membranes, with the exception of well A2, which was excluded from the final data processing (Figures 18 and 19).

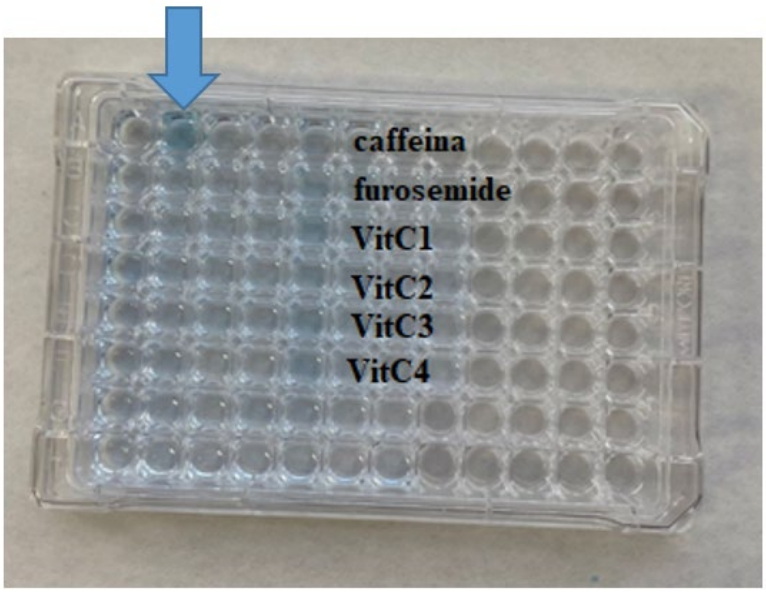

Figure 18: Integrity test. Membrane intact in all wells tested (A1 to F8) except well A2 (indicated by the blue arrow) where the more intense blue colour indicates a non-intact membrane.

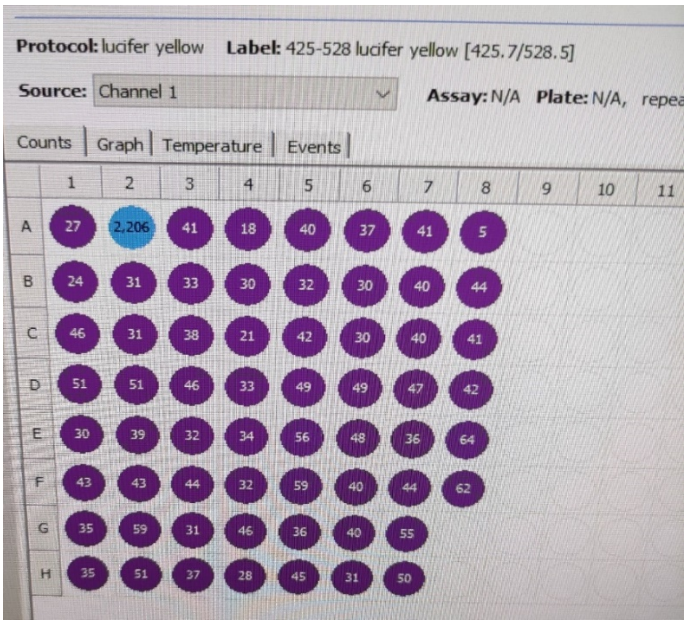

Figure 19: Yellow Lucifer assay. All wells have no luciferin in the acceptor compartment, except well A2 where the membrane is not intact.

As reported above, the passive transport of vitamin C is significant when it is taken in high doses so that the receptors responsible for active transport are saturated; because of the appropriate concentration gradient, passive diffusion is used by the body for absorption of the vitamin, and it was decided to retest the vitamin C samples 1 and 3 at the maximum usable concentration of 500 mg/mL. Figure 20 shows the chromatograms obtained from the analysis of the solutions of the acceptor compartments for samples 1 and 3.

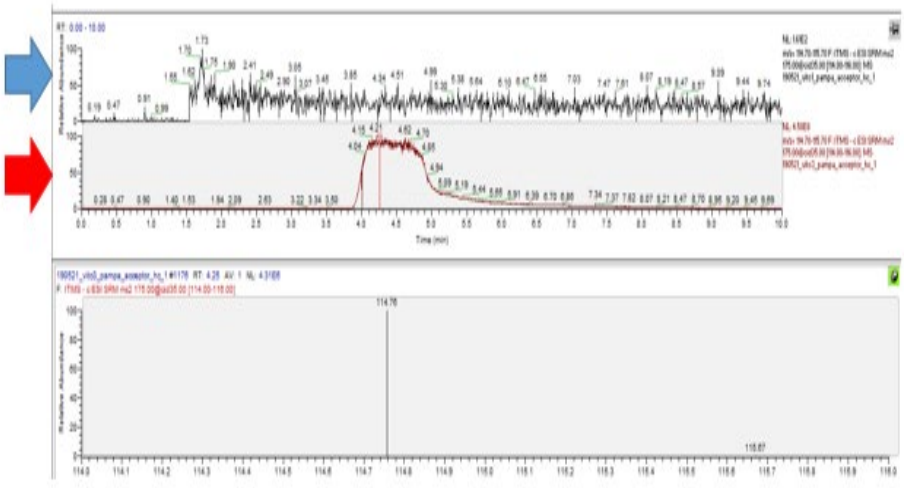

Figure 20: Chromatogram, recorded in SRM mode, of ion with *m/z* 175 → 115 of vitamin C acceptor samples. The blue arrow indicates sample 1 (natural), while the red arrow indicates sample 3 (synthetic).

The chromatogram of sample 1 (natural vitamin C; blue arrow) showed in figure 9, did not present the signal related to ion with *m/z* 175 → 115 that its identified the vitamin C, while sample 3 (synthetic vitamin C; red arrow) presented a signal of the ion with *m/z* 175 → 115. However, it cannot be quantified because of its high concentration, which exceeds the linearity range of the curve calibration. The presence of the signal relative to the synthetic vitamin C sample suggests that synthetic vitamin C passed the phospholipidic membrane, while in sample 1, the natural vitamin C did not pass through the phospholipidic membrane. These results were confirmed by physical examination of the plate. In the photos shown in figure 10, in the wells of the acceptor compartment relating to sample 3, a pale-yellow colour indicates that the passage of the compound has taken place, whereas in the wells of the acceptor compartment relating to sample 1, despite having two samples with a high concentration of vitamin C, there is no visible coloration.

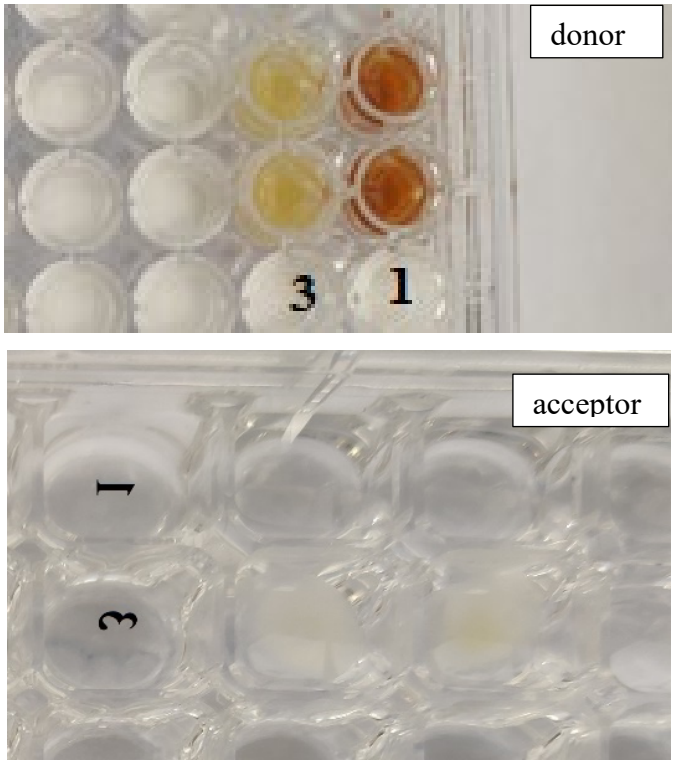

Figura 21: Donor e acceptor compartment of 1 and 3 samples tested at concentration of 500 mg/mL.

Table 15 shows the results obtained for various solutions at a concentration of 500 mg/mL.

ID SAMPLE	Equilibrium theorical (mg/mL)	DONOR concentration (mg/mL)	ACCEPTOR concentration (mg/mL)
1	122,23 ± 1,75	548 ± 2,69	-
3	120,57 ± 1,69	258 ± 1,96	High concentration

Table 15: Identification sample number, concentration of sample at equilibrium theoretical, donor, and acceptor concentrations of 500 mg/mL vitamin C samples.

Also in this case, at the end of the test, the control tests were carried out for the integrity of the cresyl blue and luciferin membrane. The cresyl blue test revealed that there was no passage of the dye into the acceptor compartment, which was due to the saturation of the membrane by the sample tested at high concentrations. Although the luciferin test showed that there was no passage of luciferin into the acceptor compartment, the artificial membrane remained intact until the end of the experiment (Figure 22).

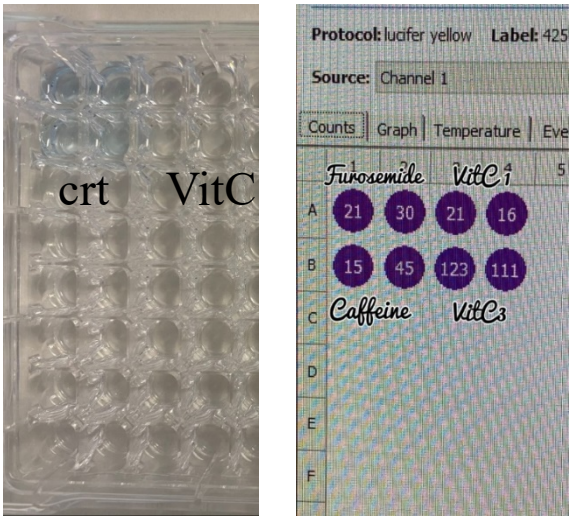

Figura 22: A) Cresyl blue assay. B) Lucifer yellow assay. Control, wells: A1, A2, B1, B2. Sample 1, wells A3 e A4; sample 3, wells B3 e B4.

The obtained results suggest that vitamin C samples at low concentrations cannot cross the membrane owing to the hydrophilic chemistry of vitamin C. Nevertheless, when samples with a high concentration (500 mg/mL) were used, synthetic vitamin C crossed the phospholipid membrane as opposed to natural vitamin C samples. In fact, under the experimental conditions applied in the PAMPA assay, the phytocomplex present in sample 1, which represents approximately 30% by weight of the sample, hinders the passage of vitamin C by creating an environment that is not favourable for the passive diffusion of vitamin C. The high viscosity of sample 1 at the tested concentration acts as an obstacle to the passive diffusion of vitamins through the phospholipid membrane. Other analyses were also performed to confirm the results.

In particular, the digested samples of natural vitamin C (sample 1) and synthetic vitamin C (sample 3) were tested at the following concentrations: 100, 50, 10, 1 mg/mL. As above, caffeine and furosemide were used as standard to check the membrane assessment.

Figure 23 shows the caffeine calibration curve and table x reported the standard concentrations, the value of absorbance recorded at 273 nm, average, blank corrected value and standard deviations (Figura23).

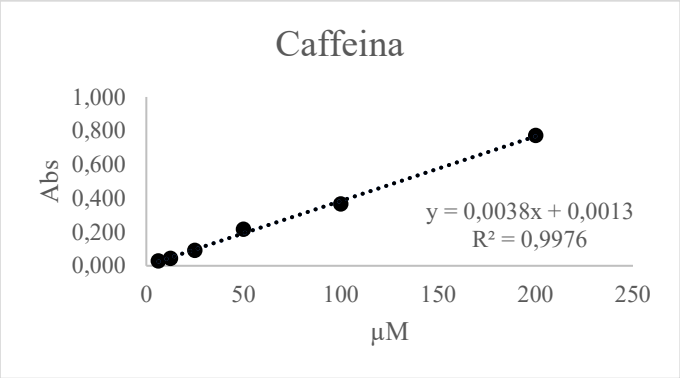

Figure 23: Calibration curve caffeine.

Caffeine concentration [µM]	OD 1	OD 2	OD 3	Average	Blank corrected average
200	0,843	0,821	0,872	0,845	0,772
100	0,438	0,433	0,445	0,439	0,365
50	0,31	0,294	0,263	0,289	0,216
25	0,168	0,161	0,163	0,164	0,091
12,5	0,112	0,118	0,121	0,117	0,044
6,26	0,1	0,102	0,103	0,102	0,028
Bianco	0,08	0,07	0,07	0,073	0,000

Table 16: Caffeine concentration, OD, average OD and Blank corrected average.

Figure 24 shows the furosemide calibration curve and table x reported the standard concentrations, the value of absorbance recorded at 330 nm, average, blank corrected value and standard deviations.

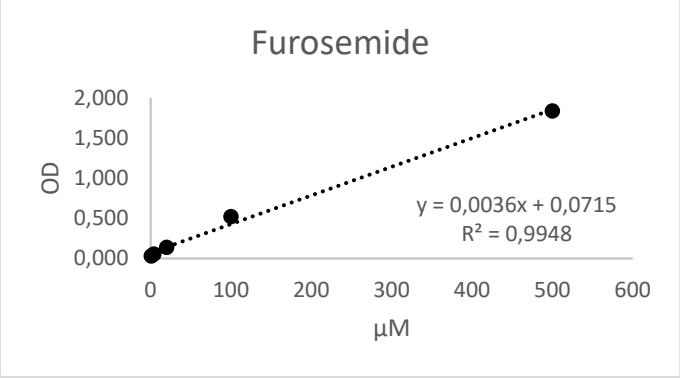

Figura 24: Calibration curve furosemide

Concentration [μM]	OD 1	OD 2	OD 3	Average	Blank corrected average
500	1,93	1,85	1,93	1,903	1,837
100	0,61	0,589	0,572	0,590	0,524
20	0,213	0,19	0,213	0,205	0,139
4	0,121	0,123	0,124	0,123	0,056
0,8	0,101	0,1	0,093	0,098	0,031
Blank	0,09	0,05	0,06	0,067	0,000

Tabella 17: Furosemide standard concentrations of standard, OD, average and blank corrected average.

Table 18 show the results obtained from analysis of acceptor compartments. Each measurement was performed in triplicate and PBS was used as blank.

Acceptor		
Compoud	Concentration (μM)	OD
Caffeine	200	0,435
Caffeine	200	0,389
Caffeine	200	0,386
Furosemide	500	0,104
Furosemide	500	0,102
Furosemide	500	0,121
PBS (273 nm)	-	0,224
PBS (273 nm)	-	0,121
PBS (273 nm)	-	0,112
PBS (330 nm)	-	0,123
PBS (330 nm)	-	0,106
PBS (330 nm)	-	0,103

Tabella 18: Absorbance registered from acceptor compartment samples.

In table 19 was reported the results obtained to different samples of vitamin C with related absorbance and concentrations (μM) for donor receptor. Each measurement was performed in triplicate and PBS was used as blank.

Donor		
Compound	Concentrazione (μM)	OD
Caffeine	200	0,879
Caffeine	200	0,832
Caffeine	200	0,842
Furosemide	500	1,64
Furosemide	500	1,71
Furosemide	500	1,67
PBS (273 nm)	0,179	0,178
PBS (273 nm)	0,17	0,183
PBS (273 nm)	0,208	0,198
Bianco PBS (330 nm)	0,179	0,129
Bianco PBS (330 nm)	0,17	0,137

Bianco PBS (330 nm)	0,208	0,143

Tabella 19: Absorbance registered from donor compartment samples.

The data reported in table 19 demonstrate that only caffeine was able to cross the artificial membrane in detectable quantities and, therefore, only for this compound was it possible to determine its apparent diffusion rate with relative Log Pe, which resulted in line with the expected data.

Compound	% Retention	P_{app} cm/s	Log P_e
Caffeina	10,03	1,779E-06	-6,11
Furosemide	-	-	-

Table 19: Apparent permeability coefficient, percentage of retention and Log P_e

Vitamin C samples were collected from acceptor compartment and analysed by HILIC-UHPLC-MS. The chromatograms reported in figure 25-28 showed the results related to acceptor compartment tested to concentration of 100 mg/ml, 50 mg/mL, 10 mg/mL e 1 mg/mL. The data show that the acceptor solutions do not show any signal corresponding to the vitamin C peak and therefore, since no quantifiable signal was obtained in the acceptor solutions, it was not possible to calculate the vitamin C P_e.

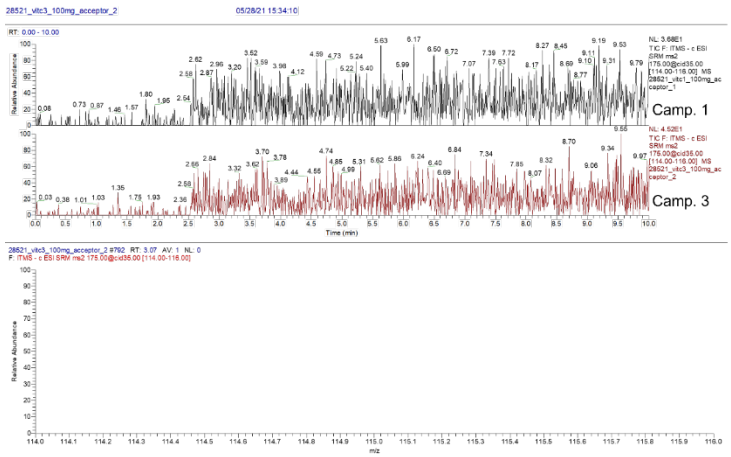

Figure 25: Chromatogram, recorded in SRM mode, of ion with *m/z* 175 → 115 of vitamin C acceptor samples 1 and 3 at concentration of 100 mg/mL.

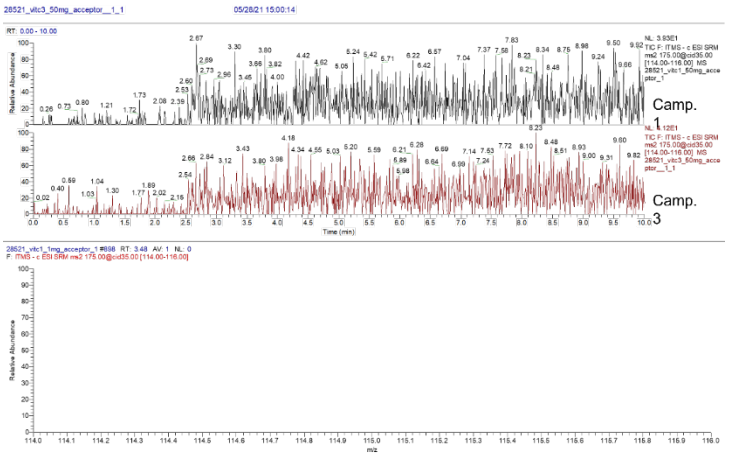

Figura 26: Chromatogram, recorded in SRM mode, of ion with *m/z* 175 → 115 of vitamin C acceptor samples 1 and 3 at concentration of 50 mg/mL.

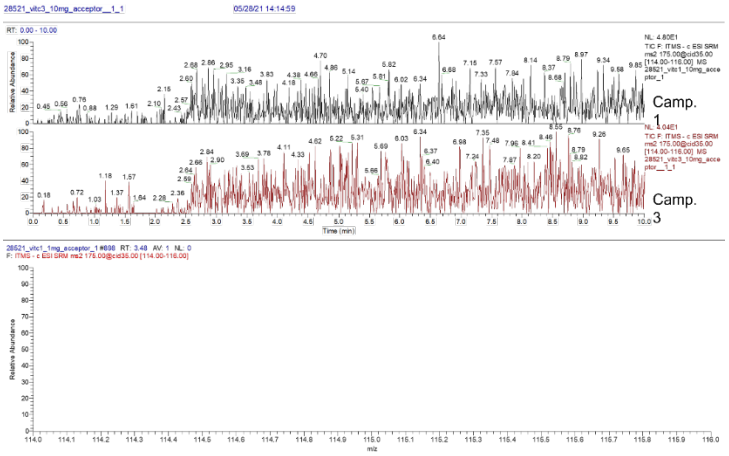

Figura 27: Chromatogram, recorded in SRM mode, of ion with *m/z* 175 → 115 of vitamin C acceptor samples 1 and 3 at concentration of 10 mg/mL.

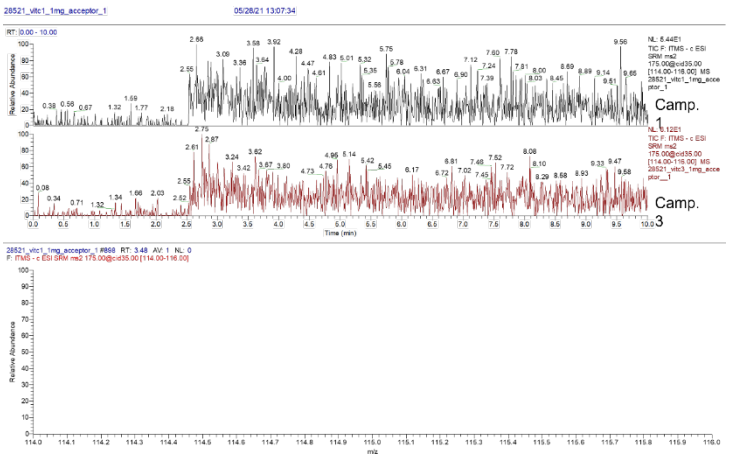

Figure 28: Chromatogram, recorded in SRM mode, of ion with *m/z* 175 → 115 of vitamin C acceptor samples 1 and 3 at concentration of 1 mg/mL.

At the end of the experiment with vitamin C samples, membrane integrity tests were performed using cresyl blue solution and luciferin. All the wells tested presented intact membranes, except for well with x, which were excluded from the final data processing (Figure 29 and 30).

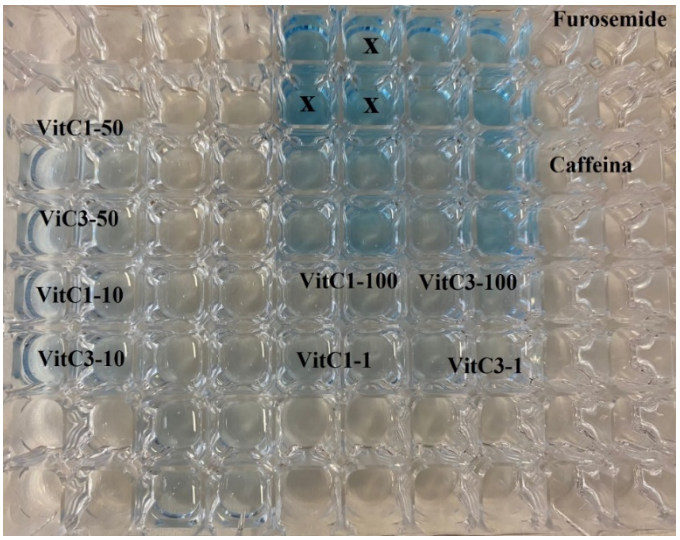

Figure 29: Integrity test. Membrane intact in all wells tested except for wells marked with the symbol X where the more intense blue color indicates a non-intact membrane. Caffein, well from C5 to C8, Furosemide wells from A5 to A8, VitC1-100 = Sample 1, concentration 100 mg/mL. VitC3-100 = Sample 3, concentration 100 mg/mL. VitC1-50 = Sample 1, concentration 50 mg/mL. VitC3-50 = Sample 3, concentratione 50 mg/mL. VitC1-10 = Sample 1, concentratione 10 mg/mL. VitC3-10 = Sample 3, Concentrazione 10 mg/mL VitC1-1 = Sample 1, concentrazione 1 mg/mL. VitC3-1 = Sample 3, Concentratione 1 mg/mL.

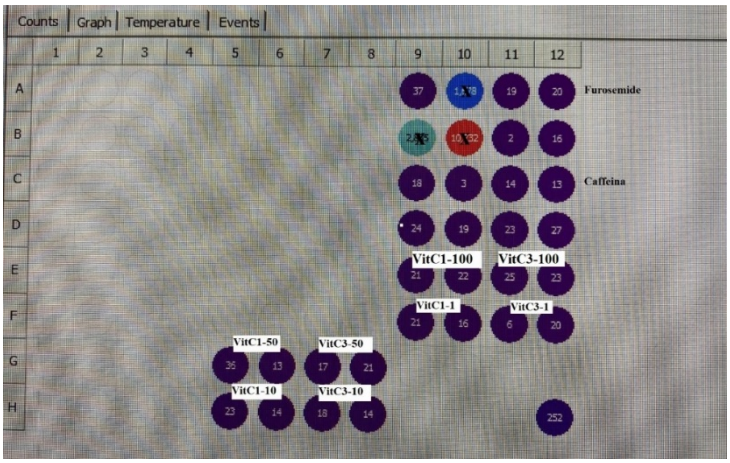

Figure 30: YL test: Membrane intact in all wells tested except for wells marked with the symbol X where the high value of fluorescent means a non-intact membrane. Caffeine, wells from C5 to C8, Furosemide wells from A5 to A8, VitC1-100 = Sample1, concentration 100 mg/mL. VitC3-100 = Sample 3, concentration 100 mg/mL. VitC1-50 = Sample 1, concentration 50 mg/mL. VitC3-50 =

Sample 3, concentration 50 mg/mL. VitC1-10 = Sample1, concentration 10 mg/mL. VitC3-10 = Sample 3, Concentration 10 mg/mL VitC1-1 = Sample 1, concentration 1 mg/mL. VitC3-1 = Sample 3, Concentration 1 mg/mL.

The results obtained from this further set of experiments conducted at different concentrations of vitamin C both of natural origin (sample 1) and of synthetic origin (sample 3) lead to the exclusion of hypothesis 2, which hypothesized a technical problem due to the high viscosity of the natural vitamin C solution caused by the phytocomplex and confirm hypothesis 1 on the basis of which only highly concentrated (500 mg/ml) synthetic vitamin C crosses the phospholipid membrane, while for natural vitamin C the phytocomplex creates an environment that is not favourable to the passive diffusion of the vitamin, preventing it from passing through the phospholipidic membrane.

2.2.6 PAMPA assay vitamin D samples.

Table 20 e 21 show the results obtained to vitamin D samples 1 and 3 in different tested concentration. For both of samples, no quantifiable concentrations were detected in the acceptor compartment as reported in the chromatograms showed in figure 31.

	Sample 1			
Concentration (µg/mL)	Theorical equilibrium concentration (µg/mL)	Concentration *donor* (µg/mL)	Concentration *acceptor* (µg/mL)	Filter retention (%)
250	102,40 ± 2,11	261,80 ± 59,25	-	0
62,5	40,70 ± 1, 30	73,02 ± 2,17	-	0
25	12,54 ± 5,07	21,710 ± 0,50	-	0,86
2,5	-	-	-	-

Table 20: Concentration of sample 1, concentration of theorical equilibrium, donor concentration and acceptor concentration.

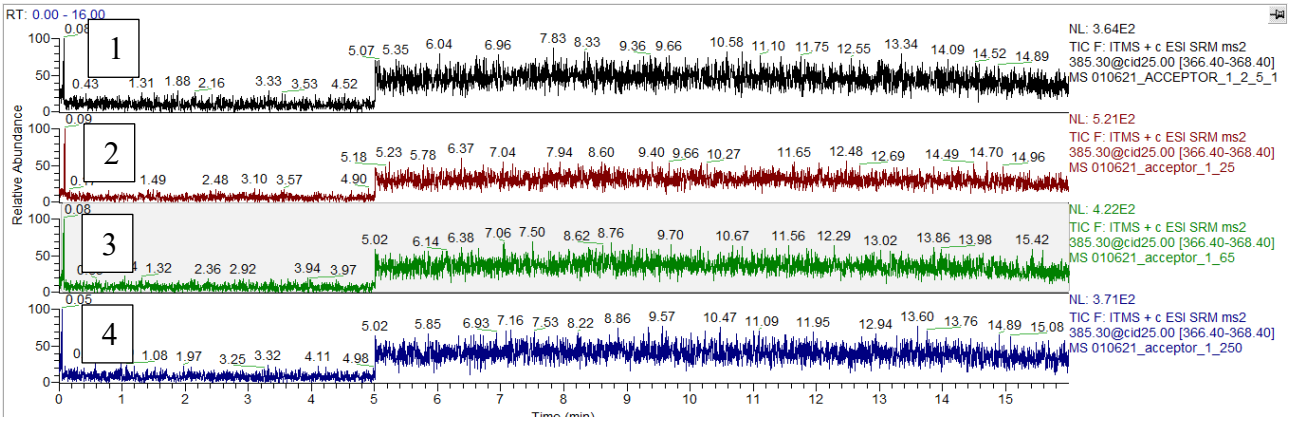

Figure 31: Chromatograms of ion with *m/z* 385,3 → 367,4 obtained from analysis of acceptor compartment sample 1. Tested concentrations:1) 2,5 µg/mL, 2) 5 µg/mL, 3) 62,5 µg/mL, 4) 250 µg/mL.

Sample 3				
Concentration (µg/mL)	Theorical equilibrium concentration (µg/mL)	Concentration *donor* (µg/mL)	Concentration *acceptor* (µg/mL)	Filter ritention (%)
250	163,90 ± 4,14	209,62 ± 12,93	-	16,15
62,5	23,54 ±1,40	48,90 ± 1,4	-	21,75
25	14,54 ± 5,66	24,65 ± 0,11	-	0,98
2,5	-	-	-	-

Tabella 21: Concentration of sample 3, concentration of theorical equilibrium, donor concentration and acceptor concentration.

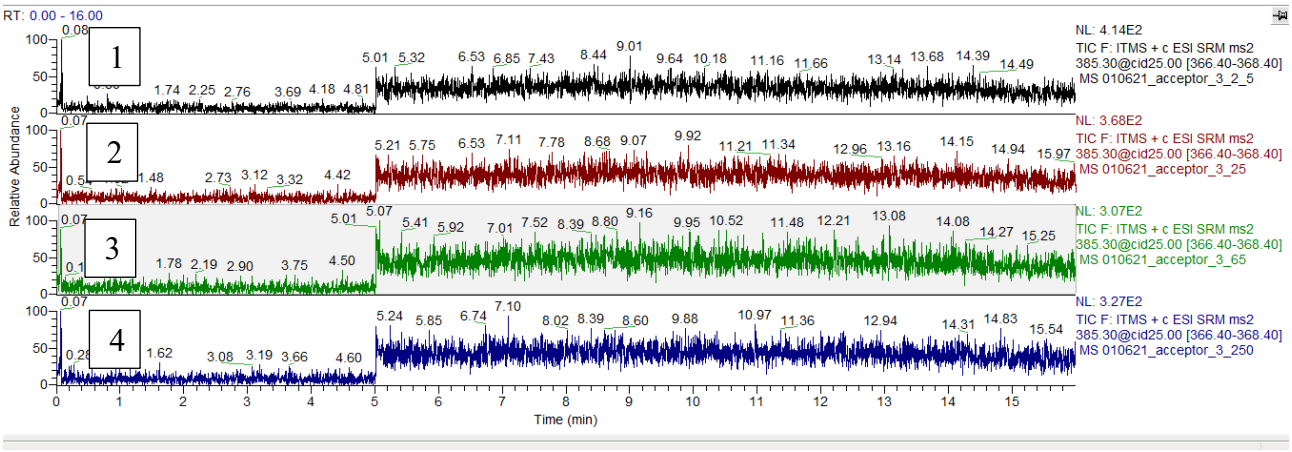

Figura 32: Chromatograms of ion with *m/z* 385,3 → 367,4 obtained from analysis of acceptor compartment sample 3. Tested concentrations: 1) 2.5 µg/mL, 2) 5 µg/mL, 3) 62.5 µg/mL, 4) 250 µg/mL.

Table 22 shows the results obtained from analysis of sample 2 at different concentrations of vitamin D. Sample 2 at concentration 2.5 µg/mL show in the acceptor compartment a concentrations of vitamin D equal to 0.069 µg/mL. Figure 33 show the chromatograms of ion with m/z 385.3 3 →67.4 obtained from the analysis of the acceptor compartments of sample 2 tested at different concentrations.

Sample 2				
Concentration (µg/mL)	Theorical equilibrium sample (µg/mL)	Concentration *donor* (µg/mL)	Concentration *acceptor* (µg/mL)	Filter retention (%)
25	8,11 ± 0,31	3,12 ± 0,69	-	87,52
12,5	3,02 ± 0,50	1,21 ± 0,10	-	75,84
5	4,71 ± 0,97	4,72 ± 0,49	-	6
2,5	1,91 ± 0,24	0,060 ± 0,006	0,060	18,52

Table 22: Concentration of sample 3, concentration at theorical equilibrium, donor concentration and acceptor concentration.

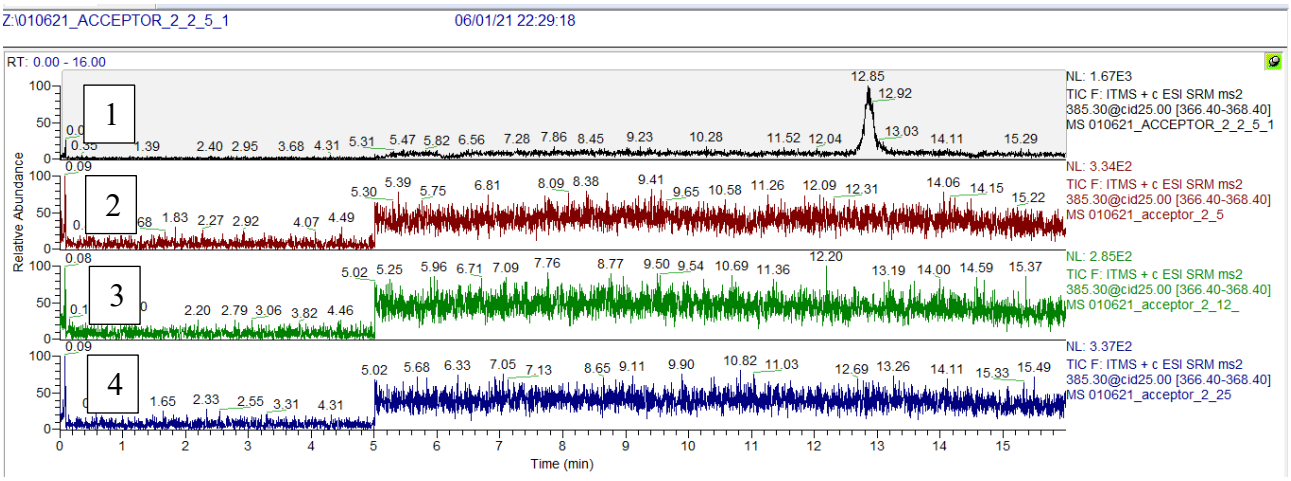

Figure 33: Chromatograms of ion with *m/z* 385.3 → 367.4 obtained from analysis of acceptor compartement sample 2: Tested concentrations: 2.5 µg/mL, 2) 5 µg/mL, 3) 12.5 µg/mL, 4) 25 µg/mL.

Sample 2 at concentration of 2.5 µg/mL present a permeability coefficient (Log P_e) equal to – 6.17 as reported in table 23.

Sample	**P_{app} (cm/s)**	**Log P_e**	**Acceptor compartemet Vitamin D (%)**
2	6.75E-07	-6.17	15%

Table 23: Concentration sample 3, concentration theorical equilibrium concentration, donor concentration e acceptor concentratione.

Table 24 show the results obtained to analysis of sample 4 at different concentrations of vitamin D. Also in this case, no sample shows in the acceptor compartment a detectable amount of vitamin D as shown by the chromatograms in figure 34.

Sample 4				
Concentration (µg/mL)	Theorical equilibrium concentration (µg/mL)	Concentration *donor* (µg/mL)	Concentration *acceptor* (µg/mL)	Filter retention (%)
25	8,28 ± 0,19	0,99 ± 0,29	-	60,04
12,5	5,05 ± 0,37	0,79 ± 0,03	-	60,24
5	1,53 ± 0,32	0,58 ± 0,51	-	76,80
2,5	0,74 ± 0,10	0,47 ± 0,32	-	18,52

Tabella 24: Concentration sample 4, concentration theorical equilibrium concentration, donor concentration e acceptor concentratione.

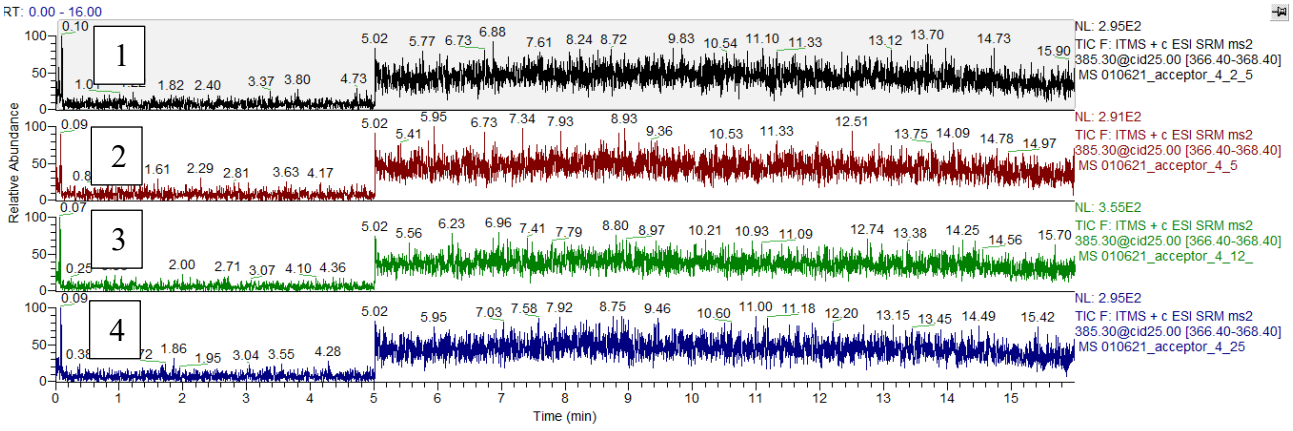

Figure 34: Chromatograms of ion with *m/z* 385.3 → 367.4 obtained from analysis of acceptor compartement sample 4: Tested concentrations: 2.5 µg/mL, 2) 5 µg/mL, 3) 12.5 µg/mL, 4) 25 µg/mL.

At the end of the experiment with vitamin D samples, membrane integrity tests were performed using cresyl blue solution and luciferin. All the wells tested presented intact membranes, except for well D4 (red arrow), which were excluded from the final data processing (Figures 35 e 36).

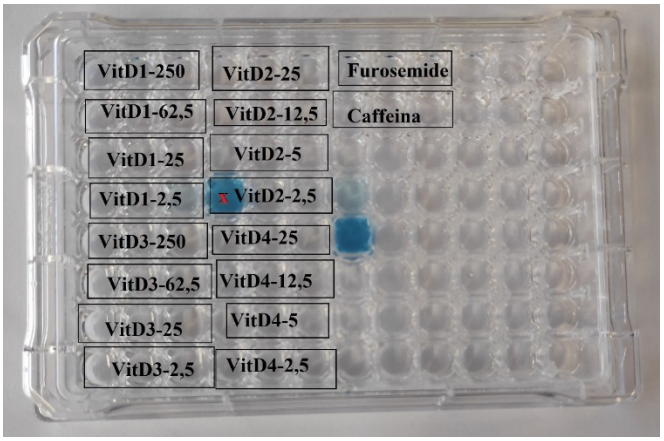

Figure 35: Integrity test: intact in all wells tested except for well D4 marked with the symbol X where the more intense blue color indicates a non-intact membrane.

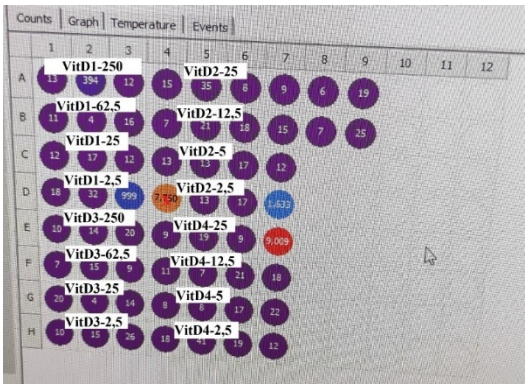

Figure 36: YL test. All wells present intact membrane except for well D4 marked with the symbol X where the high value of fluorescent means a non-intact membrane.

2.2.7 MTT test.

Digested samples of vitamin C (100 mg) were solubilized in DMEM$^+$ to obtain a stock solution of 1 mg/mL. Vitamin D samples 1 and 3 were diluted as described: an aliquot of 11 µL was diluted in 900 µL of DMSO to obtained a stock solution at concentration of 250 µg/mL of vitamin D. This stock solution were diluted in DMEM$^+$ to obtained a six different concentrations in the range between 2,5 – 0,078 µg/mL. 1 mL of sample 2 (25 µg of vitamin D) was diluted in 9 mL of DMEM$^+$ to obtain a stock solution at concentration of 2,5 µg/mL. Six concentrations were tested in a range between 2,5 – 0,078 µg/mL. Sample 3 with a content of vitamin D equal to 125 µg was diluted in DMEM$^+$ to obtain a solution at vitamin D concentration of 12,5 µg/mL. This stock solution was diluted in a ratio 1:5 od DMEM$^+$ to obtain six solutions at range of concentrations between 2,5 – 0,078 µg/mL. Digested vitamin D samples were solubilized as reported. Dried sample 1 and 3 were solubilized in 1 mL of DMSP while in sample 2 and 4 were solubilized in 5 mL of DMSO. Sample 1 and 3 present a content of 4.55 g of oil (1 mL = 0.910g), each 10 mg of oil has a content of vitamin D equal to 250 µg. The theorical concentration of vitamin D in 5 mL was 113,75 mg. Sample 1 after *in vitro* digestion and lyophilisation was solubilized in 1 mL of DMSO. 10 µL of digested sample was take and diluted it in 990 µL of DMEM$^+$ to obtain a solution with a theoretical concentration of vitamin D equal to 1.137 mg/mL (1137 µg/mL) of vitamin D. A further dilution was carried out by taking 2.20 µL from the previous solution and adding it to 998.8 µL of medium to obtain a final solution equal to 2.5 µg/mL of vitamin D. From this solution six concentrations were prepared in the range 2.5 – 0.078 µg/mL. Sample 2 present 5 mg of oil and 125 µg of vitamin D in 5 mL of solution. Digested sample 2 was suspended in 5 mL of DMSO to obtain a vitamin D concentration of 25 µg/mL. this solution was diluted taking 10 µL from the stock solution in 990 µL of DMEM$^+$ to obtain a solution with a theorical vitamin D concentration of 2,5 µg/mL. From this solution, sic concentrations were prepared in a range of concentrations between 2,5 – 0,078 µg/mL. Sample 4 present a content of oil equal to

25 mg and 625 µg of vitamin D in 5 mL of solution. Digested sample was diluted in DMSO (5 mL) to obtain a 125 µg/mL vitamin D solution. 20 µL of this solution was diluted in 984 µL of $DMEM^+$ to obtain a 2.5 µg/mL. From this solution, sic concentrations were prepared in a range of concentrations between 2,5 – 0,078 µg/mL. All of samples were filtered using a 0.22 µm membrane. Caco-2 cells (p12) were seeded in a 96-well plate at density of 5 x 10^4 cells/well. After 72 h, cells were 70% confluent and it were treated with the samples in a range of concentration of 500 – 7.81 µg/mL. For each sample was prepared 7 different concentrations as of 1 mg/mL stock solution. As positive control was used cells without any treatment and it were representing the 100% of cell viability. After 24h, the treatments were removed and the cells were rinse with PBS before added MTT solution (0.5 mg/mL). After 3 h of incubation, media was removed and cells was lysate with 500 µL DMSO and the cell viability was detected reading the samples at 580 nm using multiplate reader Envision (Perkin Elmer, Waltham, Massachusetts, USA).

2.2.8 Permeability assay

Vitamin C samples were prepared at different non-cytotoxic concentration solubilizing the samples in HBSS (Hank's balanced salt solution) at following concentration:

- Sample 1: 31,25 µg/mL
- Sample 2: 62,5 µg/mL
- Sample 3: 15,62 µg/mL
- Sample 4: 31,25 µg/mL

These concentrations represent the initial concentrations (C_i) placed in the donor compartment.

The Caco-2 cell culture medium was replaced, in the acceptor and donor compartment with HBSS and transepithelial resistance was measured. Subsequently, the solution contained in the donor compartment was replaced with the previously prepared test solutions. The plate was incubated at 37°C, 5% CO2 and with constant shaking (Corning® LSE™ Digital Microplate Shaker). Withdrawals were made from the acceptor compartment at the following times 1h, 3h, 6h and 24h. After 24h a sample was also taken from the donor compartment called final concentration (C_f).

All specimens were collected in 2 mL microtubes and stored at -20°C until analysis by UHPLC-MS. Before UHPLC-MS analysis, all samples were filtered on a 0.22 µm membrane (MiniSart® Syringe Filter, Sartorius – Milano – Italy). Specifically, the C_f samples were diluted before the chromatographic analysis until obtaining a concentration equal to 5 µg/mL, useful for returning within the linearity range of the calibration curve. The dilutions were carried out considering for each sample the initial concentration tested and diluting for a specific dilution factor (FD):

- Sample 1: Ci = 31,25 µg/mL; FD = 6,25.

- Sample 2: Ci 62,5 µg/mL; FD = 12,5.
- Sample 3: Ci 15,62 µg/mL: FD = 3,12.
- Sample 4: Ci 31,25 µg/mL; FD = 6,25.

To analyse the samples were used the HPLC-MS method reported above.

2.2.9 Determination of non-cytotoxic concentrations of vitamin C samples.

Figure 37 shows the results obtained to MTT test; we were selected as non-cytotoxic concentrations to use in permeability assay that determinate the viability of 70%. For sample 1 and sample 4 the non-cytotoxic concentration is 31,25 µg/mL, which have a viability between of 80,27% ± 1,90 e 77,81 % ± 6,25, respectively. Sample 2 have a maximum non-cytotoxic concentration of 108,35% ± 3,29. Sample 3 have a maximum non-cytotoxic concentration of 15,625 µg/mL, which viability between 96,70% ± 10,80.

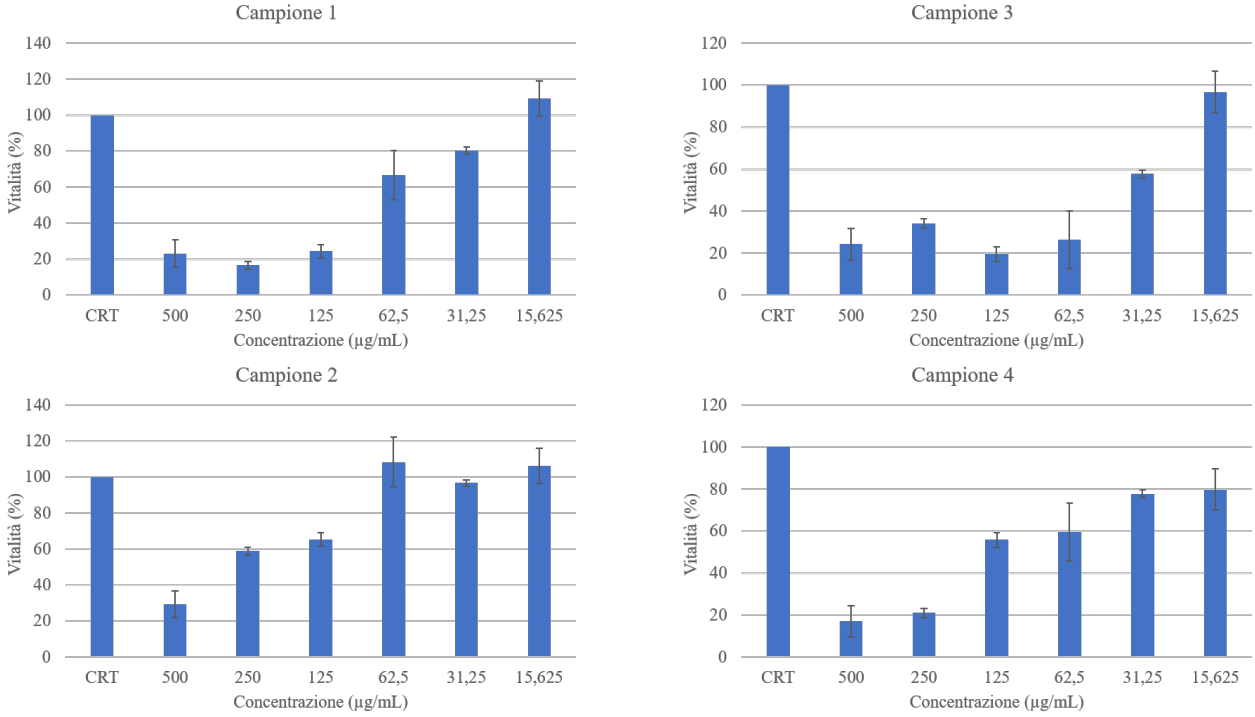

Figure 37: Viability of Caco-2 express as % viability compere to the control after a treatment with different concentrations of vitamin C samples for 24 hours.

2.2.10 Determination of non-cytotoxic concentrations of vitamin D samples.

Figure 38 shows the results obtained from the cell viability test (MTT assay) on 1-4 vitamin D samples. Sample 1, the maximum non-cytotoxic concentration is 0.625 µg/mL, which determines a cell viability of 101.27% ± 2.03. Sample 2 and 4 the maximum non-cytotoxic concentration is equal to 0.156 µg/mL, which determines a cell viability equal to 89.62% ± 3.81 and equal to 77.09% ± 3.12 respectively. Sample 3 the maximum non-cytotoxic concentration is equal to 0.625 µg/mL which

determines a cell viability equal to 91.32% ± 3.67. Sample 4 the maximum non-cytotoxic concentration is equal to 0.625 µg/mL, which determines a cell viability equal to 91.32% ± 3.67.

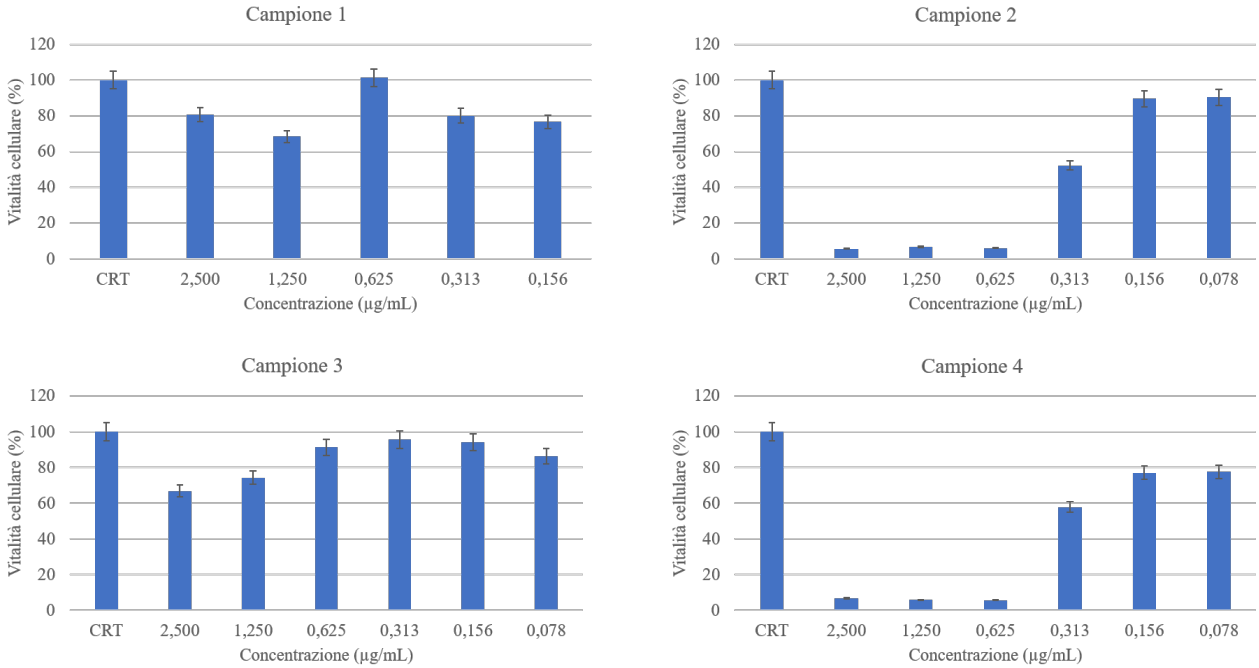

Figure 38: Viability of Caco-2 express as % viability compere to the control after a treatment with different concentrations of vitamin D samples for 24 hours.

Figure 39 shows the results obtained from the cell viability assay (MTT assay) performed by testing the digested vitamin D samples. The concentrations that determine a cell viability >70% were selected for the bioavailability study on the Transwell® model. Digested sample 1 and 2 the maximum non-cytotoxic concentration is equal to 0.313 µg/mL, which determines a cell viability of 83.18% ± 2.16 and 74.32 ± 3.75, respectively. Sample 2 the maximum non-cytotoxic concentration is equal to 0.156 µg/mL, which determines a cell viability equal to 89.62% ± 3.81 and equal to 77.09% ± 3.12 respectively. Sample 3 the maximum non-cytotoxic concentration is equal to 1.25 µg/mL, which determines a cell viability equal to 76.33% ± 2.93. Sample 4 the maximum non-cytotoxic concentration is equal to 0.156 µg/mL, which determines a cell viability equal to 72.89% ± 3.52.

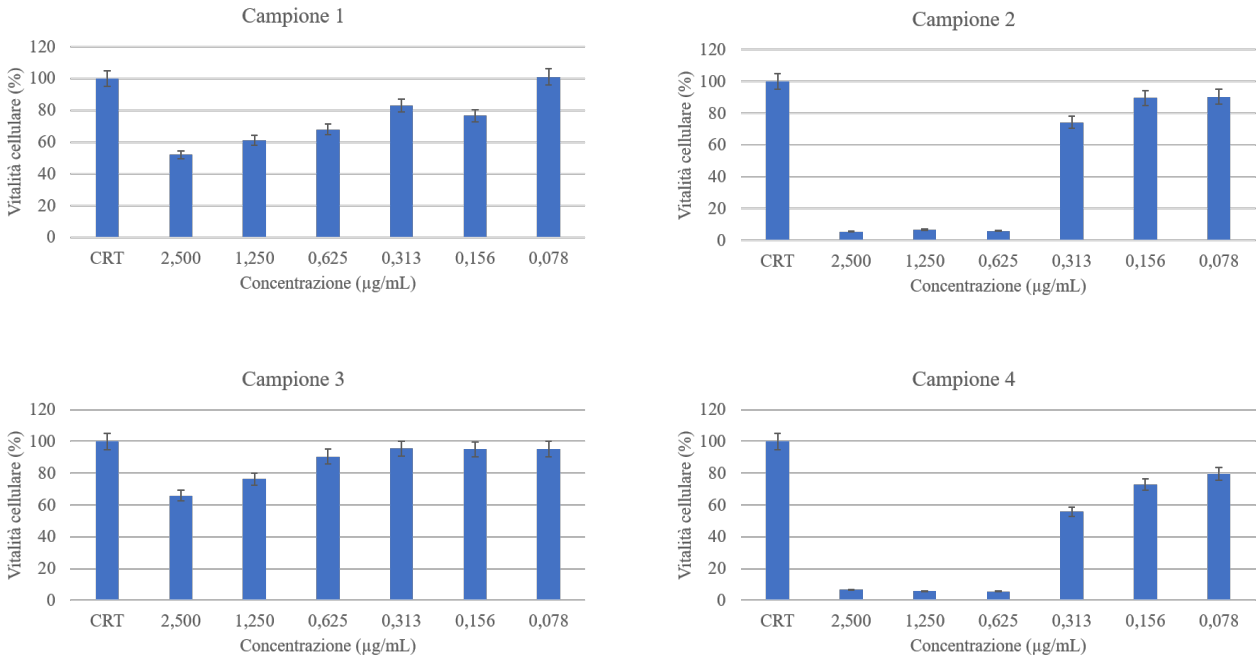

Figure 39: Viability of Caco-2 express as % viability compere to the control after a treatment with different concentrations of digested vitamin D samples for 24 hours.

2.2.11 Transwell® assay.

Table 25 reports the values of epithelial resistance measured before the permeability experiment. Values between 1800 – 2200 Ω suggest the correct formation of the cell monolayer [9], indicating that the cell monolayer is intact and ready to be used in the experiment.

Sample	TEER (Ω) (Average n=3)	TEER (Ω) (Blank corrected)
1	2002,5	1897
2	2188,5	2083
3	2168,5	2063
4	2136	2030,5
Bianco	105,5	0

Table 25: TEER value measured before the permeability assay.

The chromatograms obtained by HILIC-HPLC-MS analysis of acceptor compartment after 1h (A), 3h (B), 6h (C) shows any evidence of ion with *m/z* 175 → 115, which identified vitamin C to indicate that the concentration of vitamin C in the acceptor compartment of all the samples studied was lower than the LOD, i.e. the concentration of 0.150 µg/ml, suggesting two possible hypotheses:

1) vitamin C has not passed from the donor compartment to the acceptor compartment, as it has not penetrated the cells, stopping in the donor compartment.

2) vitamin C has not passed from the donor compartment to the acceptor one, since, although it has been absorbed, it is found inside the Caco-2 cells (Fig. 40, 41, 42).

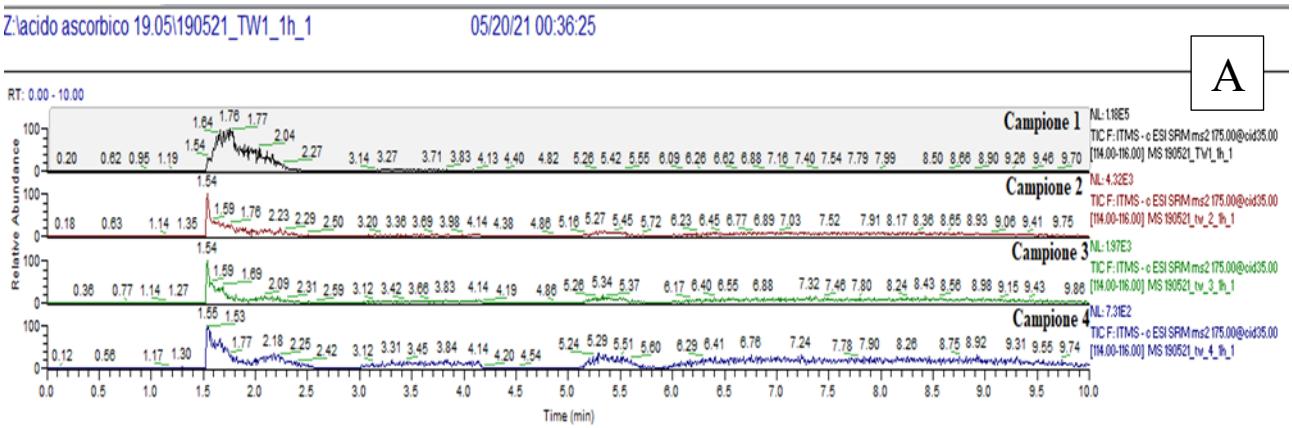

Figure 40: Chromatograms of ion with *m/z* 175 → 115 obtained from analysis of samples collected from acceptor compartment of Vitamin C samples at time point 1h..

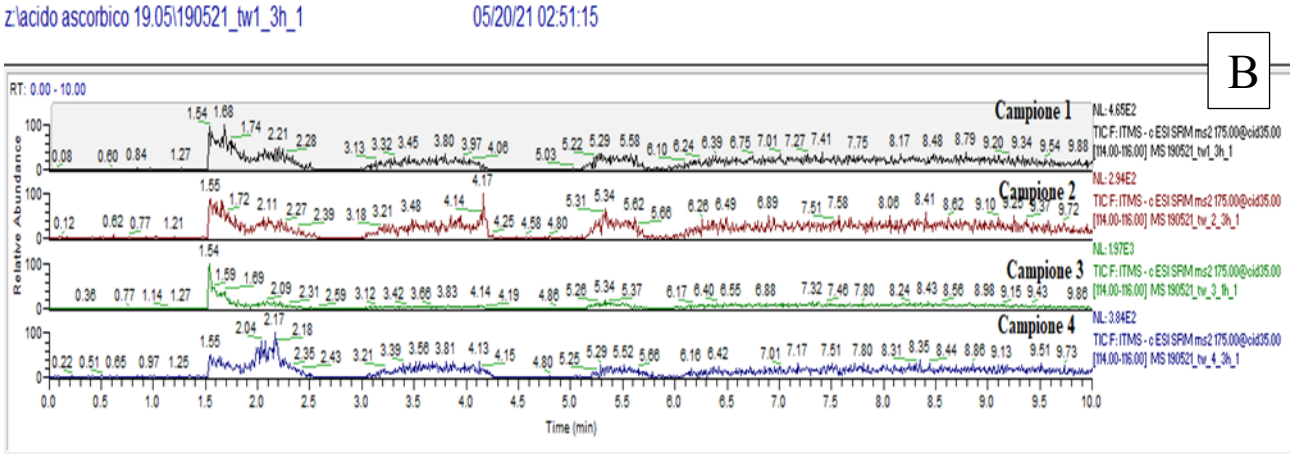

Figure 41: Chromatograms of ion with *m/z* 175 → 115 obtained from analysis of samples collected from acceptor compartment of Vitamin C samples at time point 3h.

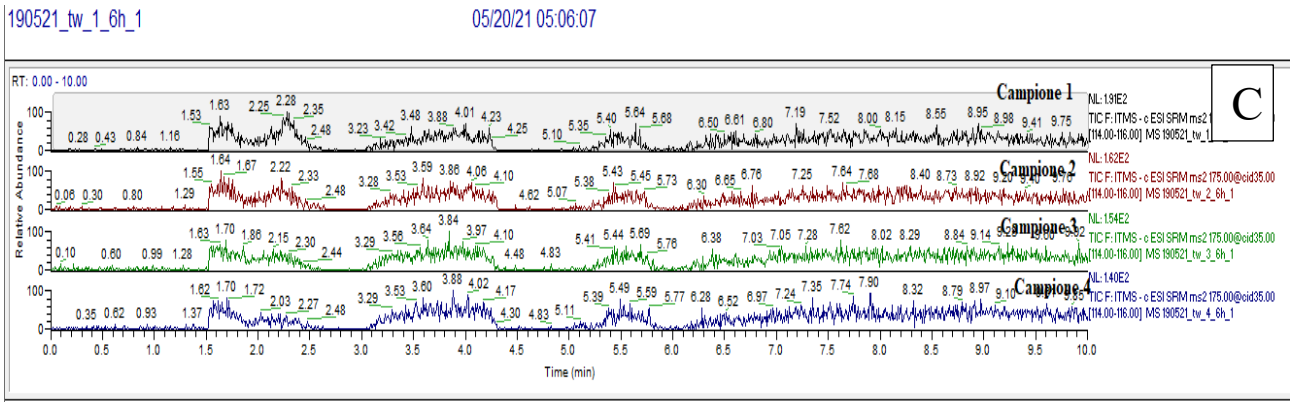

Figure 42: Chromatograms of ion with *m/z* 175 → 115 obtained from analysis of samples collected from acceptor compartment of Vitamin C samples at time point 6h.

After 6 h TEER was measured and the data was the values reported in table 16 were confirmed, indicating that the cell monolayer was intact.

CHAPTER 3: Comparative permeability study of natural source of vitamin C and synthetic vitamin C in Caco-2 monolayer grown in static and dynamic conditions.

1.2 Experimental

3.1.1 Reagents.

Acerola extract (004442) and rosa canina extract (007344) were acquired from ACEF s.p.a. (Fiorenzuola D'Ardua – Italy). L-ascorbic acid, Folin-Ciocalteu'phenol reagent were purchased from Sigma-Aldrich. Na_2CO_3 was provided by Carlo Erba (Milan, Italy). Phosphate buffered saline (PBS), triton, dimethyl sulfoxide, lucifer yellow CH, lithium salt, all reagents were acquired by Merk – Milano Italy. All the media and reagents for cell culturing were purchased from Gibco (Maia, Portugal). Hanks' balanced salt buffer (HBSS) and resazurin sodium salt were obtained from Sigma-Aldrich (Maia, Portugal).

3.1.2 Folin-Ciocalteu assay.

Total phenolic content (TPC) was determined using a colorimetric assay (Folin-Ciocalteu method), following the same protocol as set by Singleton et al. with some modifications [223]. However, Folin−Ciocalteu reagent that interacts with other different reducing nonphenolic substances (including ascorbic acid) and leads to an overestimation of polyphenol content. The purification of samples from interferents was performed using solid-phase extraction (SPE) cartridge as proposed of Georgè and co-worker [224] with same modification. Acerola and rosa canina extract were diluted in water to obtain a solution at concentration of 50 mg/mL. After that, 2 mL of solution were settled on an Oasis HLB 3 cc Vac Cartridge, 60 mg Sorbent per Cartridge (Water Corporation – Milan - Italy). The cartridge was conditioned with 4 mL of methanol and rinsed with 2 × 4 mL of water. Each sample (2 mL) were settled on the cartridge and the first phase contained the polyphenols (polyphenols phase = PF) was collected in a microtube. Interfering water-soluble components (reducing sugars, ascorbic acid) were recovered with 2 × 2 mL of distilled water (washed phase = WF). An aliquot (10 µL) of the PF and WF samples or gallic acid standard solutions (200–1000 µg/mL) was taken and added to 50 µL of Folin-Ciocalteu reagent. The solutions were cyclomixed for 4 min and added to 200 µL Na_2CO_3 (15%). The final volume was made to 1 mL with distilled water and allowed to incubate for 2 h at room temperature and under dark conditions. The solutions were read spectrophotometrically at 750 nm using Synergy Mx (Bio Tek - Winooski, Vermont, USA). Gallic acid was used as standard compound, with serial dilutions being prepared with known concentrations ranging from 200 to 1000 µg/mL. The results were expressed as mg equivalent to gallic acid/g of extract on dry weight basis.

3.1.3 Ascorbic acid quantification assay

The content of vitamin C in different samples were evaluated using Ascorbic Acid Assay Kit purchased from Abcam (Milan, Italy) following the manufacturer's instructions. Briefly, 20 mg of

samples were weighed accurately and solubilized in bi-distilled water to obtain stock solutions with a concentration of 1 mg/mL. Subsequently the stock solutions were diluted to a final volume of 120 µl/well with ascorbic acid assay buffer in a 96-well plate to obtain the test samples as follow: Acerola extract at 1 µg/well, rosa canina extract at 2 µg/well and synthetic vitamin C at 1 µg/well. A standard curve of vitamin C was prepared in according to assay protocol a concentration range of 0-10 nmol/well. All reagents were mixed in the 96-well plate and the absorbance was measured at Ex/Em = 535/590 nm using a microplate reader Synergy Mx (Bio Tek - Winooski, Vermont, USA).

3.1.4 MIVO® fluidic platform.

MIVO fluidic platform (commercialized as MIVO® by React4life S.r.l., IT) consists of a diffusive chamber made of transparent USPVI biopolymer and connected to a closed-loop fluidic circuit assembled to a pumping system, it provides a controlled and reproducible fluid flow in terms of direction, speed, and induced shear stresses, enabling to mimic different physiological flows and the real tissue complexity. The bioreactor fits commercially available 24-well trans-well inserts.

3.1.5 Culture of Caco-2 monolayer.

The Caco-2 cell line (HTB-37), derived from a human colorectal adenocarcinoma, was obtained from The American Type Culture Collection (ATCC, Manassas, VA, USA). They were grown (at passage number 9-13) in Dulbecco's Modified Eagle Medium (Lonza) supplemented with 10% heat-inactivated fetal bovine serum (Gibco, Waltham, MA USA), 1% penicillin-streptomycin (Sigma), 1% non-essential amino acids (Gibco), further referred to as $DMEM^+$. The cells were seeded at density of 3.3×10^4 cells per cm^2 in 24-well Transwell® polyester inserts (0.4 µm pore size, 0.33 cm^2 surface area, (Corning Amsterdam, The Netherlands) cultured in $DMEM^+$. During culture period, medium was changed for every other day. The cells were allowed to attach to the membrane for 24h after that 24-insert well were moved into and cultured within the MIVO chamber for 7, 14 and 21 days. The donor chamber was filler with 0.3 mL $DMEM^+$ while receiver chamber, connected to the fluidic circuit and filled with 2.5 mL of $DMEM^+$. The fluidic circuit was connected by paraben-free transparent tubes to a peristaltic pump (Watson Marlow), and $DMEM^+$ was pumped through the lower chamber in a closed-loop circuit, at a rate of 15 rpm by the peristaltic pump.

3.1.6 Caco-2 monolayer integrity.

3.1.6.1 Transepithelial electrical resistance (TEER) measurement.

To evaluate the cell monolayer integrity in Caco-2 barrier model, TEER was measured every 2 days before refreshing the medium. Briefly, the electrode was placed in a falcon contained EtOH 70% for 5 min, after that the electrode was equilibrated in $DMEM^{+}$ prior to TEER measurement of each insert. TEER measurement was performed using an EVOM2 (World Precision Instruments, Sarasota, FL, USA) apparatus.

3.1.6.2 Lucifer yellow assay.

Apical to basal translocation of lucifer yellow was measured in a Caco-2 monolayer grown up in static and dynamic conditions for 7, 14 and 21 days. At the end of culture time, MIVO chamber was opened and the insert was placed in 24-well multiplate to perform the lucifer yellow assay. A lucifer yellow solution of 500 μg/mL in HBSS was placed in the apical side of insert and 1 mL of HBSS was putted in the basolateral compartment. Sample aliquots of 200 μL were collected from the basal compartment every half hour for 2 h. At each time point 200 μL of HBSS were replaced in thr basolateral compartment to maintain the sink conditions. In the end of experiment an aliquot of samples was collected also from the apical compartment to calculate the mass balance. The fluorescence intensity (485/530 nm) of all collected samples from both systems was measured using a microplate reader (Synergy HT, BioTek, VT).

3.1.6.3 Immunohistochemistry.

Seven, fourteen and twenty-one days after seeding, Caco-2 cells, grown in MIVO platform or Transwell®, were prepared for cell and monolayer morphological assessment. The cells were fixed with 4% formaldehyde at room temperature for 10 min and rinsed twice with PBS. Cells were then permeabilized with 0.25% Triton X100 in PBS for 10 min, rinsed with PBS and blocked with 1% acetylated bovine serum albumin in PBS for 30 min. Tight junctions were stained with 10 μg/mL conjugated antibody ZO-1/TJP1-Alexa Fluor 594 (Invitrogen, Waltham, MA). The nuclei were stained with 5 μg/mL DAPI (Invitrogen, Waltham, MA) Each insert membrane (from MIVO or Transwell®) was cut out and placed between two cover slips separated by a spacer (0.12 mm depth × 20 mm diameter) with a drop of anti-fading mounting medium on the membrane. The stained monolayers of cells were analysed using a fluorescent microscope (Zeiss Axio Imager Z1; Carl Zeiss, Germany). Samples were excited with 405, 488 nm lasers. The magnification was 40× and 60×.

3.1.7 Resazurin assay.

Vitamin C samples (10 mg) were solubilized in DMEM$^+$ to obtain a stock solution of 1 mg/mL. This stock solutions were diluted in DMEM$^+$ to obtained four different concentrations for each sample. For acerola extract the range was between 2000 – 31,25 µg/mL, for rosa canina extract the range was between 31,25 – 0,48 µg/mL and for synthetic vitamin C the range was between 3000 – 46,87 µg/mL. All of samples were filtered using a 0.22 µm membrane. Caco-2 cells (p8) were seeded in a 96-well plate at density of 2 x 10^4 cells/well. After 72 h, cells were 70% confluent and it were treated with the samples. The positive and negative controls and background (positive control: cells with supplemented medium; negative control: cells with 1% (v/v) Triton-X in DMEM$^+$; background: supplemented medium only) were included in the experiment. After 24h, the treatments were removed and the cells were rinse with PBS before added Resazurin solution (20 % v/v). After 3 h of incubation (in the dark at 37°C, 5% CO2), 200 µL of each well was transferred to a black-walled, transparent-bottom 96-well plate and fluorescent was measured at Em=530 nm, Ex=590 nm.
using multiplate reader Synergy Mx (Bio Tek - Winooski, Vermont, USA). The percentage of cell viability was calculated from the absorbance obtained from the positive control (cell in DMEM$^+$) divided by that of each treatment.

3.1.8 Permeability of natural source and synthetic source of vitamin C

The static transport studies were performed following an established protocol [222]. At day 21 post-seeding, a non-toxic concentration of synthetic vitamin C and rosa canina extract were prepared in a transport medium (HBSS). The cells were washed with PBS and HBSS were added in apical and basolateral compartments for 15 min at 37 °C. Subsequently, HBSS was removed from the basolateral and the apical compartment. 1 mL of fresh HBSS was placed in the basolateral compartment while vitamin C solutions of 0.3 mL in HBSS were then added to the apical side of the inserts. In the MIVO studies, each compound solution was added in the upper channel and a flow rate of 15 rpm in HBSS was pumped through the basolateral channel. From the basolateral side, an aliquot (200 µL) was collected from the basolateral compartment at established time point of 30, 60, 90, 120 min and replace with the same volume of HBSS was replaced in the basolateral compartment to maintain the sink conditions. All the liquid from the apical and basolateral chamber was collected at the last time point to calculate a mass balance. All samples were stored in -80 °C before analysis. The transport was calculated from the experimental data using equation (2) for the Transwell data and the MIVO data [223].

(2) $P_{app} = \left(\frac{dQ}{dt}\right)\left(\frac{1}{AC_0}\right)$

Where A is the surface area (cm^2), dQ is the amount of the model compound transported (µmol) over the respective time interval dt (s), C_0 is the initial concentration (µg/mL), C is the concentration in the basolateral compartment (µg/mL).

3.1.9 Vitamin C quantification.

All samples from the transport experiments were analysed using ascorbic acid kit assay purchased from Abcam (Milan, Italy) following the manufacturer's instructions as reported above.

3.1.10 Statistical analysis.

All statistical evaluations were evaluated using an independent paired t-test (GraphPad). A p-value of ≤0.05 was considered significant.

3.2 Results and Discussion.

3.2.1 Determination of total polyphenols content.

The total phenolic content (TPC) was evaluated in acerola and rosa canina extracts (Table 27) after purification by interferences through SPE cartridge. In fact, correction of results by subtracting interfering substances appeared necessary to get appropriate values for polyphenol determination. For acerola extract the total polyphenol content is 202.298 ± 17.99 expressed as equivalent of gallic acid for g of extract (EAG mg/g of extract) while rosa canina extract show a total polyphenol content equal to 234.379 ± 11.63 EAG mg/g of extract (Tab. 27). The analysis of both fractions collected by the SPE (PF and WP) reported that the contribution of the interfering substances is 38% for acerola extract and 73% for rosa canina extract as reported in graph 1.

ID Samples	EAG mg/g of extract	
	PF	WP
Acerola extract	202.298 ± 17.99	326.843 ± 31.634
Rosa canina extract	234.379 ± 11.63	175.88 ± 16.734

Table 27: ID samples, total polyphenol content expresses as mg of equivalent of gallic acid / g extract (EAG mg/g of extract) in PF fraction and WP fraction. Average ± SD of triplicate.

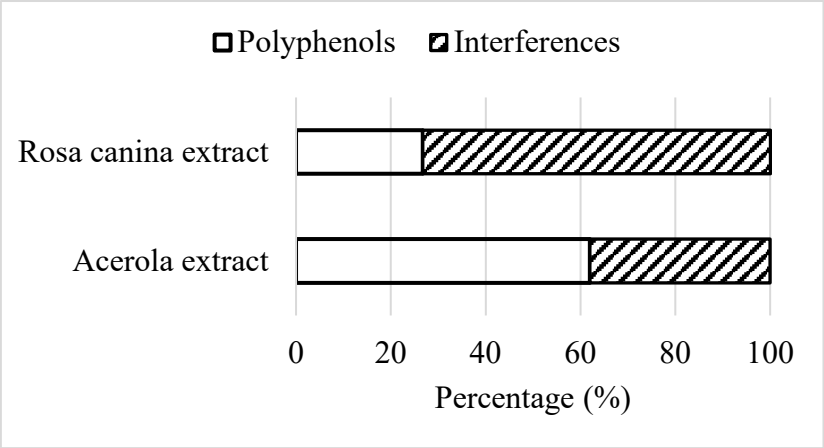

Graphic 1: Percentage of interferences and polyphenols in acerola and rosa canina extract.

Different food matrices like apple purees and juice that were analysed with this method had a percentage of interfering substances varied from 31% to 48% For food matrix like orange juice and tomato juice the percentage of interferences in between 70 - 77% [224]. In conclusion, to estimate the correct total polyphenol content in acerola and rosa canina extract was essential using the purification step with SPE cartridge to remove the interfering nonphenolic reductants including the vitamin C.

3.2.2 Vitamin C content in the samples.

The content of vitamin C was determined using ascorbic acid assay kit, yielding the results as given in figure 41 and table 26. In more detail, acerola extract presents an average concentration of vitamin C of 504.418 ± 52.262 ng/µg of sample, rosa canina extract have a content of vitamin C equal to 695.102 ± 83.148 ng/µg of sample and Vitamin C have a concentration of 957.319 ± 233.789 ng/µg of sample.

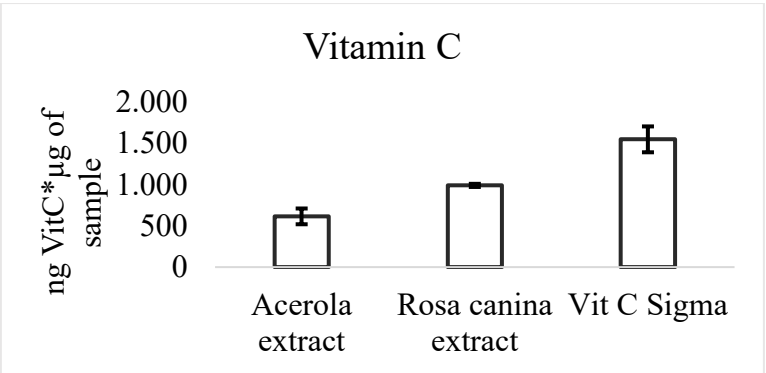

Figure 43. Content of vitamin C in different samples expressed as ng/µg of sample. The results are express as average ± standard deviation of three replicate.

ID Sample	ng VitC*µg of sample				
	Replicate 1	Replicate 2	Replicate 3	Average	Standard deviation
Acerola extract	503.677	557.046	452.531	504.418	52.262
Rosa canina extract	791.095	645.440	648.775	695.103	83.148
Vit C	1226.391	803.881	841.685	957.319	233.789

Table 26: ID samples, content of vitamin C expressed as ng VitC/µg of sample, average and standard deviation.

From the results obtained for vitamin C quantification in both extracts, rosa canina extract was choice as natural source sample due to the higher content of vitamin C to perform the subsequent permeability assay.

3.2.3 TEER monitoring in Caco-2 cells cultured in static and dynamic conditions for 7, 14 and 21 days.

Formation of a physiological barrier in most of the *in vitro* models of intestinal epithelia is detectable by trans-epithelial electrical resistance (TEER) measurements [221]. In general, this technique provides information about the state of barrier integrity of the intestinal tissue, which directly affects the paracellular passage of molecules. The TEER measuring was performed in systems culturing for 7, 14 and 21 days in static and dynamic conditions. No significant differences were revealed in the different culture conditions. However, the values of teer increase drastically after 4 days of cultures. Subsequently the values increase without reaching a plateau phase (Graph. 2, 3, 4).

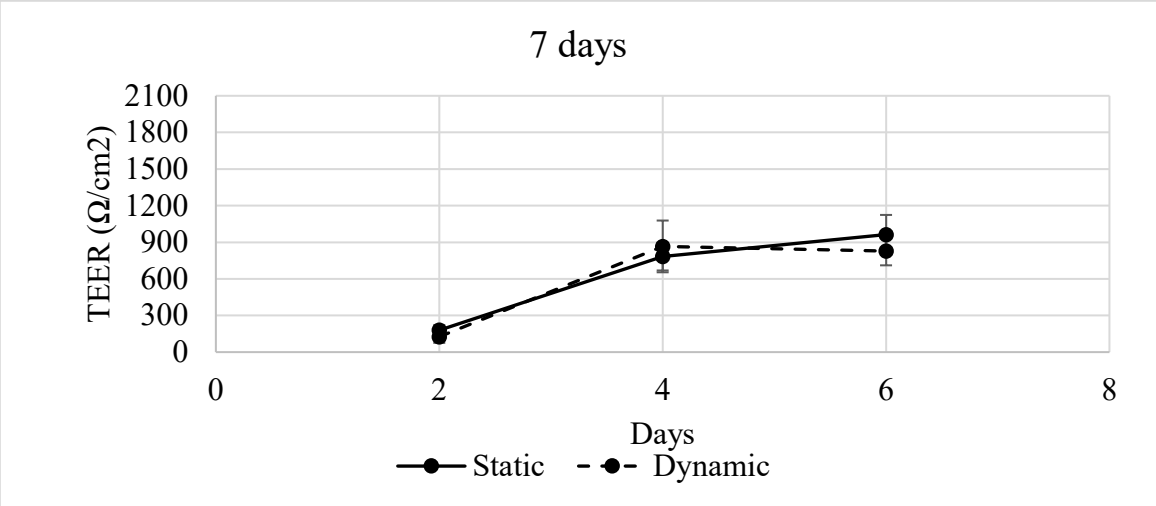

Graphic 2: TEER measuring every 2 days in static and dynamic conditions in 7 days model.

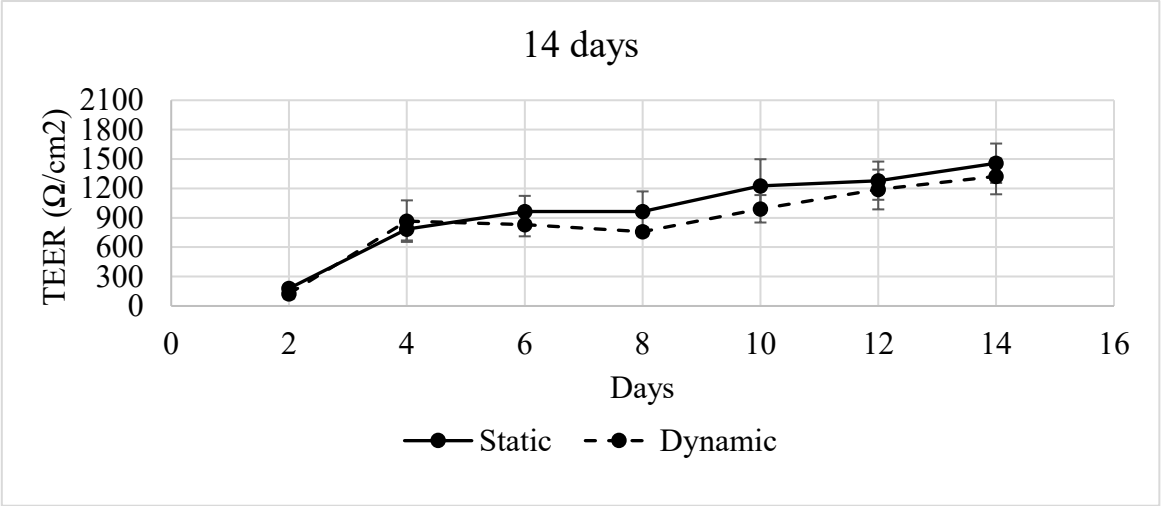

Graphic 3: TEER measuring every 2 days in static and dynamic conditions in 14 days model.

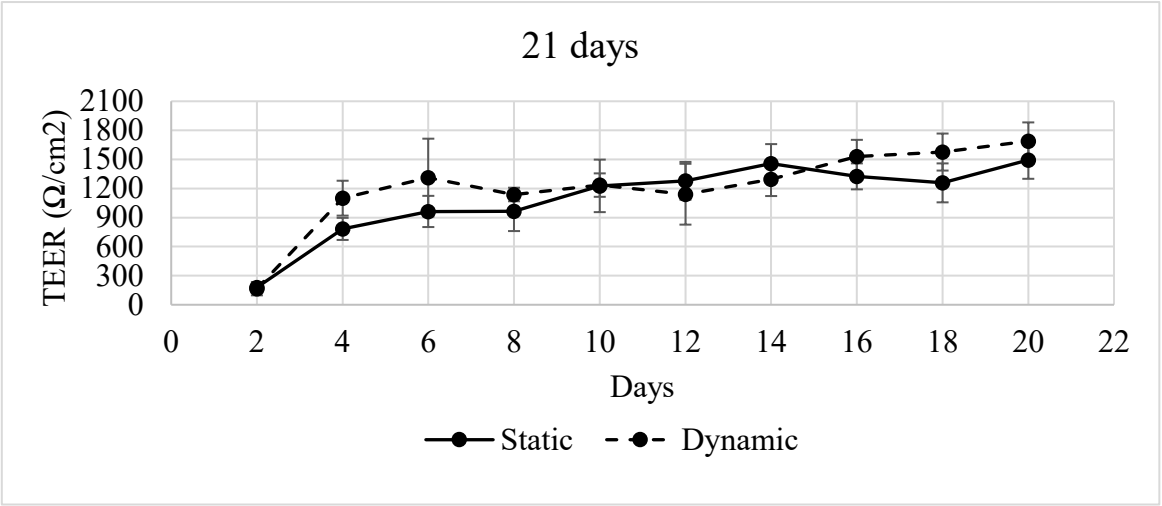

Graphic 4: TEER measuring every 2 days in static and dynamic conditions in 21 days model.

Previously, different studies demonstrated similar TEER value for Caco-2 monolayers grown in dynamic conditions and static conditions for 5 days [223, 224]. In contrast, other studies reported an increase of TEER in dynamic Coco-2 model exposed to dynamic conditions in comparations to cells grown in static Transwell® [97]. TEER is a fast technique to measure the barrier integrity, however literature data have high variability, which derived from different factors. TEER measurement is affects by temperature, type of membrane and electrode positioning. Moreover, the comparations with literature studies is complicated due to the differences in design of dynamic platform and fluid flow. From these observations, we can conclude that the only evaluation of TEER values is not enough to draw conclusion about barrier integrity. For this reason, the formation of tight junctions and the permeability of paracellular marker (yellow lucifer) were investigated in the following paragraph.

3.2.4 Formation of tight junctions.

Caco-2 cell monolayer cultured in Transwell® show tight junctions, which mimic the paracellular barrier function of the intestinal epithelium [225]. To evaluate the formation of tight junctions, the expression of ZO-1 was imaged after 7, 14 and 21 days after cell grown in static and dynamic conditions. In MIVO platform the Caco-2 cells were grown using a continuous flow of 15 rpm for 7, 14, 21 days. ZO-1 is a protein involved in the tight junctions formation in enterocyte monolayer. The most representative images are shows in figure 42. Caco-2 cells grown under both conditions show the expression of ZO-1 at day 7 to day 21. Literature data reported that cells cultured under continuous flow forms intact and polarized monolayers faster compared to Caco-2 cells cultured using traditional static conditions [120]. In this study, the visual inspection of images showed the formation of comparable pattern of tight junction in cells grown in both conditions. Nevertheless, the investigation of tight junctions through immunohistochemistry assay represents a qualitative assay. In fact, cells cultured in static conditions shows the ZO-1 staining at day 7 and 14 but it's validated that the full expression of tight junction occurs after 3 weeks in Transwell® model [70]. The quantitative evaluation of ZO-1 through western blot or PCR needs to be explored for more accurate estimation of ZO-1 expression. Unfortunately, wester blot is a time-consuming technique, which a due to time constraints, it was not possible perform in this work. Moreover, it could be interested in the future investigations study other proteins involved in the barrier integrity such as cytoskeleton proteins (i.e. F-actin, villin).

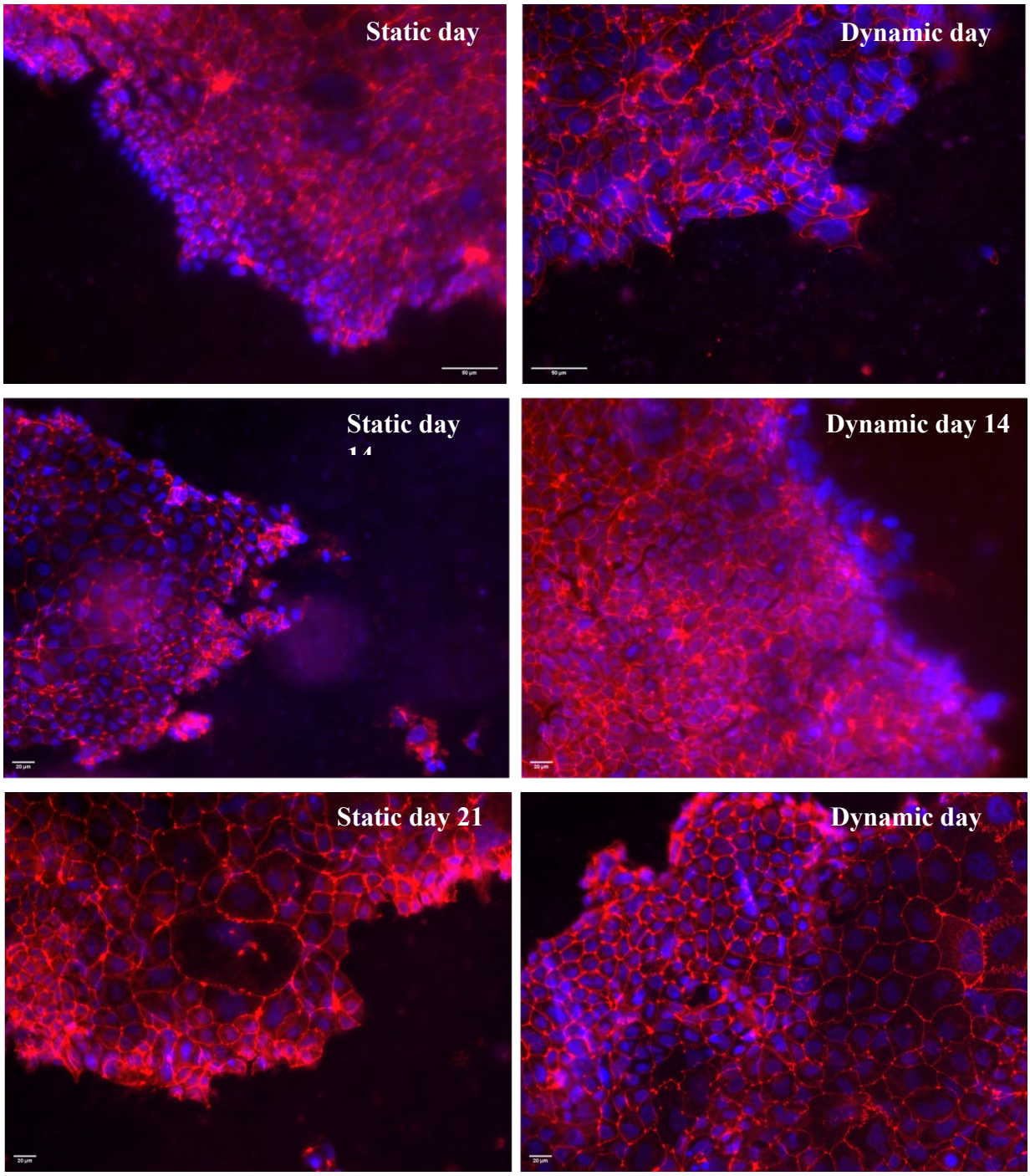

Figure 44: Morphology of Caco-2 monolayer cultured for 7, 14 and 21 days in static and dynamic conditions, visualized by fluorescent microscopy. Magnifications 20X and 40X.

3.2.5 Lucifer yellow assay.

Caco-2 cells were grown on the membrane in both the MIVO platform and the Transwell® model for 7, 14 and 21 days. Lucifer yellow is a small, hydrophilic molecule that was used as a fluorescent marker to monitor the integrity of the tight junctions between the Caco-2 cells. As shown in Fig. 42 the paracellular permeability percentage of lucifer yellow decreased in time in both tested systems.

The paracellular translocation of lucifer yellow decrease for the Caco-2 quckly for the Caco-2 monolayer grown in MIVO platform in the second week of culturing. A similar trend was observed for Caco-2 monolayer grown under static condition. On other hand, lucifer yellow permeability experiment indicated good barrier integrity of the monolayer cultured in Transwell® after 21 days and in MIVO after 7 and 14 days. Less than 5% Lucifer yellow permeability is generally used as a cut-off value for a leaky monolayer [30_Delon], and an average permeability of 2.21% ± 1.12, %, was experimentally obtained in cell monolayer grown in static conditions for 21 days while an average permeability of 0.38 % ± 0,14% was obtained in cells grown in dynamic conditions for14 days.

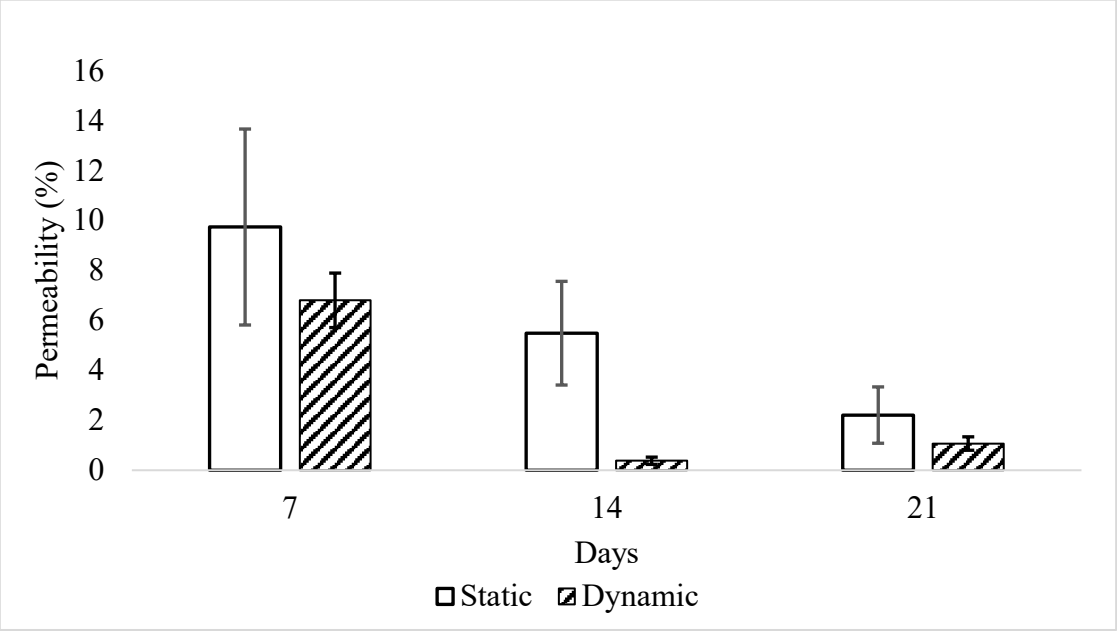

Figure 45: Percentage (%) permeability lucifer yellow in different experimental condition: Caco-2 monolayer at 7, 14 and 21 days after seeding, static and dynamic fluid flow. The values are presented as averages ± Std Dev; n = 3 Transwell® and 4 (MIVO® and Transwell®).

Conventionally, Caco-2 cells are used after 21 days of culturing in Transwell® systems, when they have developed into a leaky-free monolayer of differentiated cells. In this study, the evaluation of barrier integrity in Caco-2 monolayer was performed after growth the cells in the conventional static Transwell® *versus* dynamic conditions using MIVO platform for 7, 14 and 21 days. The evaluations of results obtained from TEER measurement, expression of ZO-1 and lucifer yellow permeability suggest that the Caco-2 monolayer grown in dynamic conditions for 14 days can be used to perform permeability studies. Previously, other research groups have characterized Caco-2 monolayer integrity in microfluidic platform, but in platform with different design. For example, using chips platform, barrier integrity was observed after 3-5 days of seeding [97, 122], which is faster than observed in MIVO® model.

3.2.6 Determination of non-cytotoxic concentrations of samples.

The resazurin assay was used to select the non-cytotoxic concentration of samples to be applied in the subsequent permeability studies. As shows in Fig. 42 the maximum non-cytotoxic concentration (> 80% viability) was found to be 3000 µg/mL for synthetic vitamin C cell viability (%) = 122,33 ± 12,4), 2000 µg/mL for acerola extract (cell viability (%) 114,75 ± 10,23) and 31,2 µg/mL for rosa canina extract (cell viability (%) 88,16 ± 7,42) as shows in figure 46, 47.

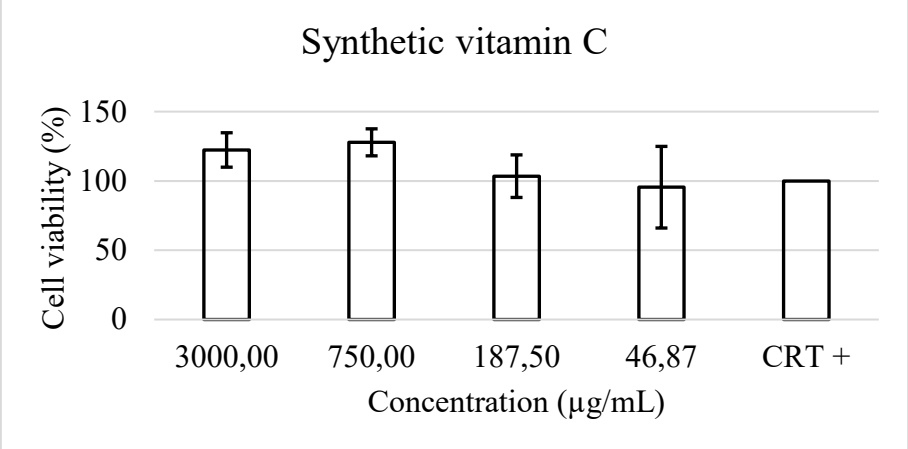

Figure 46: Cell viability (%) Caco-2 cells exposed for 24 h to different concentrations of synthetic vitamin C (n = 4).

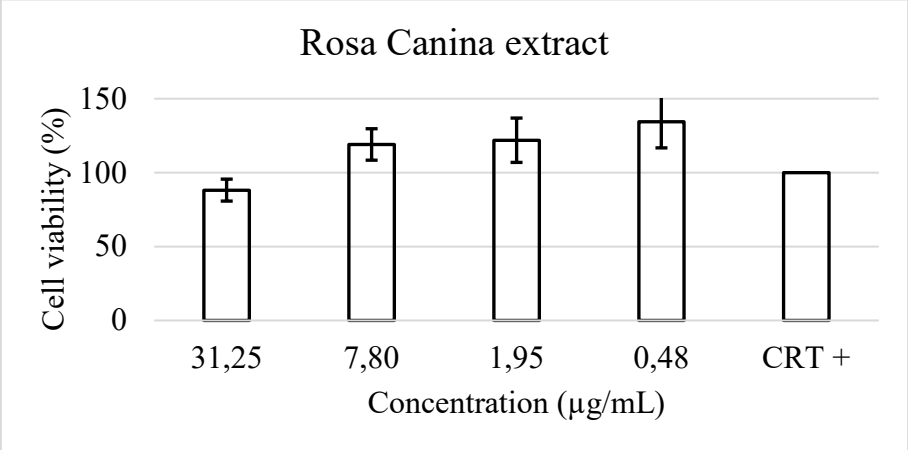

Figure 47: Cell viability (%) Caco-2 cells exposed for 24 h to different concentrations of rosa canina extract (n = 4).

3.2.7 Permeability assay Vitamin C

The percentage of vitamin C contained synthetic vitamin C and rosa canina extract through the Caco-2 monolayer cultured in conventional Transwell® system and Caco-2 monolayer cultured under dynamic conditions for 14 days were analysed. As showed in Fig. 48, the absorption profiles of vitamin C in static and dynamic are similar. However, the percentage of absorbed vitamin C in rosa canina extract was greater than that calculated for the synthetic vitamin C at each time point. A plateau was reached in vitamin C from rosa canina extract in both conditions (monolayer grown in static and dynamic conditions). In static condition, vitamin C from rosa canina reached the steady state after 30 minutes, while in dynamic conditions, the same sample reached steady state after 60 minutes.

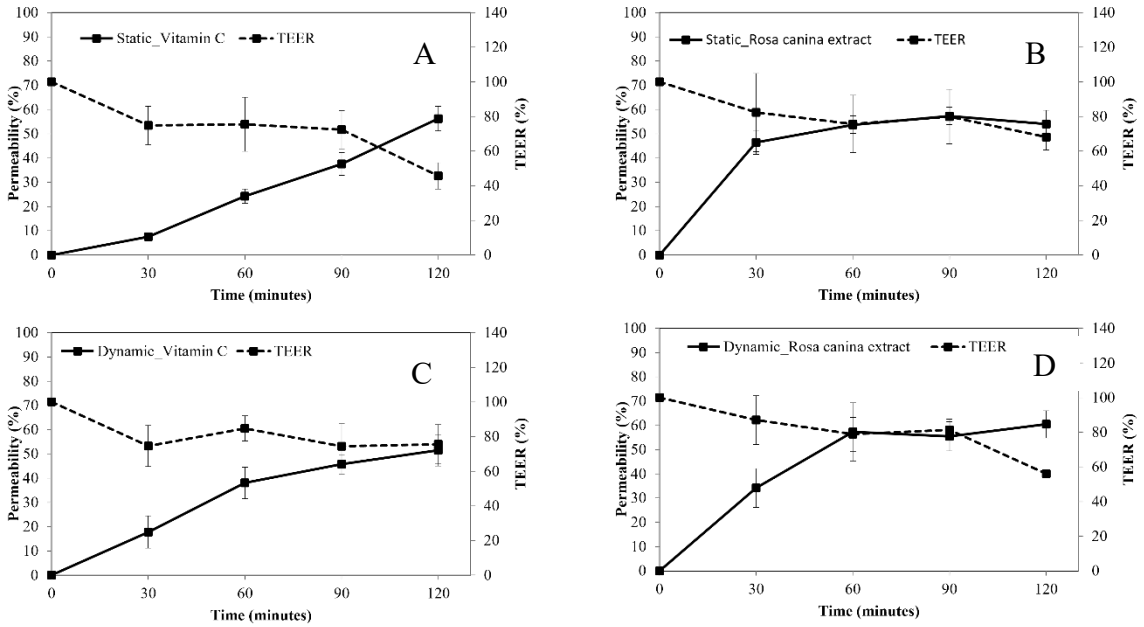

Figure 48: Vitamin C absorption from acerola extract (B-D) and from synthetic vitamin C (A-C) tested in Caco-2 monolayer in Transwell® (static) (A-B) and in MIVO platform (dynamic) (C-D). Values are presented as average ± SD. N = 3.

CHAPTER 4: General discussion and future prospective.

4.1 General discussion.

In recent years many studies support the evidence that the dynamic *in vitro* model system could represents a new tool to carry out permeability testing. The scientific progress achieved in cell biology, biofabrication and microfluidics have led to the development of new *in vitro* cellular models that can emulate specific functional tissues. These *in vitro* model systems simulate better the *in vivo* scenario because the flow of cell medium crosses the cells cultured in such a device. However, several challenges remain before these new models can become widely accepted as standard *in vitro* models. The characterization of specific validation process for these models could help the development and the qualification of this devices for a specific use. These systems can be applied in nutraceutical field to evaluate different proprieties. In particular, the number of natural products used as pharmaceuticals, components of dietary supplements have increased tremendously requiring an extensive evaluation of their pharmacokinetic properties. The work described in this thesis aimed to develop a new *in vitro* model system focused on the study of nutraceutical proprieties. An overview of the state-of-the-art *in vitro* models for the human intestine was provided in **Chapter 1**. This overview illustrated the current diversity in *in vitro* model system for transport studies divided in static system and dynamic system. The data obtained suggest that there are different new dynamic *in vitro* model systems that may more closely emulate the structure, function, physiology, and pathology of the human intestine. In **Chapter 2,** the bioaccessibility and the bioavailability of two vitamins (vitamin C and vitamin D) from two different source (natural and organic synthesis) were compared. The same experimental design was conducted, in parallel and under the same experimental conditions for both type of samples. Although synthetic vitamins and vitamins from natural sources are chemically identical, it is known that the matrix can affect the absorption and bioavailability of a nutrient [224]. **In Chapter 3**, a novel organ on chip MIVO® by React4Life model was used to culture human intestinal epithelial Caco-2 cells on a porous membrane under dynamic conditions (i.e. flow) and compare its characteristics to those of the same cells grown in a conventional static *in vitro* model. The results obtained from *in vitro* digestion, shown in **Chapter 2,** provides important information. In fact, samples VitC1 and VitC2 corresponding to natural vitamin C and the same in dosage form have a higher bioaccessibility than samples VitC3 and VitC4, corresponding to synthetic vitamin C and the same in dosage form, indicating that the natural vitamin C is more stable to oro-gastro-duodenal digestion than synthetic vitamin C. Regarding vitamin D samples, the results indicate that vitamin D after digestion is substantially stable both when subjected to digestion alone and when digested in its dosage form without any distinction between vitamin D of natural origin and of synthetic origin. The bioavailability was evaluated with different *in vitro* model systems: PAMPA assay and Transewell®. The results obtained from PAMPA assay demonstrate that, unlike what happens at low concentrations

of vitamin C, where regardless of the presence or absence of a phytocomplex, due to its hydrophilic nature, vitamin C does not cross the phospholipidic membrane, strongly increasing the concentration of vitamin C, in order to establish a favourable gradient between the donor and acceptor compartments, the synthetic vitamin C at a high concentration (500 mg/ml) widely crosses the phospholipidic membrane, unlike the vitamin C of natural origin, which although it too has been loaded in the donor compartment at high concentration (500 mg of digested sample 1/ml correspond to about 350 mg/ml of Vitamin C) does not cross the phospholipidic membrane. This result leads us to hypothesize that: 1) under the experimental conditions applied in the PAMPA assay, the phytocomplex present in sample 1, which represents about 30% by weight of the sample, hinders the passage of vitamin C by creating an environment that is not favourable to the passive diffusion of vitamin C. 2) the high viscosity of sample 1 at the tested concentration acts as an obstacle to the passive diffusion of the vitamin across the phospholipid membrane. Therefore, we decided to carry out additional tests to differentiate samples VitC1 and VitC3 and therefore the assay was repeated, including the initial phases relating to the calibration curve, the evaluation of the functionality of the phospholipid membrane and the evaluation of the membrane integrity. Regarding vitamin D samples, the results obtained from PAMPA assay show that only sample VitD2 corresponding to natural vitamin D in dosage form is absorbed by passive diffusion unlike what occurs for sample VitD4, corresponding to synthetic vitamin D in dosage form, indicating that the simultaneous presence of the phytocomplex, present in its natural form, and of the excipients contained therein induce the crossing of the phospholipidic membrane. Sample VitD1 corresponding to natural vitamin D is not able to overcome the phospholipid barrier. This suggests that in the absence of the excipients, present in sample VitD2, the phytocomplex alone is not sufficient to guarantee the passive diffusion of vitamin D. In summary, the results obtained from the test conducted with the Transwell system did not allow differentiating the absorption of vitamin C of natural origin (samples 1 and 2) from that of vitamin C of synthetic origin (samples 3 and 4). This result is not in agreement with that obtained by Takino et al. [225], which claims that the Acerola extract rich in vitamin C has a statistically greater absorption of Caco-2 than synthetic vitamin C thanks to the phytocomplex of the natural vitamin C is made up. The discrepancy between the two results could be attributed to the different operating conditions. The first difference found between the experiment we conducted and that of Takino et al. regards the fact that Takino et al. uses undigested natural and synthetic vitamin C in the assay. In our opinion, the use of the samples after digestion better mimics the physiological conditions that occur *in vivo*. However, in consideration of the aim of the research, which is to differentiate in terms of bioavailability, natural vitamin C from that of synthetic origin, in the next experiments we used the undigested samples. The second difference found between our experiment and that of Takino et al.

regards the different concentration employed in the two experiments. It is observed that in the work of Takino et al. natural vitamin C (present in an extract of Acerola) and synthetic vitamin C are tested at a concentration of 3 mM, corresponding to a concentration of 528 µg/mL. It is also observed that in the work of Takino et al. the results of the cytotoxicity assay are not reported, which is an indispensable preliminary test before carrying out the assay with the Transwell® system to be sure of the viability of the Caco-2 cells. From this new set of experiments, we can suppose that vitamin C of natural origin in dosage form, being absorbed, in the applied experimental conditions, unlike synthetic vitamin C in dosage form, has a greater bioavailability in the assay used. The results obtained in Transwell® assay for vitamin D samples not allowed to highlight differences between the samples of natural and synthetic vitamin D. In **Chapter 3** we demonstrated that Caco-2 cells can be maintained and form monolayers of cells under the applied flow rate of 15 rpm. The relationship between TEER, tight junctions and permeability of molecules with paracellular transport was investigated. TEER value and expressions of tight junction were similar for static and dynamic conditions. However, the permeability of yellow lucifer decrease for the Caco-2 monolayer grown in MIVO platform grown for 14 days reaching permeability values less than 5%, which represent the reference value accepted for the permeability of paracellular compounds in an intact barrier. To study the applicability of MIVO model system using Caco-2 human intestinal epithelial cells, the permeability of vitamin C have been performed and the observed effects were compared to those obtained using a conventional static *in vitro* model. Caco-2 cells cultured under flow for 14 days formed confluent and polarized monolayers that were visually comparable to cells cultured for 21 days under static conditions in Transwell® wells. The data obtained from the permeability assay of natural vitamin C (rosa canina extract) and synthetic vitamin C suggest no difference between the different sources of vitamin C.

In conclusion, cells that are subjected to dynamic culture conditions are affected by the flow as shown in this thesis (chapter 3) and in literature [223-225]. It is known that liquid flow resembles physiological conditions but *in vivo* depending on the intestinal location and viscosity of digesta. Therefore, to mimic the real fluidic conditions experienced by epithelial cells within the intestinal lumen is still challenging *in vitro* [6, 21, 22]. Nowadays, the development of dynamic *in vitro* model systems is performed in academia laboratories using different devices (in shape and materials) and cell culturing protocols. Moreover, the data collected from these studies show a high variability between the different laboratories. The academia knowledge in this fields is rapidly developing and for the future applications of *in vitro* model systems the researchers will be able to define and characterize protocols for a specific purpose and drive the commercialization of in dynamic *in vitro* model technology to improve manufacturing processes, robustness, cost, and ease of use.

References

1. Hubrecht R. C.; Carter E. The 3Rs and Humane Experimental Technique: Implementing Change. Animals 2019. 9, 754.
2. Mähler M.; Berard M.; Feinstein R.; Gallagher A.; Illgen-Wilcke, B.; Pritchett-Corning, K.; Raspa, M. FELASA recommendations for the health monitoring of mouse, rat, hamster, guinea pig and rabbit colonies in breeding and experimental units. Animals. 2014, 48, 178–192.
3. Decreto legislativo 4 marzo 2014, n. 26
4. Marie E.N.; Human Anatomy and Physiology 1, CA Benjamin/Cummings Publ. Company, Ine., Redwood City, 1992, 306–307.
5. Dressman J.B.; Lennernas H.; Oral Drug Absorption: Prediction and Assessment, 2000.
6. Rao J. N.; Wang J. Y. Regulation of gatrointestinal mucosa growth. San Rafael, CA: Morgan & Claypool Life Sciences. Integrated Systems Physiology: from Molecule to Function to Disease. 2010.
7. Gourevitch, D. The Anatomy and Physiology of the Small Bowel, in Upper Gastrointestinal Surgery. 2005, Springer London: London. 39-44.
8. Zheng Feei Ma, Y.Y.L. Small intestine anatomy and physiology in Clinical and Basic Neurogastroenterology and Motility, Y.Y.L. Satish S.C. Rao, Uday C. Ghoshal, Editor. 2020, Academic Press. 101-111.
9. Volk N.; Lacy B. Anatomy and Physiology of the Small Bowel. Gastrointestinal Endoscopy Clinics of North America. 2017. 27, 1, 1-13.
10. Peled J.U.; Hanash A.M.; Jenq R.R. Role of the intestinal mucosa in acute gastrointestinal GVHD. Blood. 2016. 128, 20, 2395-2402.
11. Yamada, T.; Alpers D.H. Textbook of gastroenterology. Blackwell Pub. Chichester, West Sussex. 2009.
12. Gerbe, F. C.; Legraverend P. The intestinal epithelium tuft cells: specification and function. Cellular and Molecular Life Sciences. 2012. 69, 17, 2907-17.
13. Clevers, H. The intestinal crypt, a prototype stem cell compartment. Cell, 2013. 154, 2, 274-84.
14. Walton K.D.; Freddo A.M.; Wang S.; Gumucio D.L. Generation of intestinal surface: an absorbing tale. Development. 2016. 1,143, 13, 2261-72.
15. McConnell R.E.; Higginbotham J.N.; Shifrin Jr D.A.; Tabb, R.J.; Coffey D.L.; Tyska M. J. The enterocyte microvillus is a vesicle-generating organelle, J. Cell Biol. 2009. 185, 1285–1298.
16. Herath M.; Hosie S.; Bornstein J.C.; Franks A.E.; Hill-Yardin E.L. The role of the gastrointestinal mucus system in intestinal homeostasis: implications for neurological disorders, Frontiers in cellular and infection microbiology. 2020. 10.

17. Roda G.; Sartini A.; Zambon E.; Calafiore A.; Marocchi M.; Caponi A.; Belluzzi A.; Roda E. Intestinal epithelial cells in inflammatory bowel diseases. World Journal of Gastroenterology. 2010. 16, 4264.
18. Barker N. Adult intestinal stem cells: critical drivers of epithelial homeostasis and regeneration, Nature Reviews Molecular Cell Biology. 2014. 15 19–33.
19. Barker J.H.; Van Es J.; Kuipers P.; Kujala M.; Van Den Born M.; Cozijnsen A.; Haegebarth J.; Korving H.; Begthel P.J. Identification of stem cells in small intestine and colon by marker gene Lgr5, Nature. 2007. 449 1003–1007.
20. Takuya S. Regulation of the intestinal barrier by nutrients: The role of tight junctions. Journal of Animal Science. 2020. 91 13357.
21. Gunnar C. H. Role of mucus layers in gut infection and inflammation Current Opinion in Microbiology. 2012. 15, 1, 57–62.
22. Pelaseyed T.; Bergström J.H.; Gustafsson J.K.; Ermund A.; Birchenough G.M.; Schütte A, van der Post S.; Svensson F.; Rodríguez-Piñeiro A.M; Nyström E.E.; Wising C.; Johansson M.E.; Hansson G.C. The mucus and mucins of the goblet cells and enterocytes provide the first defense line of the gastrointestinal tract and interact with the immune system. Immunol Reviews. 2014. 260, 1, 8-20.
23. Malin E. V.; Johansson M. P.; Petersson, G.C. Hansson. The inner of the two Muc2 mucin-dependent mucus layers in colon is devoid of bacteria PNAS 2008 105, 39, 15064-15069.
24. Metelsky S.T. Transport phenomena and membrane digestion in small intestinal mucosa: an electrophysiological approach. 2011, Pensoft: Sofia, Russia.
25. Byers J.P.; Sarver J.G. Chapter 10 - Pharmacokinetic Modeling, in Pharmacology, Hacker M.; Messer W.; Bachmann K. Editors. 2009, Academic Press: San Diego. 201-277.
26. Corthesy B. 2013. Multi-faceted functions of secretory IgA at mucosal surfaces. Frontiers in Immunology, 4, 185.
27. Sanz Y. De Palma G. Gut microbiota and probiotics in modulation of epithelium and gut-associated lymphoid tissue function. Int Rev Immunol, 2009. 28(6) 397-413.
28. Lu P.; Sodhi C.P.; Hackam D.J. Toll-like receptor regulation of intestinal development and inflammation in the pathogenesis of necrotizing enterocolitis. Pathophysiology. 2014. 21, 1, 81-93.
29. Castro-Sanchez P.; Martin-Villa J. M. Gut immune system and oral tolerance. British Journal of Nutrition Latest Journal. 2013. 109 Suppl 2: p. S3-11.

30. Hamman J. H.; Enslin, G. M.; Kotzé A. F. Oral delivery of peptide drugs: barriers and developments. Biodrugs: Clinical Immunotherapeutics, Biopharmaceuticals and Gene Therapy. 2005. 19, 3, 165e177.
31. Atuma C.; Strugala V.; Allen A.; Holm L. The adherent gastrointestinal mucus gel layer: thickness and physical state in vivo. American Journal of Physiology – Gastrointestinal and Liver Physiology. 2001. 280, 5, G922eG929.
32. Van der Flier L. G.; Clevers H. Stem cells, self-renewal, and differentiation in the intestinal epithelium. Annual Review of Physiology. 2009. 71, 241e260.
33. Fritsch, C.; Orian-Rousseaul V.; Lefebvre O.; Simon-Assmann P.; Reimund J. M.; Duclos B. Characterization of human intestinal stromal cell lines: response to cytokines and interactions with epithelial cells. Experimental Cell Research. 1999. 248, 2, 391e406.
34. Tang C.; Prueksaritanont T. Use of in vivo animal models to assess pharmacokinetic drug-drug interactions. Pharmceutical Research. 2010. 27, 9, 1772-87.
35. McConnell E.L.; Basit A.W.; Murdan S. Measurements of rat and mouse gastrointestinal pH, fluid and lymphoid tissue, and implications for in-vivo experiments. Journal of Pharmacy and Pharmacology. 2008. 60, 1, 63-70.
36. Hatton G.B. Animal Farm: Considerations in Animal Gastrointestinal Physiology and Relevance to Drug Delivery in Humans. Journal of Pharmacy and Pharmacology. 2015. 104, 9, 2747-76.
37. Gantzsch S.P.; Kann B.; Ofer-Glaessgen M. P.; Loos H.; Berchtold, S.; Balbach, T.; Eichinger, C.M.; Lehr U.F.; Schaefer M. Characterization and evaluation of a modified PVPA barrier in comparison to Caco-2 cell monolayers for combined dissolution and permeation testing. Journal of Pharmacy and Pharmacology. 2014. 175, 79–86.
38. Fritsch C.; Orian-Rousseaul V.; Lefebvre O.; Simon-Assmann, P.; Reimund J. M.; Duclos B. Characterization of human intestinal stromal cell lines: response to cytokines and interactions with epithelial cells. Experimental Cell Research. 1999. 248, 2, 391e406.
39. Kansy M. Physicochemical high throughput screening: Parallel artificial membrane permeation assay in the description of passive absorption processes. J Med Chem 1998. 41, 1007–10.
40. Di L. High throughput artificial membrane permeability assay for blood-brain barrier. European Journal of Medicinal Chemistry. 2003. 38, 223–232.
41. Dagenais C. P-glycoprotein deficient mouse in situ blood-brain barrier permeability and its prediction using an in-combo PAMPA model. European Journal of Pharmaceutical Sciences. 2009. 38, 121–137.

42. Mensch J. Evaluation of various PAMPA models to identify the most discriminating method for the prediction of BBB permeability. European Journal of Pharmaceutics and Biopharmaceutics. European Journal of Pharmaceutics and Biopharmaceutics. 2010. 74, 495–502.
43. Reis J.M.; Sinko B.; Serra C.H.R. Parallel artificial membrane permeability assay (PAMPA) is it better than Caco-2 for human passive permeability prediction? Mini-Reviews in Medicinal Chemistry. 2010. 10, 11, 1071-1076.
44. Yu H.; Wang Y.; Sun, M.; Shen H.; Li Y. Duan A. A new PAMPA model proposed on the basis of a synthetic phospholipid membrane, PLoS One. 2015. 10, 1–13.
45. Mensch J.; Melis A.; Mackie C.; Verreck G., Brewster M.E.; Augustijns P.; Evaluation of various PAMPA models to identify the most discriminating method for the prediction of BBB permeability, European Journal of Pharmaceutics and Biopharmaceutics. 2010. 74, 495–502.
46. Sink´o B.; Garrigues T.M.; Balogh G.T.; Nagy Z.K.; Tsinman O.; Avdeef A.; Tak´acs-Nov´ak K. Skin-PAMPA: A new method for fast prediction of skin penetration. European Journal of Pharmaceutical Sciences. 2012. 45 698–707.
47. Vizserálek, Gábor. “Examination of permeability of drugs by PAMPA method in theoretical and practical aspects Ph.” 2016.
48. Kansy M.; Senner F.; Gubernator K. Physicochemical high throughput screening: parallel artificial membrane permeation assay in the description of passive absorption processes, Journal of Medicinal Chemistry. 1998. 41, 1007–1010.
49. Gantzsch S.P.; Kann B.; Ofer-Glaessgen M.; Loos P.; Berchtold H.; Balbach S.; Eichinger T.; Lehr C.M.; Schaefer U.F., Windbergs M. Characterization and evaluation of a modified PVPA barrier in comparison to Caco-2 cell monolayers for combined dissolution and permeation testing, Journal Controlled Release. 2014. 74, 79–86.
50. Billat P.; Roger E.; Faure S.; Lagarce F. Models for drug absorption from the small intestine: where are we and where are we going? Drug Discovery Today. 2017. 22, 5, 761-775.
51. Hidalgo I.J; Raub T.J; Borchardt R.T. Characterization of the human colon carcinoma cell line (Caco-2) as a model system for intestinal epithelial permeability. Gastroenterology. 1989. 96, 3, 736-749.
52. Wilson G.; Hassan I.F.; Dix C.J. Transport and permeability properties of human caco-2 cells - an in vitro model of the intestinal epithelial-cell barrier. Journal Controlled Release. 1990. 11, 1-3, 25-40.
53. Artursson P. Epithelial transport of drugs in cell culture. I: a model for studying the passive diffusion of drugs over intestinal absorptive (Caco-2) cells. Journal of Pharmaceutical Sciences. 1990. 79, 6, 476-482.

54. Graves C.L. A method for high purity intestinal epithelial cell culture from adult human andmurine tissues for the investigation of innate immune function. Journal of Immunological Methods. 2014. 414, 20-31.
55. Kauffman A.L.; Gyurdieva A.V.; Mabus J.R.; Ferguson C.; Yan Z.; Hornby P.J. Alternative functional in vitro models of human intestinal epithelia. Frontiers in Pharmacology 2013. 4, 79.
56. Eaton A.D.; Zimmermann C.; Delaney B., Hurley B.P. Primary human polarized small intestinal epithelial barriers respond differently to a hazardous and an innocuous protein. Food and Chemical Toxicology. 2017. 106, 70-77.
57. Fogh J.; Orfeo T.; Tiso, J.;Sharkey F. E. Establishment of human colon carcinoma lines in nude mice. Experimental Cell Biology. 1979. 47, 2, 136e144.
58. Artursson P.; Palm K.; Luthman K. Caco-2 monolayers in experimental and theoretical predictions of drug transport. Advanced Drug Delivery. 2001. 46, 27–43.
59. Simon-Assman, P.; Turck, N.; Sidhoum-Jenny M.; Gradwohl G.; Kedinger M. In vitro models of intestinal epithelial cell differentiation. Cell Biology and Toxicology. 2017. 23, 4, 241e256.
60. Maubon N.; Le Vee M.; Fossati L.; Audry M.; Le Ferrec E.; Bolze S.; Fardel O. Analysis of drug transporter expression in human intestinal Caco-2 cells by realtime PCR. Fundamental & Clinical Pharmacology. 2007. 21, 659–663.
61. Olander M.; Wisniewski J.R.; Matsson P.; Lundquist P.; Artursson P. The proteome of filter-grown Caco-2 cells with a focus on proteins involved in drug disposition. Journal of Pharmaceutical Sciences. 2016. 1-11.
62. Mouly S.; Paine M. F. P-glycoprotein increases from proximal to distal regions of human small intestine. Pharmaceutical Research. 2003, 20, 10, 1595e1599.
63. Ungell A. Caco-2 replace or refine?. Drug Discovery Today: Technologies. 2004. 1, 4, 423e430.
64. Artursson P. Cell cultures as models for drug absorption across the intestinal mucosa, Critical Reviews™ in Therapeutic Drug Carrier Systems. 1991. 8, 305–330.J
65. Madara J.L.; Hecht G. Tight (occluding) junctions in cultured (and native) epithelial cells. Function Epithelial Cells Culture. 1989. 131–163.
66. Meunier V.; Bourri´e M.; Berger Y.; Fabre G. The human intestinal epithelial cell line Caco-2; pharmacological and pharmacokinetic applications. Cell Biology and Toxicology 1995. 187–194.
67. Hamalainen M. D.; Frostell-Karlsson A. Predicting the intestinal absorption potential of hits and leads. Drug Discovery Today: Technologies. 2004. 1, 4, 397e405.
68. Dahlgren D.; Lennern¨as H. Intestinal permeability and drug absorption: predictive experimental, computational and in vivo approaches. Pharmaceutics. 2019. 13, 11, 8, 411.

69. De Angelis I.; Turco L. Caco-2 cells as a model for intestinal absorption, Current Protocols in Toxicology. 2011. 1–15.
70. Hu M.; Ling J.; Lin H.; Chen J. Use of Caco-2 Cell monolayers to study drug absorption and metabolism. Optim. Drug Discov. 2004. 19–35.
71. Hubatsch I.; Ragnarsson, E.; Artursson P. Determination of drug permeability and prediction of drug absorption in Caco-2 monolayers. Nature Protocols. 2017. 2, 2111–2119.
72. Lentz K. A.; Hayashi J.; Lucisano L. J.; Polli J. E. Development of a more rapid, reduced serum culture system for Caco-2 monolayers and application to the biopharmaceutics classification system. International Journal of Pharmaceutics. 2000. 1, 41e51.
73. Sevin E.; Dehouck, L.; Fabulas-da Costa A.; Cecchelli R.; Dehouck M. P.; Lundquist S. Accelerated Caco-2 cell permeability model for drug discovery. Journal of Pharmacological and Toxicological Methods. 2013. 68, 3, 334e339.
74. Chong S.; Dando S.; Morrison R. Evaluation of Biocoat intestinal epithelium differentiation environment (3-day cultured Caco-2 cells) as an absorption screening model with improved productivity. Pharmaceutical Research. 1997. 14, 12, 1835e1837.
75. Sevin E.; Dehouck L.; Fabulas-da Costa A.; Cecchelli R.; Dehouck M. P.; Lundquist S. Accelerated Caco-2 cell permeability model for drug discovery. Journal of Pharmacological and Toxicological Methods. 2013. 68, 3, 334e339.
76. Peng Y.; Yadava P.; Heikkinen A. T.; Parrott N.; Railkar A. Applications of a 7-day Caco-2 cell model in drug discovery and development. European Journal of Pharmaceutical Sciences. 2014. 56, 120e130.
77. Turco L.; Catone T.; Caloni F.; Di Consiglio E.; Testai E.; Stammati A. Caco-2/TC7 cell line characterization for intestinal absorption: how reliable is this in vitro model for the prediction of the oral dose fraction absorbed in human? Toxicology in Vitro. 2011. 25, 1, 13e20.
78. Lyubimov A.V.; Le Ferrec E.; Fardel O. Applications using Caco-2 and TC7 cells for drug metabolism studies. Encyclopedia of Drug Metabolism and Interactions. 2012.
79. Gres M. C.; Julian B.; Bourrie M.; Meunier V.; Roques C.; Berger M. Correlation between oral drug absorption in humans, and apparent drug permeability in TC-7 cells, a human epithelial intestinal cell line: comparison with the parental Caco-2 cell line. Pharmaceutical Research. 1998. 15, 5, 726e733.
80. Mahler G. J.; Shuler M. L.; Glahn R. P. Characterization of Caco-2 and HT29-MTX cocultures in an in vitro digestion/cell culture model used to predict iron bioavailability. The Journal of Nutritional Biochemistry. 2009. 20, 7, 494e502.

81. Pontier C.; Pachot J.; Botham R.; Lenfant B.; Arnaud P. HT29-MTX and Caco-2/TC7 monolayers as predictive models for human intestinal absorption: role of the mucus layer. Journal of Pharmaceutical Sciences. 2001. 90, 10, 1608e1619.
82. Antunes F.; Andrade F.; Ferreira D.; Morck Nielsen H.; Sarmento B. Models to predict intestinal absorption of therapeutic peptides and proteins. 2012. Currurent Drug Metabolism. 2012, 14, 4–20.
83. Martínez-Maqueda D.; Miralles B.; Recio I. HT29 Cell Line BT, in: K. Verhoeckx, P. Cotter, I. L´opez-Exp´osito, C. Kleiveland, T. Lea, A. Mackie, H. Wichers (Eds.), The Impact of Food Bioactives on Health: in vitro and ex vivo models. Springer International Publishing Cham. 2015. 113–124.
84. Rousset M. The human colon carcinoma cell lines HT-29 and Caco-2: two in vitro models for the study of intestinal differentiation, Biochimie. 1986. 68, 1035–1040.
85. Araujo F.; Sarmento B. Towards the characterization of an in vitro triple co-culture intestine cell model for permeability studies. International Journal of Pharmaceutics. 2013. 458, 1, 128e134.
86. Gullberg E.; Leonard M.; Karlsson J.; Hopkins A. M.; Brayden D.; Baird A. W. Expression of specific markers and particle transport in a new human intestinal M-cell model. Biochemical and Biophysical Research Communications. 2000. 279, 3, 808e813.
87. Kerneis S.; Bogdanova A.; Kraehenbuhl J. P.; Pringault E. Conversion by Peyer's patch lymphocytes of human enterocytes into M cells that transport bacteria. Science. 1997. 277, 5328, 949e952.
88. S. Kern´eis, A.; Bogdanova J.P.; Kraehenbuhl E. Conversion by Peyer's patch lymphocytes of human enterocytes into M cells that transport bacteria, Science. 1997. 80 277, 949–952.
89. Des Rieux A.; Fievez V.; Theate I.; Mast J.; Preat V.; Schneider Y. J. An improved in vitro model of human intestinal follicle-associated epithelium to study nanoparticle transport by M cells. European Journal of Pharmaceutical Sciences. 2007. 30, 5, 380e391.
90. Antunes F.; Andrade F.; Araujo F.; Ferreira D.; Sarmento B. Establishment of a triple co-culture in vitro cell models to study intestinal absorption of peptide drugs. European Journal of Pharmaceutics and Biopharmaceutics. 2013. 83, 3, 427e435.
91. Araújo F.; Sarmento B. Towards the characterization of an in vitro triple coculture intestine cell model for permeability studies. International Journal of Pharmaceutics. 2013. 458. 128–134.
92. Negoro R. Modeling of drug-mediated CYP3A4 induction by using human iPS cell-derivedenterocyte-like cells. Biochemical and Biophysical Research Communications. 2016. 472, 4, 631-636.

93. Kabeya T.; Qiu S.; Hibino M.; Nagasaki M.; Kodama N.; Iwao T.; Matsunaga T. Cyclic AMP Signaling Promotes the Differentiation of Human Induced Pluripotent Stem Cells into Intestinal Epithelial Cells. Drug Metab Dispos, 2018. 46, 10, 1411-1419.
94. Kabeya T.; Matsumura W.; Iwao T.; Hosokawa M.; Matsunaga T. Functional analysis of carboxylesterase in human induced pluripotent stem cell-derived enterocytes. Biochemical and Biophysical Research Communications. 2017. 486, 143-148.
95. Takenaka, T.; Harada N.; Kuze J.; Chiba M.; Iwao T.; Matsunaga T. Human Small Intestinal Epithelial Cells Differentiated from Adult Intestinal Stem Cells as a Novel System for Predicting Oral Drug Absorption in Humans. Drug Metabolism and Disposition, 2014. 42, 11, 1947.
96. Kodama, N.; Iwao T.; Katano T.; Ohta K.; Yuasa H.; Matsunaga T. Characteristic Analysis of Intestinal Transport in Enterocyte-Like Cells Differentiated from Human Induced Pluripotent Stem Cells. Drug Metabolism and Disposition. 2016. 44, 10.
97. Kim H.J.; Ingber D.E. Gut-on-a-Chip microenvironment induces human intestinal cells to undergo villus differentiation. Integrative Biology. 2013. 5, 1130–1140,
98. Skardal A.; Shupe T.; Atala A. Organoid-on-a-chip and body-on-a-chip systems for drug screening and disease modelling. Drug Discovery Today. 2016. 21, 1399–1411.
99. Li N.; Wang D.; Sui Z.; Qi X.; Ji L.; Wang X. Development of an improved 3D in vitro intestinal mucosa model for drug absorption evaluation. Tissue Engineering. Part C, Methods. 2013. 19,9, 708e719.
100. Visco V.; Bava F. A.; D'Alessandro F.; Cavallini M.; Ziparo V.; Torrisi M. R. Human colon fibroblasts induce differentiation and proliferation of intestinal epithelial cells through the direct paracrine action of keratinocyte growth factor. Journal of Cellular Physiology. 2009. 220, 1, 204e213.
101. Mouly S.; Paine M. F. P-glycoprotein increases from proximal to distal regions of human small intestine. Pharmaceutical Research 2013. 20, 10, 1595e1599.
102. Moyes S. M.; Morris J. F.; Carr K. E. Macrophages increase microparticle uptake by enterocyte-like Caco-2 cell monolayers. Journal of Anatomy. 2010. 217, 6, 740e754.
103. Sung J. H.; Yu J.; Luo D.; Shuler M. L.; March J. C. Microscale 3-D hydrogel scaffold for biomimetic gastrointestinal (GI) tract model. Lab Chip. 2013. 11 ,3, 389e392.
104. Yu Q.H.; Yang Q. Diversity of tight junctions (TJs) between gastrointestinal epithelial cells and their function in maintaining the mucosal barrier. Cell Biology International. 2009. 33, 1, 78e8
105. Costa J.; Ahluwalia A. Advances and current challenges in intestinal in vitro model engineering: a digest. Frontiers in Bioengineering and Biotechnology. 2019. 7, 1–14.

106. Dedhia P.H.; Bertaux-Skeirik N.; Zavros Y.; Spence J.R. Organoid models of human gastrointestinal development and disease. Gastroenterology. 2016, 150, 1098–1112.
107. Fair K.L.; Colquhoun J.; Hannan N.R.F. Intestinal organoids for modelling intestinal development and disease, Philosophical Transactions of the Royal Society B: Biological Sciences. 2018. 373.
108. Conder R. Intestinal organoid culture: the history of intestinal organoids using intestinal organoids as a model culture system, Stem Cell Review. 2015. 1–4.
109. Zietek T.; Giesbertz P.; Ewers M.; Reichart F.; Weinmüller M.; Urbauer E.; Haller D.; Demir I.E.; Ceyhan G.O.; Kessler H.; Rath E. Organoids to study intestinal nutrient transport, drug uptake and metabolism – update to the human model and expansion of applications. Frontiers in Bioengineering and Biotechnology. 2020. 8, 1–14.
110. Rahmani S.; Breyner N.M.; Su H.M.; Verdu E.F.; Didar T.F. Intestinal organoids: a new paradigm for engineering intestinal epithelium in vitro, Biomaterials. 2019. 194, 195–214.
111. Sung J. H.; Yu J.; Luo D.; Shuler M. L.; March J. C. Microscale 3-D hydrogel scaffold for biomimetic gastrointestinal (GI) tract model. Lab Chip. 2011. 11, 3, 389e392.
112. Mehling M.; Tay S. Microfluidic cell culture, Current Opinion in Biotechnology. 2014. 25, 95–102.
113. Kim H.J.; Li H.; Collins J.J.; Ingber D.E. Contributions of microbiome and mechanical deformation to intestinal bacterial overgrowth and inflammation in a human gut-on-a-chip, Proceedings of the National Academy of Sciences. U. S. A. 2016. 113, E7–E15.
114. Steinway S.N.; Saleh J.; Koo B.K.; Delacour D.; Kim D.H. Human microphysiological models of intestinal tissue and gut microbiome. Frontiers in Bioengineering and Biotechnology. 2020. 31,8, 725.
115. Fedi A.; Vitale C.; Ponschin G.; Ayehunie S.; Fato M.; Scaglione S. In vitro models replicating the human intestinal epithelium for absorption and metabolism studies: A systematic review. J Control Release. 2021. 10, 335, 247-268.
116. Heo Y.S.; Cabrera L.M.; Song J.W.; Futai N.; Tung Y.C.: Smith G.D.; Takayama S. Characterization and resolution of evaporation-mediated osmolality shifts thatconstrain microfluidic cell culture in poly(dimethylsiloxane) devices. Analytical Chemistry. 2007. 79, 3, 1126-34.
117. Pocock K.; Delon L.; Bala V.; Rao S.; Priest C.; Prestidge C.; Thierry B.; Intestinal-on-a-chip microfluidic model for efficient in vitro screening of oral chemotherapeutic uptake, ACS Biomaterial and Science Engineering. 2017. 951–959.

118. Kulthong K.; Duivenvoorde L.; Sun H.; Confederat S.; Wu J.; Spenkelink B.; De Haan L.; Marin V.; Van der Zande M.; Bouwmeester H. Microfluidic chip for culturing intestinal epithelial cell layers: characterization and comparison of drug transport between dynamic and static models, Toxicology in Vitro. 2020. 65, 104815.
119. K. Kulthong, L. Duivenvoorde, B.Z. Mizera, D. Rijkers, G. Ten Dam, G. Oegema, T. Puzyn, H. Bouwmeester, M. Van Der Zande, Implementation of a dynamic intestinal gut-on-a-chip barrier model for transport studies of lipophilic dioxin congeners, RSC Adv. 8 (2018) 32440–32453,
120. Kim H.J.; Huh D.; Hamilton G.; Ingber D.E. Human gut-on-a-chip inhabited by microbial flora that experiences intestinal peristalsis-like motions and flow, Lab Chip. 2012, 12, 2165–2174.
121. Kim H.J.; Ingber D.E. Gut-on-a-Chip microenvironment induces human intestinal cells to undergo villus differentiation. Integrative Biology. 2013. 5, 1130–1140.
122. Gao D.; Liu H.; Lin J.M., Wang Y.; JiangY. Characterization of drug permeability in Caco-2 monolayers by mass spectrometry on a membrane-based microfluidic device, Lab Chip. 2013, 13, 978–985.
123. Tan H.Y.; Trier S.; Rahbek U.L.; Dufva M.; Kutter J.P.; Andresen T.L. A multichamber microfluidic intestinal barrier model using Caco-2 cells for drug transport studies. PLoS One. 2018, 13 1–23.
124. Chi, M., Yi B.; Oh S.; Park D.J.; Sung J.H.; Park S. A microfluidic cell culture device (muFCCD) to culture epithelial cells with physiological and morphological properties that mimic those of the human intestine. Biom Microdevices, 2015. 17, 3, 9966.
125. Delon L.C.; Guo Z.; Oszmiana A.; Chien C.; Gibson R.; Prestidge C.; Thierry B. A systematic investigation of the effect of the fluid shear stress on Caco-2 cells towards the optimization of epithelial organ-on-chip models. Biomaterials. 2019. 225, 119521.
126. Pereira C.; Costa J.; Sarmento B.; Araújo F. Cell-based in vitro models for intestinal permeability studies Concepts and models for drug permeability studies. 2016. 57-81.
127. Frei B.; England L.; Ames B.N. Ascorbate is an outstanding antioxidant in human blood plasma. Proceedings of the National Academy of Sciences. 1989. 86, 6377-6381.
128. Gershoff S.N. Vitamin C (ascorbic acid): new roles, new requirements? Nutrition Reviews. 1993. 51, 313-326.
129. Carr A.C.; Maggini S. Vitamin C and Immune Function. Nutrients. 2017. 9, 1211.
130. Webb A.L.; Villamor E. Update: Effects of antioxidant and non-antioxidant vitamin supplementation on immune function. Nutrition Reviews. 2007. 65, 181.
131. Burns J.J. Missing step in man, monkey and guinea pig required for the biosynthesis of L-ascorbic acid. Nature. 1957, 180, 553.

132. Carr A.C.; Bozonet S.M.; Pullar J.M.; Simcock J.W.; Vissers M.C. Human skeletal muscle ascorbate is highly responsive to changes in vitamin C intake and plasma concentrations. The American Journal of Clinical Nutrition. 2013b. 97, 800–807.
133. Nishikimi M.; Fukuyama R.; Minoshima S.; Shimizu N.; Yagi K. Cloning and chromosomal mapping of the human nonfunctional gene for L-gulono-gamma-lactone oxidase, the enzyme for L-ascorbic acid biosynthesis missing in man. Journal of Biological Chemistry. 1994, 269, 13685–13688.
134. Sauberlich H.E. A history of scurvy and vitamin C. In Vitamin C in Health and Disease; Packer, L., Fuchs, J.,Eds.; Marcel Dekker: New York, NY, USA, 1997. 1–24.
135. Schleicher R.L.; Carroll M.D.; Ford E.S.; Lacher D.A. Serum vitamin C and the prevalence of vitamin C deficiency in the United States: 2003–2004 National Health and Nutrition Examination Survey (NHANES). American Journal of Clinical Nutrition. 2009. 90, 1252–1263.
136. US Centers for Disease Control and Prevention. Second National Report on Biochemical Indicators of Diet and Nutrition in the US Population 2012; National Center for Environmental Health: Atlanta, GA, USA, 2012.
137. Maggini S.; Beveridge S.; Sorbara J.; Senatore G. Feeding the immune system: The role of micronutrients in restoring resistance to infections. CAB Rev. 2008. 3, 1–21.
138. Huskisson E.; Maggini S.; Ruf M. The role of vitamins and minerals in energy metabolism and well-being. Journal of International Medical Research. 2007. 35, 277–289.
139. Lindblad M.; Tveden-Nybor, P.; Lykkesfeldt J. Regulation of vitamin C homeostasis during deficiency. Nutrients 2013. 5, 2860–2879.
140. Wilson J.X. Regulation of vitamin C transport. Annual Review of Nutrition. 2005. 25, 105–125.
141. Sotiriou S.; Gispert S.; Cheng J.; Wang Y.; Chen A.; Hoogstraten-Miller S.; Miller G.F.; Kwon O.; Levine M.; Guttentag S.H.; Nussbaum R.L. Ascorbic-acid transporter Slc23a1 is essential for vitamin C transport into the brain and for perinatal survival. Nature Medicine. 2002. 8, 5, 514-517.
142. Nielsen T.K.; Hojgaard M.; Andersen J.T.; Poulsen H.E.; Lykkesfeldt J.; Mikines K.J. Elimination of ascorbic acid after high-dose infusion in prostate cancer patients: A pharmacokinetic evaluation. Basic & Clinical Pharmacology & Toxicology. 2015. 116, 343–348.
143. Buettner G.R. The pecking order of free radicals and antioxidants: Lipid peroxidation, alpha-tocopherol, and ascorbate. Archives of Biochemistry and Biophysics. 1993. 300, 535–543.
144. Du J.; Cullen J.J.; Buettner G.R. Ascorbic acid: Chemistry, biology and the treatment of cancer. Biochimica et Biophysica Acta. 2012. 1826, 443–457.
145. Lykkesfeldt J.; Tveden-Nyborg P. The Pharmacokinetics of Vitamin C. Nutrients. 2019. 11, 2412.

146. Kubler, W.; Gehler, J. Kinetics of intestinal absorption of ascorbic acid. Calculation of non-dosage-dependent absorption processes. Int Z Vitaminforsch. 1970. 40, 442–453.
147. Mayersohn M. Ascorbic acid absorption in man—Pharmacokinetic implications. European Journal of Pharmacology. 1972. 19, 140–142.
148. May J.M.; Qu Z.; Morrow J.D. Mechanisms of ascorbic acid recycling in human erythrocytes. Biochimica et Biophysica Acta (BBA). 2001. 1528, 159–166.
149. Mendiratta S.; Qu Z.C.; May J.M. Enzyme-dependent ascorbate recycling in human erythrocytes: Role of thioredoxin reductase. Free Radical Biology and Medicine. 1998a. 25, 221–228.
150. Mendiratta S.; Qu Z.C.; May J.M. Erythrocyte ascorbate recycling: Antioxidant effects in blood. Free Radical Biology and Medicine. 1998b. 24, 789–797.
151. Banhegyi G.; Braun L.; Csala M.; Puskas F.; Mandl J. Ascorbate metabolism and its regulation in animals. Free Radical Biology and Medicine. 1997. 23, 793–803.
152. Corpe C.P.; Lee J.H.; Kwon O.; Eck P.; Narayanan J.; Kirk K.L.; Levine, M. 6-Bromo-6-deoxy-l-ascorbic acid: An ascorbate analog specific for Na^+-dependent vitamin C transporter but not glucose transporter pathwaysJournal of Biological Chemistry. 2005. 280, 5211–5220.
153. Haytowitz D. Information from USDA's Nutrient Data Book. Journal of Nutrition. 1995. 125, 1952-1955.
154. Baskaran A. Acerola, an untapped functional superfruit: a review on latest frontiers. Journal of Food Science and Technology. 2018. 55, 9, 3373–3384.
155. Sirajudeen S.; Shah I.; Al Menhali A. A narrative role of vitamin D and its receptor: with current evidence on the gastric tissues. International Journal of Molecular Sciences. 2019. 20, 3832.
156. Deluca H.F. History of the discovery of vitamin D and its active metabolites. Bonekey Rep. 2014. 3, 479.
157. Lips P.; Cashman K.D.; Lamberg-Allardt C, Bischoff-Ferrari H.A.; Obermayer-Pietsch B.; Bianchi M.L.; Stepan J.; El-Hajj Fuleihan G.; Bouillon R. Current vitamin D status in European and middle east countries and strategies to prevent vitamin D deficiency: A position statement of the European calcified tissue society. European Journal of Endocrinology. 2019. 180, 23, 54.
158. EFSA NDA Panel (EFSA Panel on Dietetic Products, Nutrition and Allergies). Scientific opinion on dietary reference values for vitamin D. EFSA Journal 2016. 1, 10, 4547, 145.
159. Kristensen H.L.; Rosenqvist E.; Jakobsen J. Increase of vitamin D(2) by UV-B exposure during the growth phase of white button mushroom (Agaricus bisporus). Food & Nutrition Research. 2012. 56, 7114.
160. Tangpricha V. Vitamin D in food and supplements. American Journal of Clinical Nutrition. 2012. 95, 1299–1300.

161. Schmid A.; Walther B. Natural vitamin D content in animal products. Advances in Nutrition. 2013. 4, 453–462.
162. Mattila P.H.; Valkonen E.; Valaja J. Effect of different vitamin D supplementations in poultry feed on vitamin D content of eggs and chicken meat. Journal of Agricultural and Food Chemistry. 2012. 2, 59, 8298–8303.
163. Liu J.; Greenfield H.; Strobel N.; Fraser D.R. The influence of latitude on the concentration of vitamin D3 and 25-hydroxy-vitamin D3 in Australian red meat. Food Chemistry. 2013. 140, 432–435.
164. Tripkovic L.; Lambert H.; Hart K.; Smith C.P.; Bucca G.; Penson S.; Chope G.; Hyppönen E.; Berry J.; Vieth R.; Lanham-New S. Comparison of vitamin D2 and vitamin D3 supplementation in raising serum 25-hydroxyvitamin D status: A systematic review and meta-analysis. The American Journal of Clinical Nutrition. 2012. 95, 1357-1364.
165. Lehmann U.; Hirche F.; Stangl G.I.; Hinz K.; Westphal S.; Dierkes J. Bioavailability of vitamin D2 and D3 in healthy volunteers, a randomised placebo-controlled trial. The Journal of Clinical Endocrinology and Metabolism. 2013. 98, 4339-4345.
166. Logan V.F.; Gray A.R.; Peddie M.C.; Harper M.J.; Houghton L.A. Long-term vitamin D3 supplementation is more effective than vitamin D2 in maintaining serum 25-hydroxyvitamin D status over the winter months. British Journal of Nutrition. 2013. 109,1082-1088.
167. Tripkovic L.; Wilson L.R.; Hart K.; Johnsen S.; De Lusignan S.; Smith C.P.; Bucca G.; Penson S.; Chope G.; Elliott R.; Hyppönen E.; Berry J.L; Lanham-New SA. Daily supplementation with 15 μg vitamin D2 compared with vitamin D3 to increase wintertime 25-hydroxyvitamin D status in healthy South Asian and white European women: A 12-wk randomized, placebo-controlled food-fortification trial. The American Journal of Clinical Nutrition. 2017. 106, 481-490.
168. Amrein K.; Scherkl M.; Hoffmann M.; Neuwersch-Sommeregger S.; Köstenberger M.; Tmava Berisha A.; Martucci G.; Pilz S.; Malle O. Vitamin D deficiency 2.0: an update on the current status worldwide. European Journal of Clinical nutrition. 2020. 74, 1498-1513.
169. Deschasaux M.; Souberbielle J.C.; Andreeva V.A.; Sutton A.; Charnaux N.; Kesse-Guyot E.; Latino-Martel P.; Druesne-Pecollo N.; Szabo de Edelenyi F.; Galan P.; Hercberg S.; Ezzedine K.; Touvier M. Quick and Easy Screening for Vitamin D Insufficiency in Adults: A Scoring System to Be Implemented in Daily Clinical Practice. Medicine. 2016. 95,7, e2783.
170. Engelsen O, Brustad M, Aksnes L and Lund E. Daily duration of vitamin D synthesis in human skin withrelation to latitude, total ozone, altitude, ground cover, aerosols and cloud thickness. Photochemistry and Photobiology. 2005. 81, 1287–1290.

171. Clemens T.L.; Adams J.S.; Henderson S.L.; Holick M.F. Increased skin pigment reduces the capacity of skin to synthesize vitamin D3 Lancet. 1982. 1. 74-76.
172. Zittermann A.; Frisch S.; Berthold H.K.; Götting C.; Kuhn J.; Kleesiek K.; Stehle P.; Koertke H.; Koerfer R. Vitamin D supplementation enhances the beneficial effects of weight loss on cardiovascular risk markers. The American Journal of Clinical Nutrition. 2009. 89 1321-1327.
173. Righetto A.M.; Netoo F.M.; Carraro F. Chemical Composition and Antioxidant Activity of juices from Mature and Immature acerola (Malpighia emarginata DC). Food Science and Technology International. 2005. 11, 315–321.
174. Mezadri T.; Villano D.; Fernandez-Pachon M.S.; Garcia-Parrilla M.C.; Troncoso A.M. Antioxidant compounds and antioxidant activity in acerola (Malpighia emarginata DC.) fruits and derivatives. Journal of Food Composition and Analysis. 2008. 21, 282–290.
175. Lima V.L.A.G.; Melo E.A.; Maciel M.I.S.; Prazeres F.G.; Musser R.S.; Lima D.E.S. Total phenolic and carotenoid contents in acerola genotypes harvested at three ripening stages. Food Chemistry. 2005. 90, 565–568.
176. Fidelis M.; Maiara de Oliveira S.; Sousa Santos J.; Bragueto G. E.; Rocha R. S.; Gomes A.; Araújo Vieira do Carmo M.; Azevedo L.; Kaneshima T.; Young Oh W.; Shahidi F.; Granato D. From by-product to a functional ingredient: Camu-camu (Myrciaria dubia) seed extract as an antioxidant agent in a yogurt model, Journal of Dairy Science. 2020. 103,2, 1131-1140.
177. Chang S., Cesarettin Alasalvar & Fereidoon Shahidi. Superfruits: Phytochemicals, antioxidant efficacies, and health effects – A comprehensive review. Critical Reviews in Food Science and Nutrition. 2019. 59, 10, 1580-1604.
178. Neri-Numa I. A.; Renata A. Sancho S.; Aparecida A. P.; Pereira G. Pastore M. Small Brazilian wild fruits: Nutrients, bioactive compounds, health-promotion properties and commercial interest. Food Research International 103 (2018) 345–360.
179. Chirinos R.; Galarza J.; Betalleluz-Pallardel I.; Pedresch, R.; Campos D. Antioxidant compounds and antioxidant capacity of Peruvian camu-camu (Mirciaria dubia (H.B.K.) McVaugh) fruit at different maturity stage. Food Chemistry, 2010. 120, 1019–1024.
180. Traka M. H.; Mitchen, R. F. Plant science and human nutrition: Challenges in assessing health-promoting properties of phytochemicals. The Plant Cell, 2011. 23, 2483–2497.
181. Fracassetti D.; Costa C.; Moulay L.; Tomás-Barberán FA. Ellagic acid derivatives, ellagitannins, proanthocyanidins and other phenolics, vitamin C and antioxidant capacity of two powder products from camu-camu fruit (Myrciaria dubia). Food Chemistry. 2013. 15, 139. 1-4, 578-88.
182. National Nutrient Database for Standard Reference.

183. Günes M. Pomological and phenological characteristics of promising rose hip (Rosa) genotypes. African Journal of Biotechnology 2010, 9, 38, 6301–6306.
184. Larsen E.; Kharazmi A, Christensen LP, Christensen SB: An antiinflammatory galactolipid from rose hip (Rosa canina L.) that inhibits chemotaxis of human peripheral blood neutrophils in vitro. Journal of Natural Products. 2003. 66, 7, 994–995.
185. Keltz F.R.; Kies C.; Fox H.M. Urinary ascorbic acid excretion in the human as affected by dietary fiber and zinc. The American Journal of Clinical Nutrition. 1978. 31, 1167–1171.
186. Harper K.A.; Morton A.D.; Rolfe, E.J. The phenolic compounds of blackcurrant juice and their protective effect on ascorbic acid III. The mechansim of ascorbic acid oxidation and its inhibition by flavonoids. Int. J. Food Sci. Technol. 1969. 4, 255–267.
187. Clegg K.M.; Morton A.D. The phenolic compounds of blackcurrant juice and their protective effect on ascorbic acid II. The stability of ascorbic acid in model systems containing some of the phenolic compounds associated with blackcurrant juice. International Journal of Food Science & Technology- 1968. 3, 277–284.
188. Takino Y.; Aoki H.; Kondo Y.; Ishigami A. Acerola (*Malpighia emarginata* DC.) Promotes Ascorbic Acid Uptake into Human Intestinal Caco-2 Cells via Enhancing the Gene Expression of Sodium-Dependent Vitamin C Transporter 1. J Nutr Sci Vitaminology. 2020. 66, 4, 296-299.
189. Inoue, T. H.; Komoda, T.; Uchida T. Tropical fruit camu camu (*Myrciaria dubia*) has anti-oxidative and anti-inflammatory properties. Journal of Cardiology. 2008. 52, 127–132.
190. Thompson G.R.; Lewis B.; Booth C.C. Absorption of vitamin D3-3H in control subjects and patients with intestinal malabsorption. Journal of Clinical Investigation. 1966. 45, 94–102.
191. Lo C.W.; Paris P.W.; Clemens T.L.; Nolan J.; Holick M.F. Vitamin D absorption in healthy subjects and in patients with intestinal malabsorption syndromes. American Journal of Clinical Nutrition. 1985. 42, 644–649.
192. Jones K.S.; Assar S.; Harnpanich D.; Bouillon R.; Lambrechts D.; Prentice A.; Schoenmakers I. 25(OH)D2 half-life is shorter than 25(OH)D3 half-life and is influenced by DBP concentration and genotype. The Journal of clinical endocrinology and metabolism. 2014. 99, 9, 3373–3381.
193. Borel P.; Caillaud D.; Cano N.J. Vitamin d bioavailability: state of the art. Critical Reviews in Food Science and Nutrition. 2015. 55, 1193–1205.
194. Reboul E. Intestinal absorption of vitamin D: from the meal to the enterocyte. Food and Function. 2015. 6, 356–362.
195. Maurya V.K.; Aggarwal M. Factors influencing the absorption of vitamin D in GIT: An overview. J Food Nutr Sci. 2017. 2917, 3753-3765.

196. Glowka E.; Stasiak J.; Luek J. Drug delivery systems for vitamin D supplementation therapy. Pharmaceutics. 2019. 11, 347.
197. Grossmann R.E.; Tangpricha V. Evaluation of vehicle substances on vitamin D bioavailability: a systematic review. Molecular Nutrition and Food Research. 2010. 54, 1055–1061.
198. Jones G.; Prosser D.E.; Kaufmann M. Cytochrome P450-mediated metabolism of vitamin D. Journal of Lipid Research. 2014. 55,1, 13-31.
199. Jones K.S.; Assar S.; Harnpanich D.; Bouillon, R. 25(OH)D2 halflife is shorter than 25(OH)D3 half-life and is influenced by DBP concentration and genotype. Journal of Clinical Endocrinology and Metabolism. 2014. 99, 3373–3381.
200. Gropper, S., Smith, J. and Groff, J. Advanced Nutrition and Human Metabolism. 2013. 6th Edition, Wadsworth, Cengage Learning, Belmont.
201. Dankers W.; Colin E.M.: Van Hamburg J.P.; Lubberts E. Vitamin D in Autoimmunity: Molecular Mechanisms and Therapeutic Potential. Frontiers in immunology. 2017. 20,7, 697.
202. Holick M.F. Resurrection of vitamin D deficiency and rickets. Journal of Clinical Investigation. 2006. 116, 2062–2072.
203. Maurya V.K.; Aggarwal M. Factors influencing the absorption of vitamin D in GIT: an overview. Journal of Food and Nutrition Sciences. 2017. 3753-3765.
204. Holmberg I.; Berlin T.; Ewerth S.; Bjorkhem I. 25-Hydroxylase activity in subcellular fractions from human liver. Evidence for different rates of mitochondrial hydroxylation of vitamin D2 and D3. Scandinavian Journal of Clinical and Laboratory Investigation. 1986. 46: 785–790.
205. Tripkovic L.; Wilson L.R.; Hart K.; Johnsen S.; De Lusignan S.; Smith C.P.; Bucca G.; Penson S.; Chope G.; Elliott R.; Hyppönen E.; Berry J.L.; Lanham-New S.A. Daily supplementation with 15 μg vitamin D2 compared with vitamin D3 to increase wintertime 25-hydroxyvitamin D status in healthy South Asian and white European women: a 12-wk randomized, placebo-controlled food-fortification trial. The American Journal of Clinical Nutrition. 2017. 106, 2, 481-490.
206. Haussler M.R.; Whitfield G.K.; Haussler C.A.; Hsieh J.C.; Thompson P.D.; Selznick S.H.; Dominguez C.E.; Jurutka P.W. The nuclear vitamin D receptor: biological and molecular regulatory properties revealed. Journal of Bone and Mineral Research. 1998. 13, 325.
207. Bouillon R.; Carmeliet G.; Verlinden L.; Van Etten E.; Verstuyf A.; Luderer H.F.; Lieben L.; Mathieu C.; Demay M. Vitamin D and human health: lessons from vitamin D receptor null mice. Endocrine Reviews. 2008. 29, 726.
208. Zügel U.; Gallo R.L.; Eisenberg D.; Hewison M.; Hollis B.W.; Adams J.S.; Bloom B.R.; Modlin R.L. Toll-like receptor triggering of a vitamin D-mediated human antimicrobial response. Science. 2006. 311, 1770.

209. Sirajudeen S.; Shah I.; Al Menhali A. A narrative role of vitamin D and its receptor: with current evidence on the gastric tissues. International Journal of Molecular Sciences. 2019. 20, 3832.
210. Christakos S.; Hewison M.; Gardner D.G.; Wagner C.L.; Sergeev I.N.; Rutten E.; Pittas A.G.; Boland R.; Ferrucci L.; Bikle D.D. Vitamin D: beyond bone. Annals of the New York Academy of Sciences. 2013. 1287. 1. 45-58.
211. Amrein K.; Scherkl M.; Hoffmann M.; Neuwersch-Sommeregger S.; Köstenberger M.; Tmava Berisha A.; Martucci G.; Pilz S.; Malle O. Vitamin D deficiency 2.0: an update on the current status worldwide. European Journal of Clinical Nutrition. 2020. 74, 11, 1498-1513.
212. Griffin G.; Hewison M.; Hopkin J.; Kenny R.; Quinton R.; Rhodes J.; Subramanian S.; Thickett D. Vitamin D and COVID-19: evidence and recommendations for supplementation. Royal Society Open Science. 2020. 1, 7, 12, 201912.
213. Committee on Herbal Medicinal Products (HMPC). European Union herbal monograph on Cetraria islandica (L.) Acharius s.l., thallus. European medicines agency. 2014.
214. Freysdottir J.; Omarsdottir S.; Ingólfsdóttir K.; Vikingsson A.; Olafsdottir ES. *In vitro* and *in vivo* immunomodulating effects of traditionally prepared extract and purified compounds from *Cetraria islandica.* Int International Immunopharmacology. 2008. 8, 3, 423-30. 217.
215. Minekus M.; Alminger P.; Alvito S.; Ballance T.; Bohn C.; Bourlieu F.; Carrière R.; Boutrou M.; Corredig D.; Dupont C.; Dufour L.; Egger M.; Golding S.; Karakaya B.; Kirkhus S.; Le Feunteun U.; Lesmes A.; Macierzanka A.; Mackie S.; Marze D.J.; McClements O.; Ménard I.; Recio C. N.; Santos R.P.; Singh G.E.; Vegarud M.S.J.; Wickham W.; Weitschies A.; Brodkorb a. A standardised static in-vitro digestion method suitable for food – an international consensus Food Function. 2014,5, 1113-1124.
216. Hubatsch I.; Ragnarsson E.G.E.; Artursson P. Determination of drug permeability and prediction of drug absorption in Caco-2 monolayers. Nature Protocols. 2007. 2,9, 2111-2119.
217. Singleton V.L.; Orthofer R.; Lamuela-Raventós R.M. Analysis of total phenols and other oxidation substrates and antioxidants by averages of folin-ciocalteu reagent. Methods in Enzymology. 1999. 299, 152–178.
218. Georgé S.; Brat P.; Alter P.; Amiot M. J. Rapid Determination of Polyphenols and Vitamin C in Plant-Derived Products. Journal of Agricultural and Food Chemistry. 2005. 53, 5, 1370-1377.
219. Kim H.J.; Hamilton G.; Ingber DE. Human gut-on-a-chip inhabited by microbial flora that experiences intestinal peristalsis-like motions and flow. Lab Chip. 2012. 12, 12, 2165-2174.
220. Jun Y.; Lee J.; Choi S.; Yang J.H.; Sander M.; Chung S.; Lee S.H. In vivo-mimicking microfluidic perfusion culture of pancreatic islet spheroids. Science Advances. 2019. 27, 5, 11, eaax4520.224.

221. Srinivasan B.; Baratashvili M.; Van der Zwaag M.; Kanon B.; Colombelli, C.; Lambrechts R.A.; Schaap O.; Nollen E.A.; Podgoršek A.; Kosec G.; Petković H.; Hayflick S.; Tiranti V.; Reijngoud, D.J.; Grzeschik, N.A.; Sibon O.C. Extracellular 4'-phosphopantetheine is a source for intracellular coenzyme A synthesis. Nature Chemical Biology. 2015. 11, 10, 784-792.
222. Chi M.; Yi B.; Oh S.; Park D.J.; Sung J.H.; Park S. A microfluidic cell culture device (μFCCD) to culture epithelial cells with physiological and morphological properties that mimic those of the human intestine. Biomed Microdevices. 2015. 17, 3, 9966.
223. Furuse M.; Hirase T.; Itoh M.; Nagafuchi A.; Yonemura S.; Tsukita S.; Tsukita S. Occludin: a novel integral membrane protein localizing at tight junctions. The Journal of Cell Biology. 1993. 123, 1777–1788.
224. Lennernäs H.; Nilsson D.; Aquilonius S.M.; Ahrenstedt O.; Knutson L.; Paalzow L.K. The effect of L-leucin on the absorption of levodopa, studied by region al jejeunal perfusion in man, Br. The Journal of Clinical Pharmacology. 1993. 35. 243–250.
225. Madara J.L.; Pappenheimer J.R. Structural basis for physiological regulation of paracellular pathways in intestinal epithelia, Journal of Membrane Biology. 1987. 100, 149–164.

Acknowledgements

Questo viaggio non sarebbe stato possibile senza l'aiuto di innumerevoli persone. Vorrei cogliere l'occasione per esprimere loro i miei ringraziamenti per avermi dato un enorme aiuto.

Prima di tutti, vorrei ringraziare la Prof.ssa Maria Daglia per essere stata il mio tutor e per avermi reso, in questi anni, una persona forte, sicura e più consapevole del mio valore.

Proseguiamo con Marco con il quale ho condiviso moltissimi momenti negli ultimi anni e mi sento fortunata di aver avuto una persona come te accanto che mi sempre spinto oltre i miei limiti e mi ha fatto capire quanto io sia speciale.

Grazie ad Alessandra B. per essere una collega speciale e sempre attenta agli altri, per avermi supportato in ogni attività e per esserti presa cura di me sia a Pavia, sia a distanza.

Vorrei anche ringraziare Anna per essere stata un punto di riferimento sia dentro che fuori il laboratorio e per aver anche creduto in me quando neanche io ci credevo. Grazie per essere stata sempre presente e per aver alleviato tante piccole incombenze.

Vorrei ringraziare i miei compagni di viaggio in questo dottorato: June, Cristina, Emanuele, Raffaello, Nadia, Hammad per tutti i momenti divertenti che abbiamo trascorso insieme e per il supporto durante le situazioni difficili.

My sincere thanks next go to June, who had the same fate with me in a PhD candidate. We shared moments of deep anxiety but also excitement, travels and foods. You are also the important person of this success.

Grazie a Chiara per la sua gentilezza, per gli insegnamenti, per la fiducia che ha sempre avuto nei miei confronti. Per me Chiara è stata un punto riferimento importantissimo, lei mi ha insegnato tantissimo nel lavoro e come gestire persone e situazioni.

A Lorenza e Daniele vorrei dire grazie per avermi sostenuto sempre, specialmente nei momenti più difficili e aver accettato anche la parte peggiore di me. Siete dei magnifici amici e colleghi di laboratorio, grazie per la boccata di aria fresca che avete portato nella mia vita e per tutti i momenti che abbiamo trascorso insieme dentro e fuori il laboratorio. Ora tocca a voi iniziare questo viaggio e vi auguro il meglio per il vostro percorso di dottorato.

Gracias a Bea por su dulce sonrisa, tu amabilidad y tu gran corazón. Los quiero mucho. Hasta pronto en España.

Vorrei ringraziare le mie *pole sister*: Camilla, Daria, Marina e Renata per avermi fatto sentire parte di loro sempre e comunque. Grazie per tutte le lezioni passate insieme, per le serate, per tutte le volte che dite " il palo di Cri" e io mi sento in quella sala a ballare con voi. Grazie per darmi sempre ottimi consigli e per esserci sempre. Grazie alla She Wolf Pole Dance Studio per avermi insegnato e accolto nel loro fantastico mondo e per aver curato il mio corpo, la mia mente e il mio spirito. Grazie ad Alessandra G. per le nostre passeggiate sul lungomare, le chiacchiere e supporto reciproco.

I want to thank Prof. Bruno Sarmento for giving me an opportunity to be a member at NTDD group (Nanomedicines & Translational Drug Delivery). I really appreciate your useful guidance on my project as well as extremely fast and helpful suggestions. Your critical feedback always makes my work better and more completed. I am also deeply grateful to my tutor at NTDD lab Catarina Leite Pereira for your enthusiasm to help and be on my side during my experiments. A special person for me is Sofia Dias and the most amazing part was everything we shared together since MIVO, procrastinating mood and lots of laughter. To all of members of NTDD group thank you for this unforgettable adventure in Portugal, your kindness has filled my heart.

Grazie a Miriam per aver condiviso con me l'esperienza a Porto, per aver avuto fiducia in me nei momenti difficili e per aver viaggiato con me. La tua presenza è stata fondamentale e mi hai riempito di coraggio in tutti i momenti difficili.

A very special word of thanks goes for my lovely flatmates in Porto: Bruna, Flavio, Francesco, Gabriel, Mariana, Maria and Dino, who made me feel at home. Thank you for all the moments spent together and for the chats (especially those related to relationships).

Sofia and Natalia, my pole friends in Porto, thanks for your useful advice during my stressful moment and for the power and good vibes that you have always spread around me. Thank you for dancing and shining with me. I am very grateful to StudioUp Porto, all the staffs and members to be amazing in every class and event.

Vorrei ringraziare i miei amici di sempre, in particolare: Giusy, Emanuela, Mimma e Daniele. Nonostante la vita ci abbia portato in posti molto lontani, noi siamo sempre rimasti vicini con il cuore.

Infine, le persone più importanti, vorrei ringraziare i miei genitori e mia sorella per avermi sostenuto e incoraggiato in tutte le mie scelte e avventure.

Cristina Santarcangelo

2023